Exploring Effects of In-situ Hygrothermal Conditions on Fracture Toughness of Flax Fibre Epoxy Composite

Master Thesis

Guruesh Elangovan

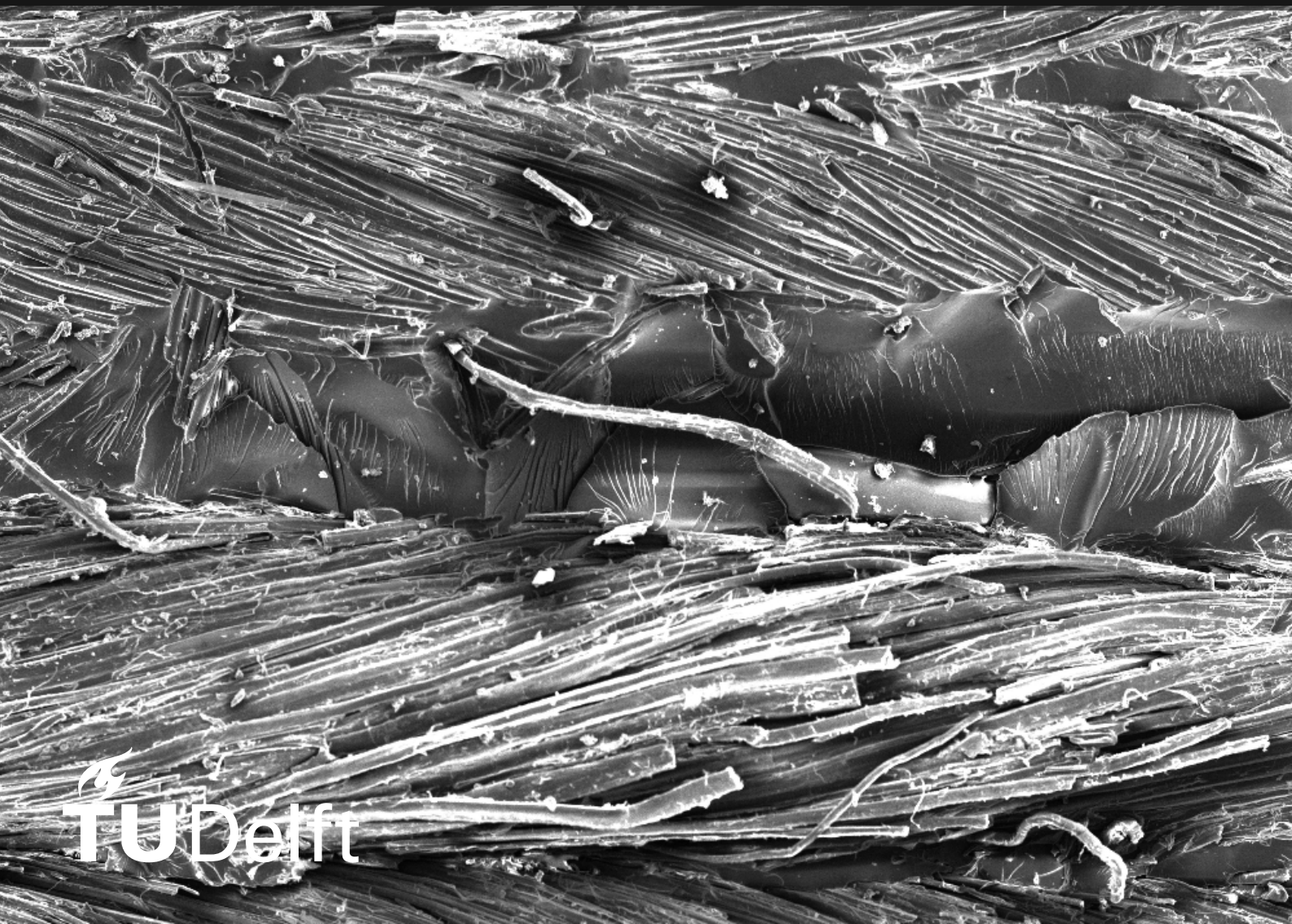

TU Delft

Exploring Effects of In-situ Hygrothermal Conditions on Fracture Toughness of Flax Fibre Epoxy Composite

by

Guruesh Elangovan

to obtain the degree of Master of Science

at the Delft University of Technology,

to be defended publicly on Wednesday, December 10th, 2025 at 15:00.

Student Number:	5994993
Project Duration:	January 2025 – December 2025
Thesis Committee:	Dr. Vera Popovich
	Dr. John-Alan Pascoe
	Dr. Yasmine Mosleh
	Dr. Pooria Pahlavan

Cover: Fracture surface photographed by the author during the course of master thesis project.

An electronic version of this thesis is available at http://repository.tudelft.nl/.

TU Delft

Acknowledgements

First and foremost, I would like to express my sincere gratitude to my supervisors Dr. Yasmine Mosleh and Dr. John-Alan Pascoe for their invaluable guidance, insightful feedback, and continuous support throughout this thesis. I am also grateful to Dr. Vera Popovich for providing the necessary support and for facilitating the progress of this work. I owe a great deal to Valentin for introducing me to the manufacturing procedures and to Francisco for sharing practical and helpful tips on post-processing. I also wish to express my appreciation to the laboratory technicians in the Mechanical, Civil, and Aerospace Engineering departments, whose technical assistance and hands-on help were essential for carrying out the experimental work.

Many people have helped me, both directly and indirectly, during this project. I would like to thank the PhD candidates, postdoctoral researchers, and fellow master's students who contributed through discussions, small pieces of advice, and encouragement during long days in the lab. Each of them has been like a small drop in a vast ocean, collectively shaping this work and my overall experience. Finally, I am deeply grateful to my family for their continuous support and encouragement throughout my studies. Their belief in me has been a constant source of motivation and has played an important role in the completion of this thesis.

Guruesh Elangovan
Delft, December 2025

Abstract

Composites are widely used in structural applications due to their high strength-to-weight ratio, stiffness, and design flexibility, but their sustainability remains a limitation. To address this, flax fibre-reinforced polymer (FFRP) composites offer competitive mechanical performance while being biodegradable and less energy-intensive to produce. However, the use of FFRPs in load-bearing structural applications is constrained, in particular, by the susceptibility of flax fibres to environmental conditions such as temperature and humidity, and by a limited understanding of their delamination behaviour in the primary loading modes. Therefore, this study investigates the interlaminar fracture toughness of FFRP composites under various hygrothermal conditions in Mode I loading.

The experimental analysis was conducted under environmental conditions representative of natural weathering, including hot-wet, hot-dry, room, and cold environments. The samples were initially conditioned at the respective hygrothermal conditions and subjected to quasi-static and fatigue loading in an environmental chamber. The results demonstrate a strong dependence of fracture toughness on the applied hygrothermal conditions, indicating that FFRP composites are highly sensitive to both temperature and relative humidity. Under quasi-static loading, the fracture toughness increased with higher humidity and lower temperature, indicating enhanced crack growth resistance due to moisture and improved fibre bridging, while a reduction in fracture toughness was observed under low-humidity conditions. Fatigue results showed distinct Paris curves, with a rightward shift observed under high-humidity and low-temperature conditions, indicating improved resistance to fatigue crack propagation, whereas Paris curves corresponding to low-humidity environments shifted leftward, reflecting decreased resistance to fatigue crack growth.

Fractographic analysis using optical microscopy and scanning electron microscopy (SEM) revealed common microstructural features such as technical fibre bridging, fibre pull-out, yarn loosening, fibre patches, scarps, and matrix cracking. The nature of fracture transitioned from ductile under high humidity and elevated temperature to brittle at low temperature, highlighting a shift in the dominant failure mechanism from interfacial debonding to matrix-dominated cracking. Surface roughness measurements, however, exhibited considerable statistical scatter across all environmental conditions, likely due to the strong influence of technical fibre bridging on the measured roughness. Consequently, the observed changes in Mode I interlaminar fracture toughness with humidity and temperature were not clearly reflected in the roughness parameters.

Overall, the findings emphasise the strong dependence of the fracture behaviour of FFRP composites on environmental exposure. Understanding these effects is critical for the reliable design and durability prediction of FFRP composites in structural applications. The results contribute to establishing a foundational understanding of the fracture mechanics of FFRPs.

Contents

List of Figures

List of Tables

Nomenclature

Abbreviations

Abbreviation	Definition
ANOVA	Analysis of variance
ASTM	American Society for Testing and Materials)
CCM	Compliance Calibration Method
CFRP	Carbon fibre reinforced polymer
CLSM	Confocal laser scanning microscope
CMC	Ceramic matrix composite
CNTs	Carbon nanotubes
CTBN	Carboxyl terminated butadiene acrylonitrile
DCB	Double cantilever beam
DSC	Differential scanning calorimetry
FFRP	Flax fibre reinforced polymer
FRP	Fibre reinforced polymer
GFRP	Glass fibre reinforced polymer
ISO	International Organization for Standardization
LEFM	Linear elastic fracture mechanics
MBT	Modified beam theory
MCC	Modified compliance calibration
MMC	Metal matrix composite
MWCNT	Multi walled carbon nanotube
NFRC	Natural fibre reinforced composite
PMC	Polymer matrix composite
PPS	Polyphenylene sulfide
PW	Plain weave
R-Curve	Resistance Curve
RH	Relative Humidity
SEM	Scanning electron microscope
SERR	Strain energy release rate
UD	Unidirectional

Symbols

Symbol	Definition	Unit
a	Delamination length	$[m]$
b	Width	$[m]$
C	Compliance	$[m/N]$
δ	Load-point displacement	$[m]$
Δ	Effective crack-length correction term	$[m]$
e	Insert length	$[m]$
E	Young's modulus	$[N/m^2]$
F	Large-displacement correction factor	[–]
G	Critical strain energy release rate	$[J/m^2]$
G_I	Mode I interlaminar fracture toughness	$[J/m^2]$
G_{II}	Mode II interlaminar fracture toughness	$[J/m^2]$
G_{III}	Mode III interlaminar fracture toughness	$[J/m^2]$
h	Thickness	$[m]$
ℓ	Distance from loading-block pinhole center to block edge	$[m]$
L	Length	$[m]$
M	Moisture uptake / evolution (mass fraction)	[–]
N_{LB}	Load-block correction factor	[–]
N_{cycles}	Number of cycles	[cycles]
P	Applied load	$[N]$
$P_{\max}$	Maximum applied load	$[N]$
$P_{\min}$	Minimum applied load	$[N]$
R	Load ratio ($P_{\min}/P_{\max}$)	[–]
S_a	Arithmetical mean height (surface roughness)	$[m]$
S_q	Root mean square height (surface roughness)	$[m]$
S_z	Maximum height (surface roughness)	$[m]$
T_g	Glass transition temperature	$[^\circ C]$
W_0	Initial mass of specimen	$[kg]$
W_i	Mass of specimen at measured time	$[kg]$
σ_{ult}	Ultimate tensile strength	$[N/m^2]$
$\varepsilon_{\max}$	Strain at break	$[\%]$

1

Introduction

A fundamental consideration in the design of any structural component is ensuring that it can withstand applied loads and prevent failure throughout its service life. Therefore, understanding the mechanical behaviour, damage mechanisms, and environmental sensitivity of materials is essential for achieving structural reliability and durability [1]. Composite materials have become increasingly important in this regard due to their high strength-to-weight ratio, stiffness, corrosion resistance, and design flexibility, which make them suitable for a wide range of applications in aerospace, automotive, marine, and civil engineering [2].

However, a major limitation of conventional composites reinforced with synthetic fibres, such as glass or carbon, lies in their poor sustainability. They are non-biodegradable and require high energy for production, which contributes to environmental concerns [3]. To address these issues, flax fibre-reinforced polymer (FFRP) composites have emerged as a promising alternative. FFRPs combine biodegradability and renewability with competitive mechanical performance, making them attractive for sustainable engineering applications [4].

Despite these advantages, flax fibres are known to be sensitive to environmental conditions, particularly temperature and humidity, which can significantly influence the mechanical integrity and interfacial bonding of the composites [5]. These combined environmental effects are referred to as hygrothermal effects, representing the interaction between moisture absorption and temperature variation. Moisture absorption can lead to matrix plasticisation, fibre swelling, and interfacial degradation, whereas temperature fluctuations can cause thermal degradation of the fibres and plastisacation of matrix [5]. Together, these effects can alter the fracture toughness, stiffness, and overall durability of the composite, especially under long-term outdoor exposure [5] [6].

Among the key parameters defining the performance and reliability of composites, fracture toughness is one of the most critical. It characterises a material's resistance to crack initiation and propagation, and therefore its ability to absorb energy before catastrophic failure occurs [7]. In fibre reinforced composites, a dominant mode of failure associated with crack growth is delamination, the separation of adjacent plies due to interlaminar normal or shear stresses [7]. Delamination can be triggered by quasi static or fatigue loading . Once initiated, it can propagate rapidly, leading to a significant reduction in load-bearing capacity and stiffness.

This study investigates the interlaminar fracture toughness of FFRP composites under various hygrothermal conditions in Mode I quasi static and fatigue loads. The experimental work examines four environmental conditions (hot wet, hot dry, room, and cold) selected to represent geographically realistic weather conditions. The results provide insight into the sensitivity of FFRP composites to both temperature and relative humidity and how these factors influence crack propagation behaviour and fracture resistance.

The structure of this report is as follows. Chapter 2 reviews existing literature on flax fibres and their composites, with particular emphasis on fracture toughness and the influence of hygrothermal envi-

ronments. Chapter 3 formulates the research objectives and states the problem definition. Chapter 4 presents the specimen design, manufacturing procedures, quality control processes, and specimen preparation. Chapter 5 describes the experimental methodology, data reduction techniques, and the systematic approach used to achieve the research objectives. Chapter 6 provides an in-depth analysis and discussion of the results obtained. Chapter 7 summarises the main conclusions derived from the study. Chapter 8 presents the recommendations and suggests directions for future research.

2

State of the art

Composites are multiphase materials designed to combine two or more distinct constituents to produce a material with superior mechanical and physical properties compared to the individual components. These materials typically consist of a continuous *matrix phase* that binds and protects a *reinforcement phase*, which is usually in the form of fibres or particulates. The matrix serves to transfer stress between reinforcements and provides resistance against environmental degradation and mechanical damage, while the reinforcement contributes to stiffness, strength, and toughness [1].

In general, composites can be broadly classified into three categories, polymer matrix composites (PMCs), metal matrix composites (MMCs), and ceramic matrix composites (CMCs) [2]. Among these, PMCs are the most widely used in structural applications, because of their properties such as high-strength to weight ratio, low density, corrosion resistance, cost-efficiency, and ease of manufacturing. Among PMCs, fibre-reinforced polymers (FRPs) is a key subclass, wherein high-performance continuous fibres (such as glass, carbon, etc.,) are embedded in a polymer matrix, resulting high specific strength and stiffness materials [8]. Therefore, they are widely used in various applications across aerospace, automotive, marine, and civil engineering industries.

Fibre-reinforced composites are used in structural applications in the form of a laminate, which is made by stacking a number of thin layers of fibres and matrix and consolidating them into the desired thickness. Fibre orientation in each layer, as well as the stacking sequence of various layers in a composite laminate, can be controlled to generate a wide range of physical and mechanical properties for the composite laminate.

In recent years, driven by growing environmental concerns and sustainability initiatives, research attention has increasingly focused on natural fibre–reinforced composites (NFRCs). These materials employ renewable, plant-derived fibres such as flax, hemp, jute (bast fibres), sisal (leaf fibres), and cotton (seed fibres) as reinforcements [9]. Natural fibres offer several advantages, including biodegradability, low cost, low density, and a reduced environmental footprint during production and disposal. When combined with biodegradable or recyclable polymer matrices, NFRCs provide a sustainable alternative to conventional composites, aligning with the principles of the circular economy and green engineering [9].

Among the various natural fibres, flax has attracted particular interest due to its excellent specific stiffness, strength, and favourable mechanical performance compared to other bast fibres. To understand the origins of these properties, it is essential to examine the hierarchical structure of the flax fibre in detail.

2.1. Structure and production of flax fibres

Flax (Linum usitatissimum L.), a member of the Linaceae family, is one of the oldest cultivated plants, with its use dating back thousands of years for textile, oil, and industrial applications [4]. The stalk of the flax plant contains bast fibres that are extracted primarily from the phloem tissue located in the outer regions of the stem. These bast fibres, once separated and processed, can be used to reinforce

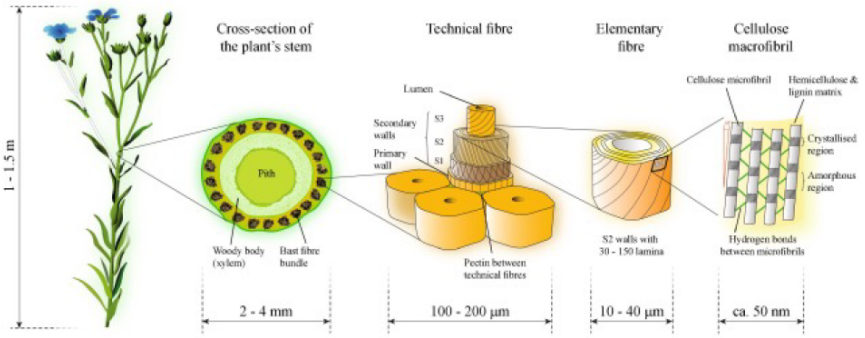

Figure 2.1: Schematic representation of structure of flax fibre [10]

polymer matrices, forming flax FFRP composites.

The hierarchical microstructure of flax fibres is central to their mechanical behaviour. Each fibre is composed of numerous elementary fibres, bound together by natural matrices of hemicellulose and pectin. The elementary fibre, in turn, has a hollow central lumen surrounded by cell walls with spirally wound cellulose microfibrils. The microfibril angle ,typically 5–10° in flax has strong influence in the stiffness and load-bearing capacity of the fibre [11]. This anisotropic structure contributes to flax fibres relatively high Young's modulus (ranging from 37.6 to 103 GPa) and tensile strength (ranging from 343 to 2000 MPa), depending on the source and processing conditions.

One of the distinguishing features of flax compared to other bast fibres (such as jute or hemp) is its relatively fine diameter and higher cellulose crystallinity. These properties contribute to superior stiffness and vibration damping characteristics, making flax fibres suitable for automotive panels, bicycle components, musical instruments, and other vibration sensitive applications [12]. Moreover, flax fibres have a relatively lighter colour, which is advantageous for visible or semi-transparent composite surfaces where aesthetics are important.

The production of flax fabrics begins with a growth period of approximately 100 days, after which the plants are harvested and subjected to retting, a crucial process that facilitates fibre extraction by decomposing the pectin that binds fibres to the stalk. Retting can be performed through various methods, including dew retting, water retting, and enzymatic retting, each of which significantly affects fibre quality [13]. Among these, proper retting is essential to loosen the fibre bundles effectively without damaging the fibres or leaving residual impurities that may impair mechanical performance and fibre–matrix adhesion in composite applications. Following retting, the fibres are mechanically separated from the stem via scutching and hackling processes, which produce individual technical fibres with diameters typically ranging from 100– 200 µm and lengths up to 1 m. Within these technical fibres are elementary fibres, which are finer in diameter (19–25 µm) and shorter in length (20–50 mm)[14]. The elementary fibres themselves consist of a primary cell wall and a secondary wall comprising three distinct layers, which collectively contribute to the mechanical properties and functionality of FFRP composites [13]

2.2. Moisture absoprtion Mechanism in NFRP

Unlike synthetic fibres such as glass and carbon, which are more resistant to environmental degradation, natural fibre composites are much more vulnerable to moisture-induced damage. This makes moisture absorption in NFRPs more complex than in synthetic FRPs, leading to a range of progressive degradation mechanisms as follows:

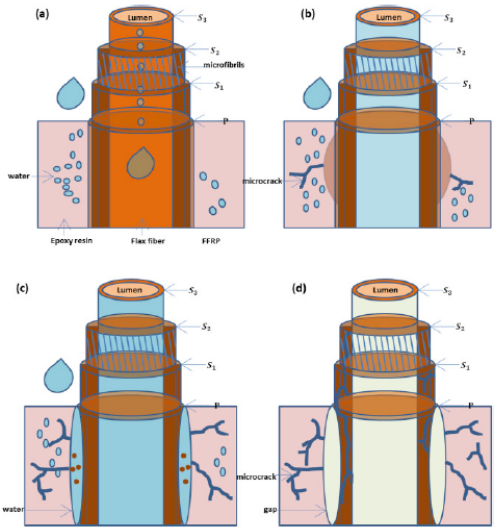

Figure 2.2: Hygrothermal ageing Mechanisms in NFRPs [5]

(a) **Reversible Physical Changes: Plasticisation and Swelling** - As shown in Figure 2.2-(a), moisture enters the composite primarily through diffusion into the polymer matrix and capillary flow along the fibre–matrix interface [5] . The internal lumen structure and surface porosity of natural fibres facilitate rapid water uptake. Water molecules bind to hydroxyl-rich regions in hemicellulose and amorphous cellulose, causing the fibres to swell. This fibre swelling, in turn, induces internal stresses that can trigger microcracking in the adjacent matrix. The plasticisation of the matrix and swelling of fibres are partially reversible upon drying. [15][5].

(b) **Irreversible Mechanical Damage: Stress-Induced Microcracking** - Figure 2.2-(b) highlights the development of internal stress concentrations due to uneven swelling across different layers of the fibre cell wall[5]. This non-uniform expansion distorts the microfibrillar angle and generates cracks within the matrix, eventually compromising fibre–matrix adhesion. These changes often result in a permanent reduction in mechanical performance, including loss of stiffness and tensile strength.

(c) **Irreversible Chemical Degradation: Leaching and Hydrolysis** - With continued exposure to humid or wet environments, irreversible chemical transformations occur within the fibre phase[5]. As shown in Figure 2.2-(c), components such as pectins, hemicellulose, and low-crystallinity cellulose are leached from the fibres. This leaching weakens the fibre's internal structure and degrades the bonding interface with the matrix.

(d) **Irreversible Dimensional Changes: Shrinkage and Interfacial Voids** - Figure 2.2-(d) shows the long-term effects of moisture cycling, where fibres shrink upon drying after prolonged wet conditions[5]. This shrinkage causes separation at the fibre–matrix interface, leaving behind microvoids that serve as stress concentration points during mechanical loading.

2.3. Hygrothermal Effects on Mechanical properties

A study investigated the effect of moisture absorption on the mechanical properties of short roselle and sisal fibre reinforced hybrid polyester composites, comparing them with composites made using dried fibres [16]. Under dry conditions, increasing the fibre content and length led to improvements in both tensile and flexural strength. However, under wet conditions, these properties showed a significant reduction up to 11.7 % . The impact strength decreased with increasing fibre content and length in both dry and wet states. Overall, exposure to moisture caused a showed the decline in mechanical performance, primarily due to degradation at the fibre–matrix interface.These insights underscore the need to assess hygrothermal performance in NFRCs to ensure long-term durability, particularly for structural applications exposed to fluctuating environmental conditions.

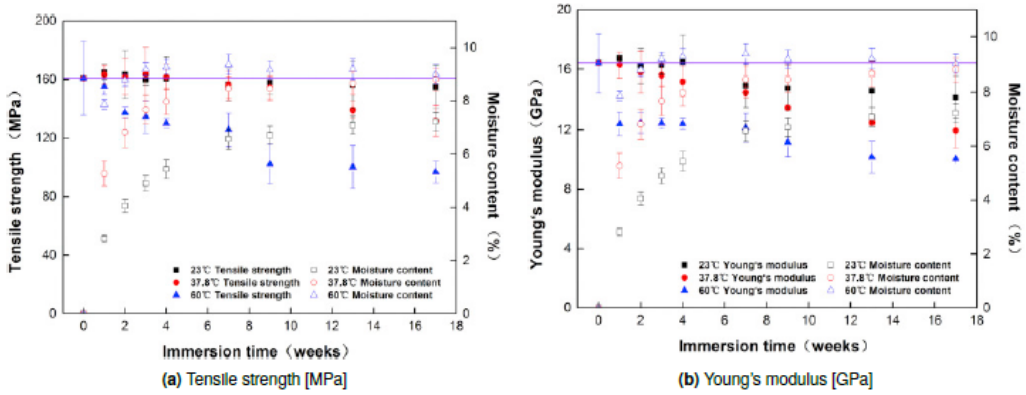

Figure 2.3: Effect of hygrothermal ageing and subsequent drying on tensile properties of unidirectional FFRP [5]

A study investigated the tensile behaviour of flax fibre-reinforced epoxy specimens after immersion in water at different temperatures [5]. The tensile strength initially increased in specimens aged at 23 °C before stabilizing; at 37.8 °C, a slight decline was observed; and at 60 °C, a substantial and irreversible drop occurred. Figure 2.3 illustrates these results, showing that specimens aged at 23 °C experienced a permanent reduction in stiffness after four weeks of immersion, while tensile strength remained stable. For specimens at 60 °C after seven weeks, severe splitting was observed, accompanied by peeling of cell walls from flax yarns. This behaviour was attributed to the multilayered structure of the fibres, which induced delamination among the different layers of flax fibres due to interface modifications caused by ageing. It has been reported that a series of variations occured within flax fibres during hydrothermal ageing, including changes in the microfibrillar angle, dissolution of pectins, hemicelluloses, and poorly crystallized celluloses, as well as fibre peeling and splitting. These structural damages in flax fibres led to degradation of the tensile strength of FFRP aged at 37.8 °C and 60 °C. In contrast, due to the relatively low water absorption of specimens aged at 23 °C, no decreasing trend in tensile strength was observed.

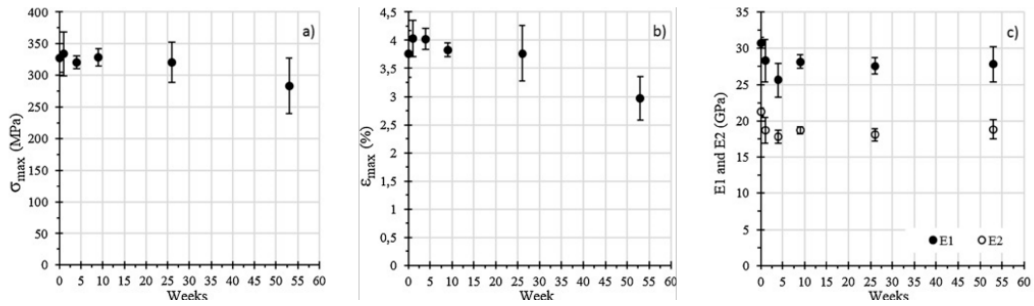

Figure 2.4: Effect of hygrothermal ageing duration on tensile strength, strain at break, and Young's modulus of FFRP [17]

Van Schoors et al conducted the study in which the flax fibre epoxy composite specimens were exposed to hygrothermal ageing cycles for up to one year, and tensile tests were performed on all aged samples [17]. As shown in Fig 2.4, the ultimate tensile strength (σ_{max}) and deformation at break (ε_{max}) remained stable up to 26 weeks of exposure. Between 26 and 52 weeks, ε_{max} decreased by about 20%, while σ_{max} showed a smaller reduction of approximately 12%. In contrast, the evolution of both moduli E_1 and E_2 began earlier, with decreases observed from the 1st to the 4th week of exposure, reaching 8% and 12% respectively, before stabilizing up to 52 weeks. The reductions in ultimate tensile strength and strain observed between 26 and 52 weeks were mainly attributed to the increased formation of cracks and the degradation of fibre/matrix interfaces within the material.

The influence of in-situ temperature and humidity on the tensile behaviour of FFRP has been examined by Perruchoud et al. [18]. In their study, the in-service performance of cross-ply Glass fibre reinforced polymer (GFRP) and FFRP laminates was compared, revealing clear differences in environmental sen-

sitivity. FFRP showed a stronger dependence on temperature than GFRP, and for FFRP, tests at $-20\,^{\circ}\mathrm{C}$ yielded higher tensile strength than those at room temperature. Moisture effects assessed at 50% and 90% RH indicated that relative humidity had little influence on GFRP, whereas FFRP laminates were significantly affected, highlighting the susceptibility of flax fibres to moisture. Increased humidity was also associated with enhanced ductility in FFRP. Figure 2.5 shows an increase in tensile strength with decreasing temperature and an increase in ductility with increasing humidity. Taken together, these observations underscore the pronounced impact of in-service environmental conditions on the mechanical response of flax fibre composites.

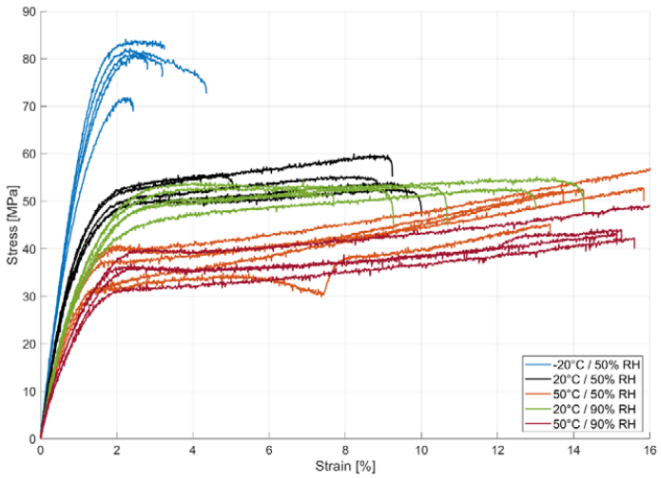

Figure 2.5: Stress-strain curves of the FFRP in insitu hygrothermal conditons. [18].

The hygrothermal effect on the toughness of flax fibre composites was investigated by Calabrese et al [6]. The study examined the influence of cyclic salt fog and drying exposure on the toughness characteristics of FFRPs. The experimental procedure involved subjecting flax/epoxy specimens to 10 days of salt fog ageing at 35 °C, followed by 18 days of drying at 22 °C and 50% relative humidity, repeated for three consecutive cycles. Mechanical performance was assessed using three-point bending tests in accordance with ASTM D790 standards. As illustrated in Figure 2.6a, the ageing protocol resulted in a reduction in stiffness and a corresponding increase in ductility, attributed to the plasticisation and softening of both the epoxy matrix and the flax fibres.

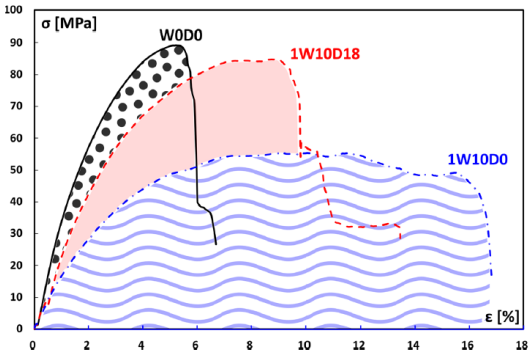

(a) Stress–strain curves at different ageing conditions in the first cycle (W0D0: unaged; 1W10D0: 0 drying days; 1W10D18: 18 drying days) [6].

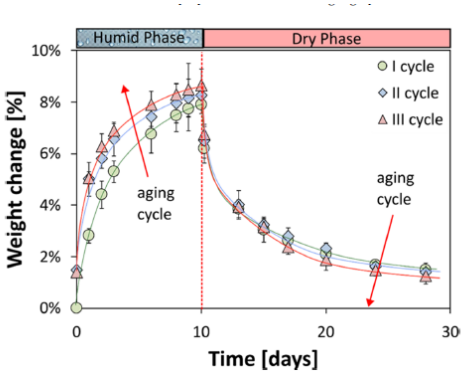

(b) Weight change vs. time during humid and dry phases for the flax composite laminate across ageing cycles (cycle I: circle marker; cycle II: diamond marker; cycle III: triangle) [6].

It is noteworthy that the exhibited different weight changes in each ageing cycle. The maximum weight gain increased progressively with the number of cycles, reaching 8.65% in the third cycle [6]. A slight decrease in residual weight due to leaching was also observed at the end of each dry phase, reaching 1.25% by the third cycle as shown in figure 2.6b.

Figures 2.7-a and 2.7-b demonstrate that the drying stages partially restored both flexural strength and modulus following each ageing cycle [6]. These results indicate that although humidity exposure leads to matrix softening and mechanical degradation, subsequent drying phases promote partial recovery, with the composite remaining more ductile than the unaged reference. The enhanced ductility contributes to improved toughness. These findings further suggest that toughness is highly sensitive to humid–dry cycling. Toughness increases due to a slight reduction in peak stress combined with a significant increase in deformation at break under humid conditions. Interestingly, after drying, the composite subjected to three cycles exhibited a permanently higher toughness than the unaged composite.

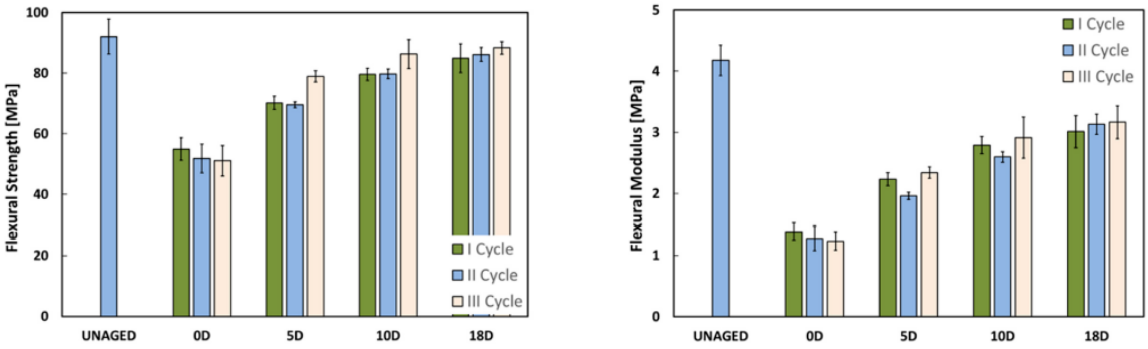

(a) Flexural strength evolution

(b) Flexural modulus evolution

Figure 2.7: Flexural property degradation in FFRC due to salt fog and drying cycles[6].

Therefore, cyclic hygrothermal exposure not only affects stiffness and strength but also enhances the energy absorption capability of FFRCs, potentially leading to improved toughness under variable environmental conditions.

2.4. Fracture toughness of composites

Fracture mechanics in FRP composites presents significant challenges due to their inherent anisotropy and heterogeneous microstructure, which result in complex crack initiation and propagation behaviour. Unlike isotropic materials, where cracks typically follow predictable paths, the fibre–matrix architecture in FRP composites leads to multiple interacting damage mechanisms, such as fibre breakage, matrix cracking, fibre–matrix debonding, and delamination. Among these, delamination is a critical failure mode that compromises the structural integrity and service life of composite components, this is because laminated fibre reinforced composites delaminate quickly under compressive loads due to sub laminate buckling.

Fracture toughness, a key parameter for evaluating resistance to crack growth, is typically quantified by the critical strain energy release rate, G_C [J/m^2], which defines the energy required to advance a crack per unit area of the newly created fracture surface. The value of G_C is highly dependent on the mode of delamination, which is generally classified into three idealized modes: Mode I (G_{IC}) – opening or tensile mode, Mode II (G_{IIC}) – in-plane shear or sliding mode, and Mode III (G_{IIIC}) – out-of-plane shear or tearing mode. These modes are schematically represented in Figure 2.8.

In real-world applications, however, loading conditions rarely produce pure modes of fracture. Instead, mixed-mode delamination, involving simultaneous contributions from two or more fracture modes, is commonly observed. As a result, accurate characterization of fracture toughness must account for mixed-mode interactions to better reflect the actual performance and failure behaviour of FRP structures under service conditions.

The fracture toughness of FRP composites is typically evaluated using various standardised testing procedures developed by organisations such as the International Organization for Standardization (ISO) and the American Society for Testing and Materials (ASTM). Mode I fracture toughness is most commonly assessed using Double Cantilever Beam (DCB) specimens, as specified in ASTM D5528 and ISO 15024 [20] [21]. For Mode II delamination, ASTM D7905 recommends the use of End-Notched Flexure (ENF) specimens [22], while ISO 15114 proposes the Calibrated End-Loaded Split (C-ELS)

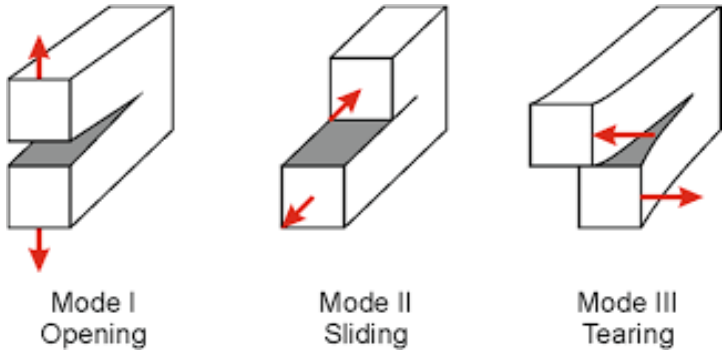

Figure 2.8: Schematic representation of three principal fracture modes [19]

method [23]. Mode III testing, though less common due to the inherent difficulty of inducing pure out-of-plane shear, is typically conducted using Edge Crack Torsion (ECT) or Split Cantilever Beam (DCB) specimens [24]. However, these Mode III methods have not yet been standardised due to the complexity involved in generating isolated Mode III loading conditions.

To initiate controlled crack propagation in the test environment, all specimens are typically manufactured with a precrack. This is often achieved by inserting a thin non-adhesive film, such as PTFE at the mid-plane during lay-up. While this artificial starter crack is essential for test repeatability, real-world delamination usually originates from flaws introduced during manufacturing, such as voids, porosity, fibre misalignment, or resin-rich zones. Additionally, delamination can occur in-service due to accidental impacts, fatigue loading, or exposure to harsh hygrothermal conditions.

The fracture toughness of composite materials is not a fixed property but is strongly influenced by various material and processing parameters. Factors such as fibre orientation, matrix properties, fibre volume fraction, and the integrity of the fibre–matrix interface all play critical roles in determining a composite's resistance to crack initiation and propagation. A comprehensive understanding of how these factors affect fracture behaviour is essential for optimizing composite structures and improving their damage tolerance under actual service conditions.

2.5. Factors influencing Fracture Toughness

Crack propagation in fibre-reinforced composites is governed by both intrinsic and extrinsic toughening mechanisms, as illustrated in Figure 2.9. Intrinsic mechanisms act ahead of the crack tip and are associated with the inherent material characteristics, such as matrix toughness and the strength of the fibre–matrix interface. In contrast, extrinsic mechanisms operate behind the crack front and serve to hinder further crack growth through phenomena such as fibre bridging, fibre pullout, and crack deflection.

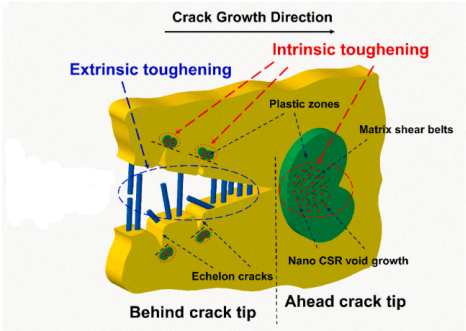

Figure 2.9: Intrinsic and extrinsic toughening mechanisms in FRP[25]

2.5.1. Matrix

The type of matrix selected in a composite system plays a crucial role in determining its fracture toughness. Studies have demonstrated that matrices with inherently higher toughness tend to improve the interlaminar fracture resistance of the composite. In general, the polymer resin used as the matrix can be classified into two types: thermoplastic and thermosetting. Typically, thermoset composites exhibit lower toughness compared to thermoplastics due to cross-linking, which limits plastic deformation and reduces the ability to absorb energy during fracture [26]. Thermosetting resins (e.g., polyesters, epoxies, and polyimides) are highly crosslinked and provide adequate modulus, strength, and creep resistance, but the same cross-linking of molecular chains leads to extreme brittleness and very low fracture toughness. The commonly used polyester resins for FRP composites are epoxy and polyester, which are often modified by introducing carboxyl-terminated butadiene-acrylonitrile (CTBN) copolymers. The modification can be achieved through simple mechanical blending of the soft, rubbery particles with the resin or by copolymerisation of a mixture of the two. Figure 2.10 shows the increase in fracture surface energy of an epoxy as a function of the weight percentage of CTBN elastomer [26].

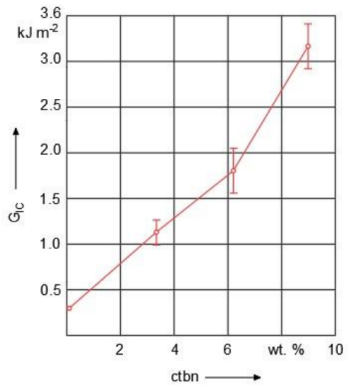

Figure 2.10: racture surface energy of an epoxy as a function of weight % of carboxyl-terminated butadiene-acrylonitrile (ctbn) [26]

Another method to reinforce fracture toughness is through the addition of fillers such as carbon nanotubes (CNTs), which enhance crack-bridging and promote fibre pull-out mechanisms [27]. In the study conducted by Hibbs et al. on the effect of resin toughness on composite delamination fracture toughness, they highlighted that increasing the resin toughness without improving the bonding strength will be of little practical use, since the composite will then delaminate by debonding without fully utilizing the resin toughness [28]. Therefore, any attempt to improve the toughness of the composite by increasing the resin toughness must be accompanied by improved bonding of the new resin to the fibres. All the studies discussing the improvement of matrix toughness have given paramount importance to the matrix–fibre interface.

2.5.2. Fibre-Matrix Interface

Delamination in fibre-reinforced composites typically occurs due to matrix failure and/or fibre–matrix interface failure. The adhesion between fibres and the surrounding polymer matrix plays a crucial role in governing the fracture behaviour of such materials. One of the primary factors influencing this adhesion is the surface texture and chemical compatibility of the fibre with the matrix. When strong interfacial bonding is achieved, fibres can effectively transfer stress from the matrix, leading to improved load distribution and enhanced resistance to crack propagation. This, in turn, contributes significantly to the overall fracture toughness of the composite.

Numerous studies have investigated the influence of fibre surface treatments aimed at improving fibre–matrix adhesion. In GFRPs, treatments that enhance interfacial bonding have been reported to increase Mode II interlaminar fracture toughness by up to 2.5 times, with minimal effect on Mode I fracture toughness [29]. To improve Mode I fracture toughness, alternative mechanisms are often explored. In the case of carbon fibre-reinforced polymers (CFRPs), approaches such as the incorporation of multi-walled carbon nanotubes (MWCNTs) and the application of veils like polyphenylene sulfide (PPS) have

shown significant improvements in fracture toughness, with reported increases of approximately 70% and 215%, respectively [30].

Achieving effective interfacial adhesion is particularly challenging in biocomposites. Natural fibres such as flax, jute, and hemp are inherently hydrophilic due to their cellulose content, whereas common thermosetting matrices like epoxy are hydrophobic. This fundamental mismatch in surface chemistry often results in weak interfacial bonding, adversely affecting the mechanical performance and damage tolerance of bio-based composites.

To address this challenge, various surface modification techniques have been explored, including chemical treatments, plasma activation, and nanoparticle coatings, all of which aim to enhance fibre-matrix compatibility. For example, in a study conducted by V. Prasad *et al.*, flax fibres were coated with nano-sized titanium dioxide (TiO_2) particles and embedded in an epoxy matrix. The results demonstrated a 37% increase in Mode I fracture toughness at a 0.4 wt% TiO_2 content and a 24% increase in Mode II fracture toughness at a 0.6 wt% content, as shown in Figure 3.3 [31]. These findings highlight the potential of surface engineering to overcome adhesion limitations in natural fibres and achieve fracture toughness improvements comparable to those observed in synthetic composite systems. Furthermore, the strength of the fibre–matrix interface directly influences fibre bridging behaviour, which will be discussed in the following section.

2.5.3. Fibre Bridging

Fibre bridging is a phenomenon where fibres from adjacent plies span across the crack plane behind the crack tip as the crack propagates, as shown in 2.11. This phenomenon acts as a crack resistor, as it creates additional resistance by enabling the bridging fibres to transfer load between the plies. As a result, a greater force is required to propagate the crack, leading to increased delamination resistance and enhanced interlaminar fracture toughness.

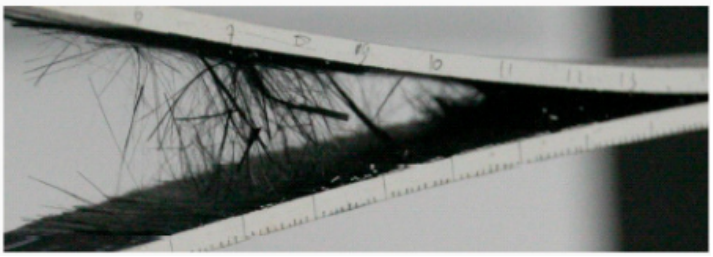

Figure 2.11: Fibre bridging [32]

Fibre bridging arises due to the nesting of adjacent fibre layers and the presence of weak interfaces in laminated fibre-reinforced composites[33]. It has been reported that unidirectional composites exhibit more pronounced fibre bridging compared to other laminate configurations. Johnson et al. observed that merely inclining the midplane laminate by 1.5 to 3 degrees resulted in a reduction of fracture toughness, primarily due to a significant decrease in fibre bridging. Although unidirectional laminates display prominent fibre bridging, inclined laminates still exhibit this phenomenon to a lesser extent [33].

It has been reported that different mechanisms contribute to fibre bridging in laminated composites, particularly those with weak fibre-matrix interfaces and larger crack tip yield zones [33]. In fibre-reinforced polymer (FRP) composites with high fibre volume fractions, interface debonding is a common phenomenon, which can result in fibre bridging. In such cases, the fracture surface associated with interface debonding typically exhibits large fibre imprints with minimal matrix failure. Similarly, laminated composites with tougher resin matrices often exhibit larger crack tip yield zones. In these materials, the yield zone extends through several plies above and below the delamination plane. As a result, delamination is observed to occur within these extended plies, where the fibres act as bridging elements. However, the global delamination remains at the original interface, as the debonded fibres span the crack plane in the surrounding plies, thereby contributing to fibre bridging [33].

In the case of cross-ply laminates or angled laminates, the amount of fibre bridging behind the crack tip is relatively low, but this does not terminate the occurrence of fibre bridging; instead, it leads to another

complex fibre bridging mechanism. In cross-ply laminates, it has been observed that the direction of crack propagation is not parallel to the fibre axis in the laminates. Therefore, the delamination deviates from the main crack plane into adjacent plies, ensuing in fibre bridging occurring within the delamination plane [34].

Several other factors influence fibre bridging during delamination, including ply thickness, loading conditions (static or fatigue), and environmental parameters such as moisture and temperature. Studies on carbon fibre/epoxy composites have shown that laminate thickness significantly affects fibre bridging behaviour [35]. In particular, the initiation (G_{Ic}) value has been reported to depend on specimen thickness, while the propagation G_{Ic} values increase continuously with crack growth. Thinner specimens exhibit higher G_{Ic} values and more pronounced fibre bridging compared to thicker ones. The loading profile also plays a key role in fibre bridging behaviour. Fibre bridging is generally more prominent under quasi-static loading compared to fatigue loading, with bridging stresses observed to be significantly higher under quasi-static conditions [36].

Moisture and temperature also play an important role in determining the extent of fibre bridging. It has been reported that increasing both moisture content and temperature can enhanced fibre bridging, leading to a increased the R-curve under Mode I loading [34]. However, while such effects have been documented in laminated carbon fibre/epoxy composites, the influence of temperature and moisture on fibre bridging in flax fibre-reinforced composites has not yet been thoroughly investigated.

The effects of fibre bridging can be clearly observed in all crack growth resistance curve (R-curve), as illustrated in Figure 2.12. As the crack extends, the fracture toughness increases because more fibres begin to bridge the crack, absorbing energy and slowing down further crack growth. Eventually, the R-curve reaches a plateau, indicating that the fibre bridging zone has stabilised. At this stage, the number of new fibres forming bridges at the crack tip is equal to the number of fibres breaking or pulling out as the crack opening becomes too large. This balance results in a steady-state fracture resistance [53].

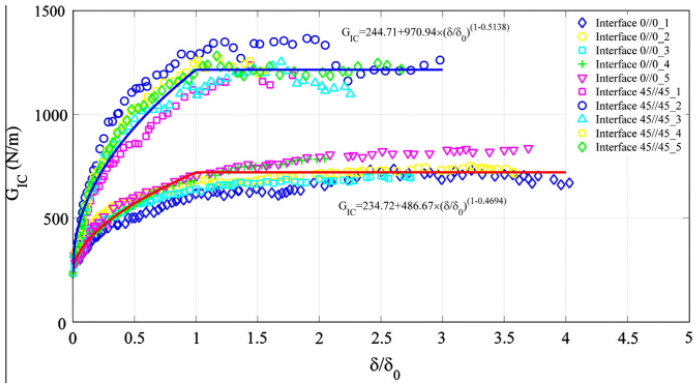

Figure 2.12: Bridging effect on mode I fatigue delamination behaviour on CFRP [36]

Its important to note that the when fibre-matrix interface is too strong, the fibres tend to break as the crack opens. This prevents the formation of fibre bridging, as the fibres are unable to span the crack and contribute to crack resistance. On the other hand, if the fibre-matrix interface is too weak, fibre bridging may still occur but it can result in excessive fibre pull out. This reduces the energy absorption during crack propagation and weakens the material's toughness. Therefore, it is important to maintain a balanced fibre-matrix interface strength. The interface should be strong enough to allow efficient load transfer between the fibre and the matrix and to prevent early fibre pull-out. At the same time, it should not be so strong that it causes fibre breakage, which would reduce or eliminate the benefits of fibre bridging.

2.5.4. Loading Rate

The influence of loading rate on the fracture toughness of fibre reinforced polymer (FRP) composites has been the subject of extensive investigation. Numerous experimental studies have explored how

varying the loading rate affects crack initiation and propagation, particularly under Mode I delamination conditions. Jacob et al. reviewed a wide range of studies addressing this topic and concluded that there is currently no clear consensus regarding the overall impact of loading rate on the fracture toughness of FRP materials [37].

Its importnat note that one of the key factors influencing rate sensitivity is the viscoelastic nature of the polymer matrix. As loading rate increases, polymer matrices may exhibit stiffer behaviour and reduced time for energy dissipation through plastic deformation, potentially resulting in different fracture responses. Additionally, variations in loading rate can trigger different failure mechanisms [37]. For instance, at higher rates, matrix-dominated failures may be more prevalent, whereas at lower rates, mechanisms such as fibre pull-out or interfacial debonding may become more dominant.

Due to these effects, fracture toughness may not remain constant across all testing conditions. To ensure consistency in test results and to minimize variability introduced by loading rate, standardised testing protocols have defined specific rate limits. For Mode I fracture toughness tests, both ASTM and ISO standards prescribe loading rates within the range of 1 to 5 mm/min [21]. These guidelines aim to reduce the influence of rate-dependent behaviours, enabling more reliable comparisons between materials and test campaigns.

2.6. Fracture Toughness of Flax Fibre Composites

A notable study by Saadati et al investigated Mode I fracture toughness of unidirectional (UD) flax/epoxy composites, reporting G_{Ic} values of 574 J/m^2 at crack initiation and 903 J/m^2 during crack propagation [38]. Their load–displacement curve exhibited a linear elastic region up to approximately 95% of peak load, followed by a gradual drop indicating stable crack growth and the corresponding R-curve plateaued after a delamination length of about 60 mm as shown in figure 2.13 .

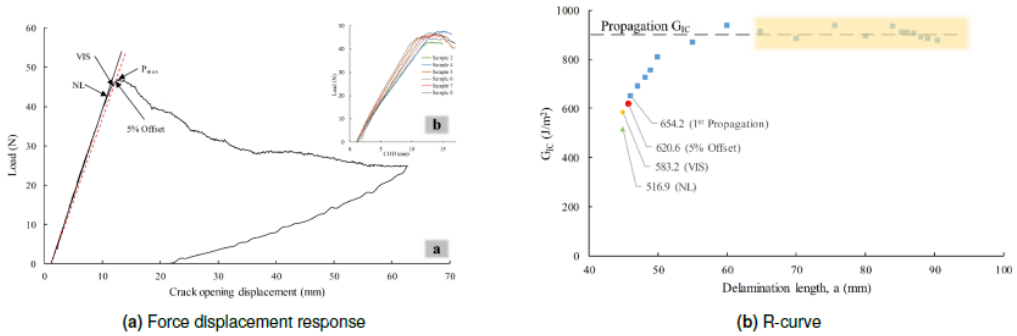

(a) Force displacement response (b) R-curve

Figure 2.13: Mode I Fracture toughness under Quasi static load regime for UD flax fibre reinforced epoxy composite [38]

Other notable research has produced comparable static fracture toughness values. Rajendran et al. evaluated UD and plain-weave flax/epoxy composites, recording initiation values in the range of 363 J/m^2 and steady-state values around 485 J/m^2. Other Researchers like Li. Ravadi, Yu has reported fracture toughness with flax as reinforcement fibres [39][40][41]. These studies collectively suggest that GIc for flax composites typically falls between 300 and 1400 J/m2, with variability influenced by fibre architecture, test methods, measurement techniques and matrix type.

The work done by the researchers mentioned above focusses only on the quasi static regime. The fatigue-driven delamination flax composites remains largely unexplored. Reviews by Mahboob and Bougherara confirm that fatigue degradation strongly affected by parameters such as stress ratio, frequency, and environmental conditions are critical for structural composites yet remains poorly understood in natural fibre systems [42].

A recent fatigue study by Barouni et al on flax/epoxy and flax-glass hybrid laminates under tension–tension cycling showed that hybrid configurations significantly improve fatigue life compared to pure flax systems [43]. They also demonstrated that fibre-matrix interface quality plays a key role in fatigue

performance. However, these works primarily address static or general tensile fatigue behaviour; Mode I fatigue delamination testing using DCB under cyclic loading is still missing for flax composite, a critical gap in understanding their long-term durability.

2.7. Hygrothermal effect on fracture toughness of composites

Although biofibres such as flax are increasingly regarded as promising, sustainable reinforcements in composite materials, there remains a significant research gap regarding the effects of hygrothermal ageing on their fracture toughness. Most existing literature focuses on synthetic fibres like carbon and glass, which serve as fundamental models for understanding how temperature and moisture influence fracture properties. In these systems, the resin typically bears the brunt of hygrothermal damage, while the fibres remain largely unaffected.

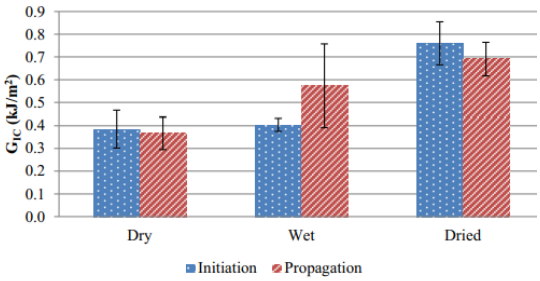

(a) Comparison of the dry, wet, and dried Mode-I initiation and propagation of BZ9120B laminates [44].

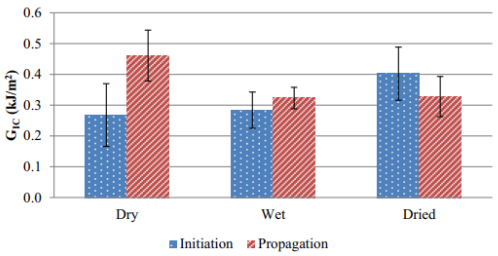

(b) Comparison of the dry, wet, and dried Mode-I initiation and propagation of BZ9130B laminates [44].

The Mode-I quasi static results for the BZ9120B laminates tested under dry, wet, and dried conditions are presented in Figure 2.14a [44]. The presence of moisture did not produce any noticeable change in the resistance to crack initiation; however, it resulted in a slight increase in resistance to crack propagation. This behaviour was attributed to matrix plasticisation and degradation of the fibre/matrix interface, which enhanced fibre bridging. Interestingly, drying the specimens after saturation did not reverse the influence of moisture on either the matrix or the fibre/matrix interface. Instead, the drying stage further amplified the effect, leading to nearly a twofold increase in both the initiation and propagation G_{IC} values.

In the case of BZ9130B laminates, the results shown in Figure 2.14b demonstrated a comparable trend with respect to crack initiation [44]. Moisture exposure did not alter the resistance to crack initiation; however, unlike BZ9120B, it caused a slight reduction in the resistance to crack propagation. Subsequent drying of the saturated laminates again did not restore the material behaviour to its original state. While a minor increase in initiation G_{IC} was observed, the propagation G_{IC} values remained essentially unchanged. This study clearly indicates the influence of the matrix on Mode-I fracture toughness under hygrothermal ageing. The ageing cycle can either improve or deteriorate the fracture toughness of the composites.

In a study on the effect of hygrothermal conditioning on the fracture toughness of carbon/epoxy composites cured in autoclave & Quickstep, the samples were dried at $105\,^{\circ}\mathrm{C}$ and then conditioned at $70\,^{\circ}\mathrm{C}$ and 85% RH [45]. The equilibrium moisture content of both panels was reported to be the same. In the fracture toughness tests, both autoclave- and QS-cured wet samples showed a reduction in the average values of G_{IC} compared to the dry state, as shown in Figure 2.15, but the statistical analysis indicated that the differences were insignificant.

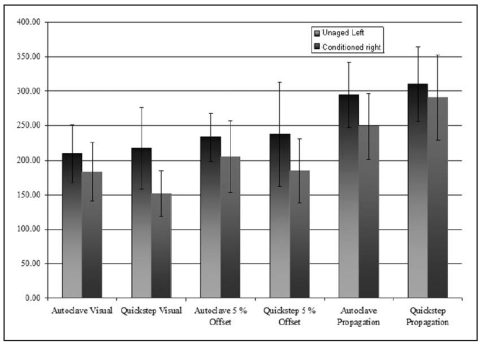

Figure 2.15: Comparison of the mean initiation (visual, 5% offset) and propagation G_{IC} values for Mode-I DCB testing of dry and wet autoclave and Quickstep-cured panels [45].

In a NASA Technical Memorandum on "Hygrothermal Influence on Delamination behaviour of Graphite/Epoxy Laminates" [46], the specimens were initially dried at $70\,^{\circ}\mathrm{C}$, then immersed in water and exposed to $70\,^{\circ}\mathrm{C}$ and 50% RH. Specimens with different moisture levels were tested at room temperature. It was shown that the interlaminar fracture toughness in Mode-I delamination increases slightly with increased moisture content and increased temperature, as shown in Figure 2.16. SEM images revealed distinct morphological features: matrix cleavage, river patterns, chevron markings, and branched crack structures. The study concluded that moisture does not appear to significantly influence the fracture-surface morphology under Mode-I loading conditions.

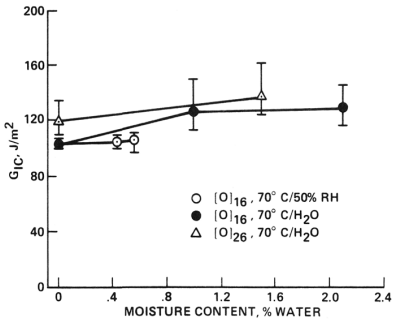

Figure 2.16: Effect of moisture content on fracture toughness in Mode-I delamination of a graphite/epoxy laminate [46].

A study on Mode-I delamination tests conducted at different R ratios for samples exposed to hygrothermal conditions [47] used $70\,^{\circ}\mathrm{C}$ and 85% RH and immersion in a $70\,^{\circ}\mathrm{C}$ water bath. Figure 2.17a shows the fatigue R-curves for Mode-I delamination at $R = 0.1$ and $R = 0.5$ at water bath. The graph shows that the shapes of the fatigue R-curves are R-ratio dependent. The magnitude of the R-curves for fatigue delamination with a higher stress ratio ($R = 0.5$) is larger than that for fatigue delamination with a lower stress ratio ($R = 0.1$), indicating more fibre-bridging generation in fatigue delamination at higher R.

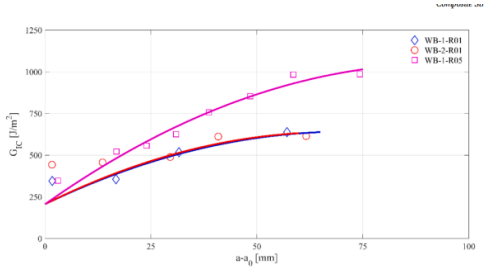

(a) Fatigue R-curves for composite laminates after water-bath ageing at different stress ratios [47].

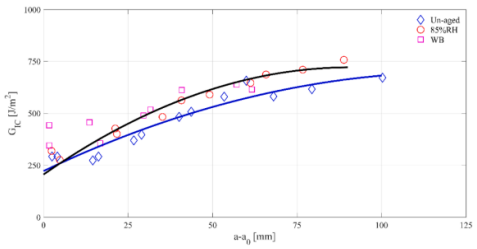

(b) Fatigue R-curves for composite laminates after different environmental ageing at the same stress ratio, $R = 0.1$ [47].

Figure 2.17: Comparison of fatigue R-curves for composite laminates under different ageing and stress ratio conditions.

It is clear that as the crack propagates, fatigue resistance gradually increases and tends to form a plateau, the level of which indicates the propagation fracture toughness and is defined by fibre bridging [47]. The resistance increases for each tested DCB specimen. Figure 2.17b provides a comparison of these fatigue R-curves for fatigue delamination in composite laminates after different environmental ageing at the same stress ratio ($R = 0.1$), demonstrating the environmental ageing effects on the development of fibre bridging. The difference in hygrothermal ageing (85% RH vs. water bath) does not have visible effects on the magnitude of the R-curves at the same R ratio. In the fatigue analysis, a two-parameter fatigue model is used to determine the effect of hygrothermal ageing. It is concluded that hygrothermal ageing has a significantly detrimental effect on fatigue crack growth, it becomes five times faster compared to that without ageing [47]. It is interesting to note that microscopy of specimens before and after ageing indicates a change in morphology; micro-voids are observed in samples subjected to hygrothermal ageing. Fracture-surface analysis shows fibre imprints in both aged and unaged specimens, indicating fibre–matrix interface debonding as the failure mechanism. It is concluded that the damage mechanisms in Mode-I fatigue delamination of composite laminates after different hygrothermal ageing remain the same.

Across these collective studies, it becomes evident that hygrothermal ageing can subtly to significantly affect fracture toughness in GFRP or CFRP composite materials. In the case of FFRP composites, the hydrophilic nature of the fibres and the ageing of the composite system impact both the fibre and the matrix, potentially altering fibre–matrix interactions and failure mechanisms differently than glass/carbon fibre composite materials. However, explicit data on hygrothermal effects on the fracture toughness of biofibre composites remain lacking, highlighting a critical gap and an opportunity for research into their long-term performance.

3

Research Scope

3.1. Problem Statement

Despite increasing interest in flax fibre-reinforced polymer (FFRP) composites as renewable materials with competitive mechanical properties and reduced environmental impact, their adoption in structural and semi-structural applications remains limited. This is primarily because their long-term mechanical reliability under varying environmental conditions is not yet fully understood. Since FFRPs are hydrophilic in nature, hygrothermal conditions can significantly alter the material's fracture and fatigue behaviour, thereby affecting their durability and safety in service environments.

While several studies have explored the mechanical properties and moisture absorption behaviour of natural fibre composites, there remains a lack of systematic investigation into how hygrothermal conditions influence the fracture toughness and fatigue crack growth resistance of flax fibre composites. Most available studies focus on strength or stiffness degradation, often neglecting fracture mechanics-based parameters that govern delamination and long-term damage evolution.

This knowledge gap hinders the accurate prediction of the long-term performance and reliability of FFRPs in structural applications, especially in outdoor or humid environments where fluctuations in temperature and moisture are inevitable. Therefore, a detailed experimental investigation is required to quantify how hygrothermal conditions affect the crack growth behaviour in FFRPs. Such understanding will contribute to the development of design guidelines and durability models for natural fibre composites under real-world service conditions.

3.2. Research Questions

Based on the outcome of the extensive literature review, the following overarching research question is formulated:

> *How does the hygrothermal environment influence the Mode I fracture toughness of flax epoxy composites under quasi-static and fatigue loading conditions?*

To address this main question, the following sub-research questions are proposed:

1. How does temperature variation affect the fracture toughness of flax epoxy composites under Mode I quasi-static and fatigue loading conditions?
2. How do dry and wet environmental conditions influence the fracture toughness of flax epoxy composites under Mode I quasi-static and fatigue loading conditions?
3. What is the effect of hygrothermal exposure on the surface morphology and damage mechanisms in flax epoxy composites subjected to Mode I quasi-static and fatigue loading conditions?

4

Materials & Manufacturing

As a first step towards achieving the research objectives, this chapter focuses on the materials and manufacturing procedures used in this study. It details the specimen design, composite plate fabrication, sample preparation, and quality control measures.

The preparation of test specimens is critical to ensuring consistency and reliability in fracture toughness testing. As flax fibres and their composites are inherently hydrophilic, particular attention was given during specimen preparation to minimize moisture absorption and maintain the integrity throughout the process.

4.1. Specimen Design

This section discusses the specimen configuration used in this research. The ASTM D5528 standard was selected to determine the Mode I interlaminar fracture toughness of the composite laminates [20]. According to the standard, the basic geometry for the test specimen follows the Double Cantilever Beam (DCB) configuration as shown in the figure 4.1-(a). The standard specifies that specimens shall be at least 125 mm in length and nominally between 20 mm and 25 mm in width. In this study, a specimen dimension of 200 mm $\times$ 25 mm was chosen to ensure sufficient crack propagation for evaluating both the fracture initiation and propagation toughness values. The standard also recommends a specimen thickness between 3 mm and 5 mm.

During preliminary experiments and also from Luca Baak results, it was noted that FFRPs tend to undergo permanent deformation during opening prior to crack initiation, which can invalidate the assumptions of Linear Elastic Fracture Mechanics (LEFM) [48]. To mitigate this effect and improve the bending stiffness of the specimen, the DCB samples were modified by bonding aluminium plates on both outer surfaces. This modification enhances the overall rigidity of the specimen and ensures that crack propagation occurs in a controlled and stable manner. The DCB design is shown in the figure 4.1-b

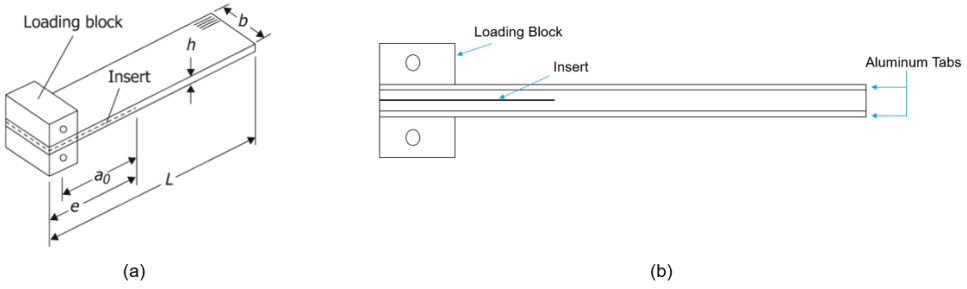

Figure 4.1: (a) DCB design according to ASTM 5528 [20] (b) Side view of the modified DCB design

Perruchoud *et al.* reported that flax fibre laminates with a lay-up configuration of $[+45/-45]_{2S}$ exhibit a thickness of approximately 3.8 $\pm$ 0.7 mm [18]. Based on this reference, a stacking sequence of $[0_4//0_4]$ was selected for this study, incorporating a mid-plane delamination of 60 mm. With the addition of 1 mm aluminium plates on both sides, the total thickness of the modified DCB specimen was expected to be approximately 5.8 mm. In this notation, "//" denotes the delamination plane located at the mid-thickness of the laminate. The nominal dimensions of the DCB specimens are shown in Table 4.1.

Table 4.1: Nominal specimen dimensions.

Dimension	Value (mm)
Length (L)	200
Width (b)	25
Insert length (e)	60
Thickness (h)	5.8

4.2. Composite Manufacturing

The specimen preparation process began with the fabrication of large composite plates, from which the DCB specimens were later cut. The fibre material used in this study is Amplitex 280, a unidirectional non-crimp flax fabric supplied by Bcomp Ltd. (Switzerland). The polymer matrix consists of SWANCOR 2511-1AL/BL epoxy resin, a thermosetting system manufactured by Swancor Advanced Materials Co. (Shanghai, China).

The Amplitex 280 flax fabric is composed of twisted flax yarns reinforced with fine polyester threads that hold the yarns parallel and maintain fabric stability. These fabrics are specifically engineered for infusion-based composite manufacturing and are known for their uniform fibre alignment, non crimps, and compatibility with epoxy systems. The SWANCOR 2511-1AL/BL epoxy system, composed of a resin (AL) and a hardener (BL), was selected due to its low viscosity, extended pot life, high heat deflection temperature (HDT), and superior wetting characteristics, all of which make it highly suitable for vacuum-assisted resin infusion processes.

The composite laminates were manufactured as square plates with dimensions of 500 mm × 500 mm using a modified vacuum infusion technique. In this modified process, the conventional peel ply and flow mesh were replaced with aluminium plates, which act as both mould surfaces and flow guides. The manufacturing process began by selecting two large aluminium plates that could accommodate the 500 mm × 500 mm fibre plies. The plates were first thoroughly cleaned using isopropanol and acetone to remove any surface contaminants such as oils or dust particles. Following cleaning, the plates were coated with three layers of Marbocote 227 release agent, with an interval of approximately 15 minutes between each coating. This release coating ensured that the composite did not adhere to the aluminium surface during curing and facilitated easy demoulding of the panels.

The flax fibre plies were then cut from the roll into 500 mm × 500 mm sheets. Adhesive tapes were carefully applied along the edges of each ply to prevent fraying and to maintain alignment during lay-up and infusion. To manufacture panels with the stacking sequence [0_4 // 0_4], four plies of flax fibre were first placed on the prepared aluminium plate with their fibre direction aligned along the intended infusion flow path. A 30 µm thick fluorinated ethylene propylene (FEP) release film was then positioned at the mid-plane to act as the delamination starter for the DCB specimens. Although the ASTM D5528 standard recommends a release film thickness of less than 13 µm, a slightly thicker film was used for the experiment. The remaining four flax plies were then stacked above the release film, replicating the bottom ply orientation.

To control the panel thickness and prevent resin leakage, three layers of tacky tape were applied along the panel edges, serving both as a sealant and as a mechanical spacer during infusion. The top aluminium plate was then positioned over the lay-up, and a vacuum bag was placed over the entire assembly to create an airtight seal. A vacuum pump and resin inlet system were connected at opposite sides of the assembly, allowing for efficient and uniform resin flow between the aluminium plates in the fibre direction during the infusion process. The schematic representation of the setup is shown in the figure 4.2

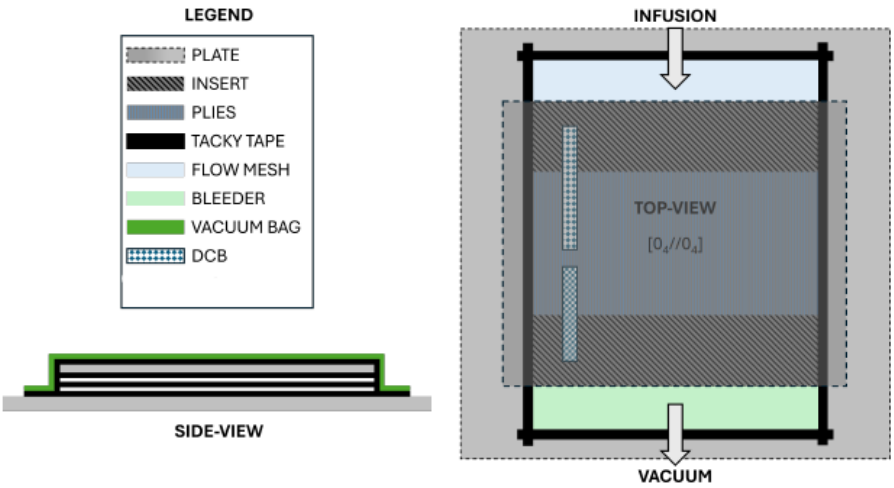

Figure 4.2: Schematic representation of the modified vacuum infusion setup showing the top and side views of the laminate lay-up.

The modified vacuum infusion setup ensured the fabrication of high-quality composite plates with smooth, uniform surface finish and consistent thickness across the entire laminate. The use of aluminium surfaces minimized surface roughness variations and improved fibre impregnation uniformity. This smooth surface finish is particularly critical for subsequent hygrothermal conditioning experiments, as it allows the specimens to absorb moisture uniformly across all exposed surfaces, thereby ensuring the reliability and consistency of the fracture toughness subjected to hygrothermal conditons.

The resin system was first prepared according to the manufacturer's specifications and placed in the resin container prior to infusion. A thorough vacuum integrity check was conducted before initiating the infusion process to ensure the absence of leaks and to maintain uniform resin flow throughout the laminate. Once the vacuum conditions were verified, the plates were infused and subsequently cured at room temperature for 24 hours.

Curing at room temperature, however, does not always result in complete polymerisation of the epoxy matrix. Under such conditions, typically only about 90% of the reactive functional groups form cross-links. Therefore, the infused composite plates were subjected to a post-curing process to achieve complete polymerisation, ensuring that all reactive sites were converted and that the glass transition temperature (T_g) was stabilised. This step is crucial because an incomplete cure can cause variability in thermal and mechanical behaviour, particularly under hygrothermal conditions, where exposure to moisture and temperature can further alter the T_g.

For post-curing, the composite plates were placed inside an autoclave for a controlled thermal cycle lasting 18 hours. The temperature was gradually increased to 70,°C at a rate of 5,°C/min, after which it was held constant for 18 hours under a pressure of 7,bar. This post-curing cycle promotes complete cross-linking within the epoxy matrix, stabilising both the thermal and mechanical properties of the composite material. The entire manufacturing process, including vacuum infusion and post-curing, was conducted at the TU Delft Composites Laboratory within the Faculty of Aerospace Engineering. The manufacturing setup and manufactured plate is shown in figure 4.3

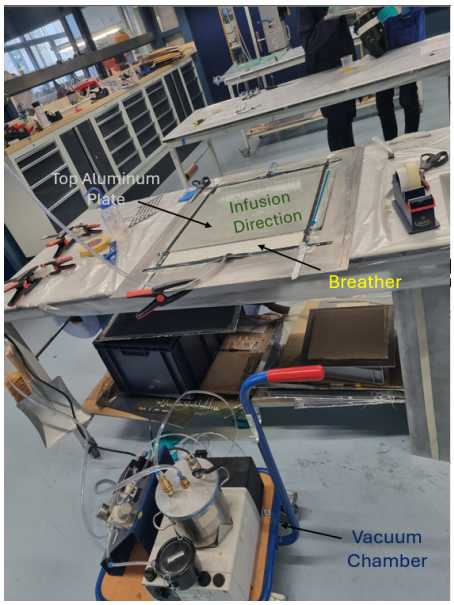

(a) Manufacturing setup of the vacuum infusion process.

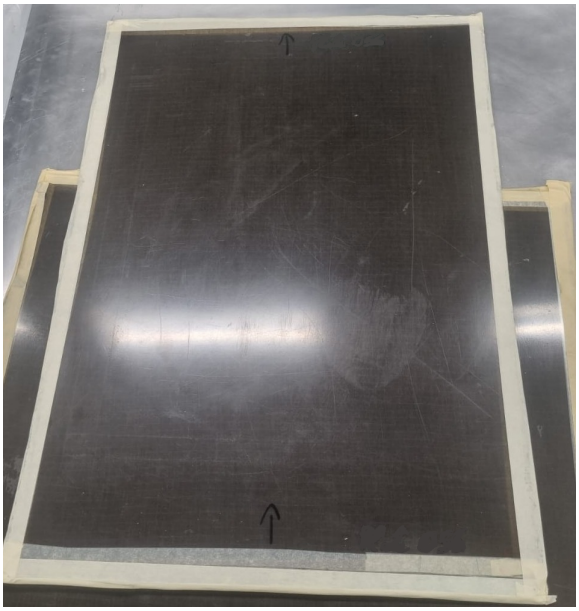

(b) Manufactured plate after post-curing process.

Figure 4.3: Manufacturing process

A total of 34 DCB specimens were prepared from the cured composite plates. To ensure dimensional accuracy and minimise fibre damage during sectioning, the specimens were cut using a high-precision waterjet cutting process. This method was selected to avoid the shear stresses and heat generation typically associated with mechanical cutting tools such as diamond saws. The cutting was performed at Van Nobelen Delft, a company specialised in precision fabrication of composite and metallic materials. The cutting operation was executed with a tolerance of ±0.1 mm, producing specimens with dimensions of 200 mm × 25 mm as defined in the design.

To prevent delamination initiation caused by the initial impact of the high-pressure waterjet, the cutting path was programmed to begin at least 5 mm outside the specimen boundary. This approach allowed the waterjet stream to stabilise before engaging the actual specimen geometry, resulting in smooth edges and corners while minimising surface and subsurface damage.

Although every step of the manufacturing process was performed with high precision and care, minor variations and imperfections can still occur due to uncontrolled or process-related factors. Consequently, a comprehensive quality control procedure was implemented during and after manufacturing to verify specimen integrity and conformity to design requirements. These procedures included dimensional measurements, Differential Scanning Calorimetry (DSC) testing, and microscopic examinations.

Dimensional measurements were carried out to confirm that the samples remained within the specified tolerance limits and to detect any local thickness variations introduced during fabrication. The DSC tests were performed to determine the glass transition temperature (T_g) of the cured composites, verifying the effectiveness of the post-curing process and ensuring that the specimens were fully cured before hygrothermal exposure experiments.

Despite best manufacturing practices, no composite fabrication process can be considered entirely free of imperfections. In vacuum infusion processes, a common defect is the formation of voids, which can adversely affect mechanical performance. To identify such potential defects, microscopy analyses were conducted on cross-sectional samples to assess fibre-volume fraction, void content, fibre alignment, and the presence of delaminations or other microstructural irregularities. These evaluations ensured that the manufactured specimens met the required quality standards for subsequent testing and analysis.

4.3. Quality Assessment

This section presents the implementation of quality assessment procedures carried out to verify the integrity and consistency of the manufactured specimens. The evaluation includes dimensional measurements, Differential Scanning Calorimetry (DSC) testing, and microscopic examinations performed to ensure conformity with the design specifications and to identify any potential manufacturing defects.

4.3.1. Dimensional Check

Dimensional verification was performed after the waterjet cutting process to ensure that all specimens conformed to the design specifications. The measurements were conducted using a vernier caliper with a precision of 0.01 mm. The average dimensions obtained from specimens cut from different composite plates are presented in Table 4.2.

Table 4.2: Average specimen dimensions (width and thickness) of samples obtained from the manufactured plates.

	Plate 1	Plate 2
Thickness	25.01 ± 0.07 mm	25.06 ± 0.02 mm
Width	3.62 ± 0.13 mm	3.72 ± 0.08 mm

The length of each specimen was measured using a standard ruler scale. Since the DCB specimens were intentionally designed with sufficient length to allow stable crack propagation, minor deviations in length were considered acceptable and did not affect the integrity of subsequent tests. The width measurements confirmed that the specimens were within the specified design tolerance range, demonstrating consistency in the cutting process.

The thickness of the specimens was designed to be approximately 3.8 mm. Although slight variations were observed compared to the nominal design thickness, the comparison between samples taken from different plates showed only minimal deviations. Such small variations are expected in vacuum infusion processes, particularly since the three layers of tacky tape used along the plate edges were applied manually, which can introduce minor inconsistencies in panel thickness. Overall, the dimensional checks confirmed that all specimens were within acceptable tolerances for fracture testing.

4.3.2. Differential Scanning Calorimetry (DSC)

Differential Scanning Calorimetry (DSC) testing was performed using the mDSC 250 instrument to evaluate the thermal behaviour of the specimens and verify the completion of the curing process. DSC is a thermal analysis technique that measures the difference in heat flow between a sample and an inert reference material as the temperature is varied in a controlled manner. This method enables the identification of thermal transitions such as the glass transition temperature (T_g), curing reactions, and other heat-related events associated with the polymer matrix.

During testing, the specimens absorb or release heat depending on whether physical or chemical transitions occur. These changes appear as distinct features or peaks on the *heat-flow versus temperature* curve. A well-cured epoxy typically shows a stable and reproducible T_g without any residual exothermic peaks, which would otherwise indicate incomplete crosslinking or post-curing reactions.

Since flax fibre composites are inherently hygroscopic, residual moisture within the specimens can influence the measured heat flow. To mitigate the effect of moisture variation during heating and cooling, each sample was sealed in a hermetic aluminium pan prior to testing. This approach ensured that the thermal response reflected the material's intrinsic behaviour rather than moisture-related fluctuations.

Each specimen was subjected to three continuous heating and cooling cycles under controlled conditions to ensure measurement consistency and repeatability. The temperature program was as follows:

- Equilibration at $0\,^\circ\mathrm{C}$ for $5\,\mathrm{min}$
- Heating at a rate of $10\,^\circ\mathrm{C\,min^{-1}}$ to $150\,^\circ\mathrm{C}$
- Isothermal hold for $5\,\mathrm{min}$ at $150\,^\circ\mathrm{C}$
- Cooling at a rate of $10\,^\circ\mathrm{C\,min^{-1}}$ back to $0\,^\circ\mathrm{C}$

The results of the DSC measurements are presented in figure 4.4 The heat-flow curves obtained from the three consecutive cycles exhibited consistent glass transition temperatures (T_g), with no observable residual curing peaks. This stability confirms that the composite plates underwent complete polymerisation during the autoclave post-curing stage, ensuring thermal stability and uniform crosslinking throughout the material.

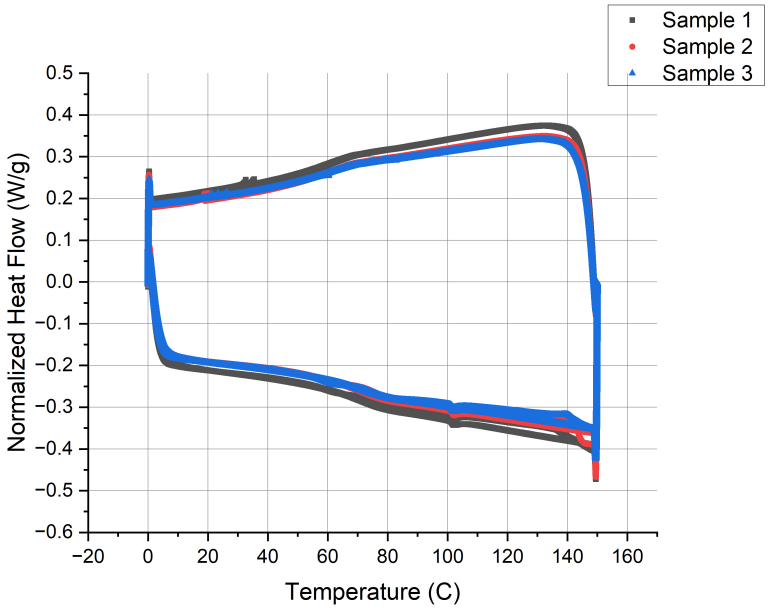

Figure 4.4: Normalized heat flow vs Temperature curves from the DSC tests

4.3.3. Microscopy Analysis

Microscopic analysis was carried out to evaluate the internal structure of the composites and to identify any possible manufacturing defects such as voids, fibre misalignment. The cross sections of the specimens were examined using the Keyence VHX 7000X digital microscope, which provides high resolution imaging and excellent depth of field, making it suitable for detailed inspection of composite materials.

Before microscopic observation, the specimens were prepared through a sequence of surface preparation procedures to ensure a smooth and damage free cross section. Each sample was first embedded with clarocit resin using a cold mounting procedure. This resin was selected because it cures at room temperature and is particularly suitable for bio based composite materials such as FFRP, which are sensitive to thermal degradation at high temperatures. The embedding process provides mechanical support to the specimen, enabling smooth and controlled polishing of the cross-section.

After curing, the mounted specimens were subjected to progressive grinding using Struers silicon carbide abrasive papers of grit sizes 320, 500, 1200, and 4000 to gradually remove surface irregularities and achieve a uniform surface roughness cross section. Following the grinding process, the specimens were polished using the Struers Tegramin 20 polishing system, first with a polishing suspension containing 3 µm diamond particles, and then with a 1 µm suspension to obtain a mirror like finish suitable for microscopic imaging.

The polished samples were then examined under the Keyence VHX 7000X microscope at various magnifications. The resulting micrographs are presented in Figure 4.5. In these images, dark regions correspond to voids or areas with incomplete resin impregnation, while the lighter areas represent the fibre and matrix regions. A comparison of the images revealed that the composite specimens were largely free from visible defects, showing only a few small voids which are typical for vacuum infusion processes. Overall, the microscopy results confirm that the specimens possess good fibre and matrix distribution, minimal void content, and strong interfacial bonding, demonstrating the reliability of the selected manufacturing process.

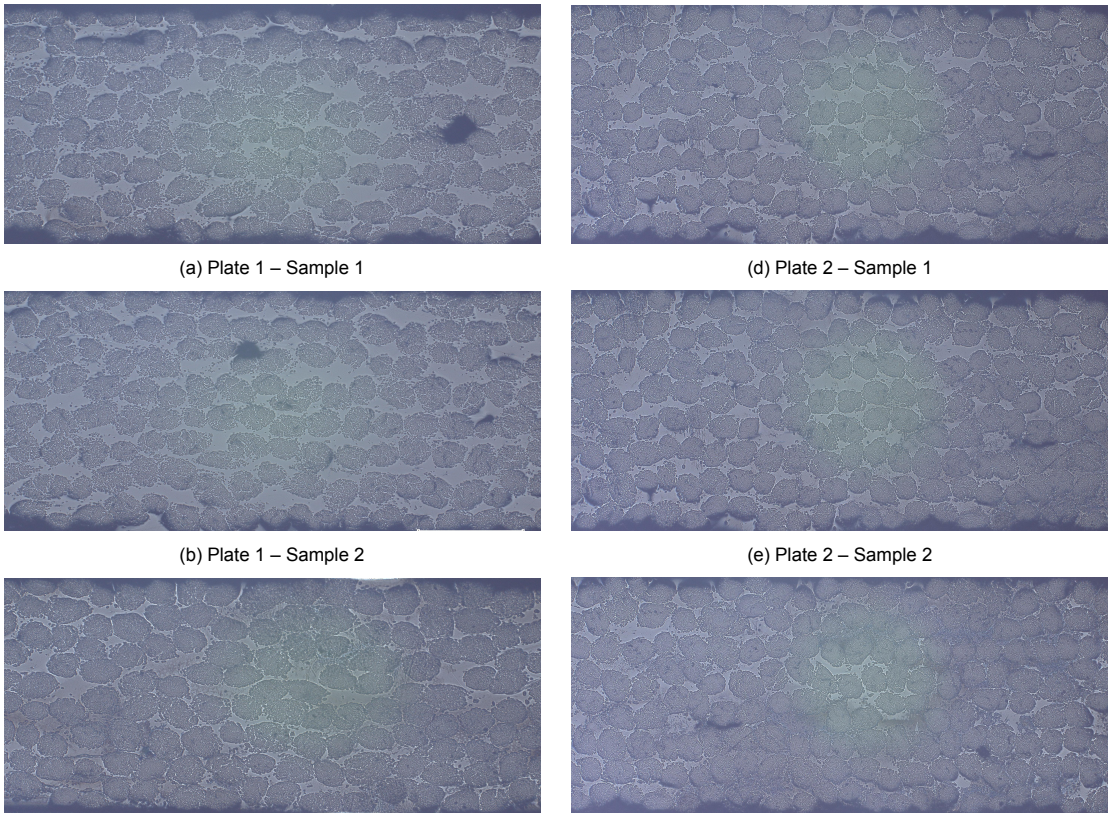

(a) Plate 1 – Sample 1 (d) Plate 2 – Sample 1

(b) Plate 1 – Sample 2 (e) Plate 2 – Sample 2

(c) Plate 1 – Sample 3 (f) Plate 2 – Sample 3

Figure 4.5: Cross-sectional images of samples at 40x magnification from Plate 1 (a–c) and Plate 2 (d–f), showing fibres perpendicular to the polished plane for quality check.

4.4. Fibre Volume Fraction

Microscopic observations indicate that voids within the composite cross-sections are minimal; therefore, their influence on the calculated fibre volume fraction is considered negligible. The fibre volume fraction for each plate was determined from the measured mass and geometric volume of the specimens, together with the known densities of the constituent materials. According to material data sheets, the Swancor 2511 A/B epoxy resin has a density of approximately $1.15\,\mathrm{g\,cm^{-3}}$, and the AmpliTex flax fabric has an areal density of $250\,\mathrm{g\,m^{-2}}$.

Using these values, in combination with the average mass and dimensions of the prepared specimens, the fibre volume fraction (V_f) was estimated to be $44.3\,\%$ and $46.7\,\%$ for the samples obtained from the two manufactured composite plates. These results fall within the expected range for vacuum infused natural fibre composites and indicate a relatively uniform fibre distribution throughout the laminates.

In summary, the specimens were successfully fabricated with nominal dimensions of $200\,\mathrm{mm} \times 25\,\mathrm{mm} \times 34\,\mathrm{mm}$, using the modified vacuum infusion process described earlier. The resulting composites exhibited an average glass transition temperature (T_g) of approximately $75\,^\circ\mathrm{C}$, fibre volume fractions of $44.3\,\%$ and $46.7\,\%$, and negligible structural defects. Although slight variations in thickness and fibre content were observed between the two plates, such deviations are typical of the vacuum infusion process. Nevertheless, these variations were minor and did not compromise the integrity or suitability of the specimens for subsequent mechanical and hygrothermal testing.

4.5. Sample Preperation

The sample preparation process was conducted in three stages according to the requirements of the experiments performed.

4.5.1. Stage 1 : Preperation for the quality checks

In Stage 1, the specimens were prepared for microscopy analysis, which served as part of the post-manufacturing quality assessment and also for the hygrothermal conditioning experiments discussed in Section 5.1. The procedures for microscopy preparation are described in detail in Section 4.3.3 under the quality control section, and the same preparation steps were followed for the samples used in hygrothermal testing.

4.5.2. Stage 2 : Preperation for fracture toughness tests

In Stage 2, the specimens were prepared for the Mode I fracture toughness (DCB) tests presented in Section 5.2. Aluminium sheets with a thickness of 1 mm were used to fabricate the aluminium plates that were bonded to the specimens. These sheets, initially measuring 500 mm $\times$ 500 mm, were laser-cut into individual plates of 200 mm $\times$ 25 mm at the TU Delft Faculty Workshop (Mechanical Engineering Department). Laser cutting was selected for its high dimensional accuracy and its ability to produce smooth edges, thereby ensuring proper alignment of the plates with the composite specimens.

Prior to bonding, the aluminium plates were cleaned with isopropanol to remove surface contaminants and subsequently sandblasted to generate a rough surface texture, promoting better mechanical interlocking between the plate and the adhesive layer. For the same purpose, the hygrothermally conditioned specimens were removed from the chamber and gently abraded with 320 grit sandpaper to enhance surface roughness. To prevent adhesive flow into the delamination plane during bonding, scotch tape was carefully applied along the specimen edges. The tape also helped maintain smooth edges, which are necessary for precise optical measurement markings prior to testing and their subsequent analysis.

Finally, the plates were bonded to the specimens using Loctite EA 3430 epoxy adhesive. A uniform layer of adhesive was applied on each tab surface, and the plates were aligned with the specimen surfaces under constant pressure using three mechanical clamps to ensure a consistent bond thickness and alignment as shown in the figure 4.6. During curing, the specimens was placed inside the hygrothermal chamber to prevent moisture absorption or desorption.

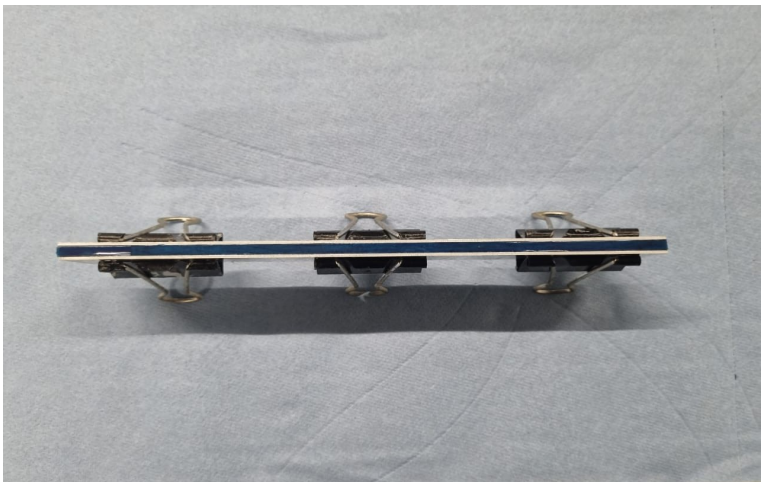

Figure 4.6: Specimens bonded with aluminum plates.

Its important to note that since sample preparation was performed immediately after conditioning at respective hydrothermal conditions, care was taken to minimize any alteration in the moisture content of the specimens. To achieve this, each specimen was removed individually from the climatic chamber, prepared within a time frame of approximately $30\,\mathrm{min}$, and then returned to the chamber for an additional $24\,\mathrm{h}$. This procedure allowed sufficient time for the adhesive bonding to cure while ensuring that the specimens reached moisture equilibrium before testing.

The subsequent step involved the fabrication and attachment of loading blocks to the specimens required for the fracture toughness testing. The loading blocks were machined from aluminium blocks of

dimensions $15\,\mathrm{mm} \times 15\,\mathrm{mm} \times 25\,\mathrm{mm}$, with a $5\,\mathrm{mm}$ through-hole drilled along the midline of the $15\,\mathrm{mm}$ face. This hole served as the gripping point for the test fixture during mechanical testing. All machining operations were performed at the TU Delft Faculty Workshop at Mechanical Engineering Department.

After the aluminium blocks were prepared, the conditioned specimens were again removed from the climatic chamber for bonding. The loading blocks were cleaned using acetone, followed by sandblasting to roughen the bonding surface, and cleaned once more to remove residual particles. These surface preparation steps were performed for the same reasons outlined earlier for the aluminium plates attachment to improve surface adhesion and mechanical interlocking. Alignment during bonding was achieved using 3D printed fixtures to ensure precise positioning. The Loctite EA 3430 epoxy adhesive was then applied to the bonding surfaces, after which the loading blocks were positioned and clamped to maintain uniform pressure as shown in the figure 4.7. The bonded assemblies were then returned to the climatic chamber for $24\,\mathrm{h}$, allowing both adhesive curing and moisture re-equilibration. As in earlier steps, all bonding operations were completed within $30\,\mathrm{min}$ of specimen removal from the chamber.

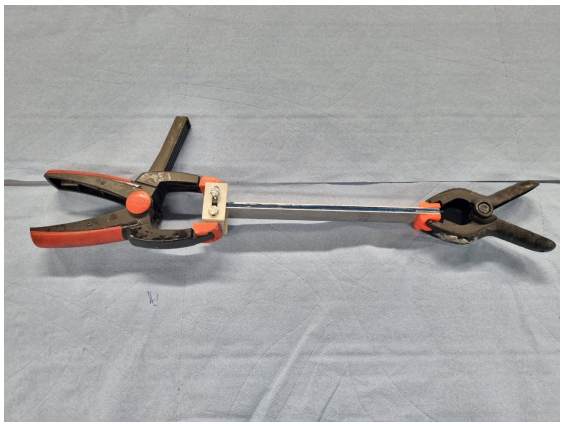

Figure 4.7: Bonding procedure for the loading blocks.

After the 24-hour conditioning period, the fixtures were removed, and one side of each specimen along the longer edge was spray painted with a white paint. Fine vertical reference lines were then marked at $1\,\mathrm{mm}$ intervals along the edge of each specimen, starting from the end of the insert to the outer edge, as prescribed by ASTM D5528. These markings were used to facilitate visual monitoring of delamination growth during the fracture toughness tests. Figure 4.8 shows the fully prepared specimen ready to be mounted on the tensile testing bench.

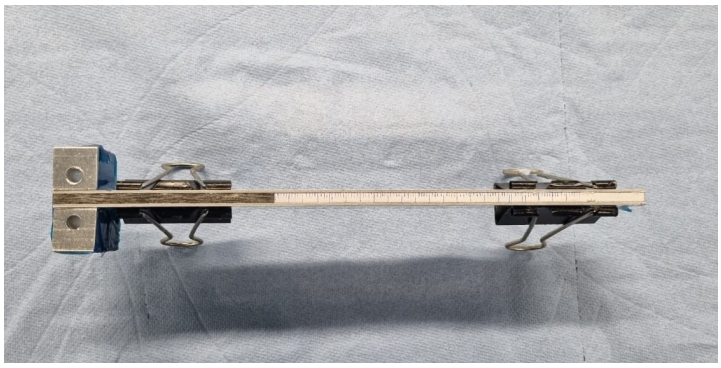

Figure 4.8: Manufactured Specimen

4.5.3. Stage 3: Preparation of Post-Fracture Specimens

The final stage of specimen preparation involved post-fracture handling of specimens after the primary experimemts for surface roughness and Scanning Electron Microscopy (SEM) analysis. After fracture testing, the specimens were loaded in the Zwick Z010 universal testing machine and pulled until complete delamination occurred along the mid-plane, separating the two halves of the specimen. Sections of approximately $10\,\mathrm{mm} \times 10\,\mathrm{mm}$ were then carefully cut from the fracture surface using a hand saw to produce samples suitable for microscopy. These samples were cleaned gently with dust free air spray to remove any debris or surface contaminants resulting from the cutting process.

5

Methodology

To achieve the research objectives, four different experimental procedures were systematically conducted. These include Hygrothermal Aging, Fracture Toughness Tests, Microscopy Analysis, and Fractography Studies. The experiments were carried out across three faculties at TU Delft — the Faculty of Aerospace Engineering, the Faculty of Civil Engineering and Geosciences, and the Faculty of Mechanical Engineering. .

In order to investigate the effect of environmental exposure, four distinct hygrothermal conditioning environments were selected to examine how temperature and relative humidity influence the interlaminar fracture toughness of flax fibre-reinforced composites. The primary aim of this study was to understand how the interlaminar fracture toughness of the material varies under environmental conditions representative of real-world service scenarios. Therefore, the conditioning parameters were chosen to reflect typical and extreme climatic conditions, namely: hot-wet, hot-dry, room temperature, and severe cold environments.

Although actual outdoor exposure often includes ultraviolet (UV) radiation, this study intentionally excluded the UV component to isolate the specific effects of temperature and humidity on the mechanical response of the material. The selected hygrothermal conditions used in this research are summarized in Table 5.1.

In Table 5.1, the term “hot” refers to temperatures significantly above room temperature, while “cold” corresponds to sub-zero conditions. Similarly, “wet” indicates relative humidity levels substantially above $50\,\%$, whereas “dry” represents conditions with comparatively low humidity.

The influence of humidity was assessed by comparing the results obtained from specimens conditioned under Hot-Wet and Hot-Dry environments, where the temperature was maintained at $50\,^{\circ}\mathrm{C}$ and the relative humidity was varied between 30% RH and 90% RH. Similarly, the influence of temperature was evaluated by comparing the results of the Hot-Wet and Severe Cold conditions. Finally, the results from all environmental conditions were compared against the Room Temperature baseline to develop a comprehensive understanding of how combined temperature and humidity exposure affect the interlaminar fracture toughness of flax fibre composites.

Table 5.1: Hygrothermal test conditions for the fracture toughness tests

Condition	Temperature ($^{\circ}\mathrm{C}$)	Relative Humidity ($\%$)	Quasi-static Tests	Fatigue Tests
Hot-Wet	50	90	3	3
Hot-Dry	50	30	3	3
Room Condition	20	50	3	3
Cold	-20	N/A	3	3

5.1. Hygrothermal Aging Experiments

Throughout their service life, structural components such as bridges, wind turbine blades, and other outdoor load-bearing systems are exposed to a wide range of harsh and fluctuating environmental conditions. These variations in temperature and humidity can significantly influence the mechanical response and long-term durability of the materials used in such applications. Therefore, understanding the combined effects of temperature and moisture on key mechanical properties, such as fracture toughness, is essential for reliable design and life prediction. This is particularly important for bio-based materials, whose mechanical and physical characteristics can change rapidly when subjected to hygrothermal environments.Therefore, the samples are conditioned through an artificial climatic environment before the mechanical tests.

Although relative humidity can be controlled under ambient conditions, its effect on the material properties is difficult to evaluate at room temperature because the rate of moisture diffusion through the polymer matrix and fibre network is relatively slow. Under such conditions, the equilibrium moisture content is reached only after a long duration, often leading to negligible absorption or desorption within practical testing times. To accurately study the influence of humidity, the conditioning must be performed at elevated temperatures, where the rate of diffusion increases significantly, promoting measurable changes in the moisture uptake or release of the material. For this reason, Hot-Wet and Hot-Dry environments were selected to represent the high-temperature scenarios in this study, allowing the influence of relative humidity to be systematically examined.

Even though the diffusion rate is enhanced at higher temperatures, it typically requires several days or even weeks for the material to reach moisture equilibrium. Therefore, the experimental campaign conducted in this work is referred to as hygrothermal aging experiments, emphasizing that the conditioning period is intended to simulate long-term environmental exposure effects.

To investigate the effect of temperature variation, experiments were also performed under cold conditions. However, it is technically challenging to regulate relative humidity at sub-zero temperatures, as the available laboratory equipment was not designed to maintain stable humidity levels in such environments. Consequently, the influence of temperature was examined by comparing specimens conditioned under Hot-Wet and Severe Cold environments, while ensuring that the specimens contained comparable moisture contents prior to testing. To achieve this, a sequential hygrothermal conditioning procedure was developed to control and stabilize the equilibrium moisture content of each specimen before mechanical testing.

To evaluate the influence of hygrothermal conditions on the Mode I interlaminar fracture toughness of flax fibre-reinforced epoxy composites, the specimens were conditioned using two Weiss climatic chambers: the Weiss LF7M45 and Weiss C34070a models. These chambers allow precise control over both temperature and humidity, with an operational temperature range of $-40\,^{\circ}\mathrm{C}$ to $90\,^{\circ}\mathrm{C}$ and a humidity range up to $100\,\%$.

Initially, all specimens were stored under laboratory room conditions, which served as the reference environment for the experimental campaign. During this stage, the mass of each specimen was monitored over a two-week period, and no significant changes in weight were observed. This confirmed that the specimens were already in a moisture equilibrium state prior to exposure to the controlled hygrothermal environments.

Following the initial reference conditioning, the specimens were divided into three experimental batches:

- **Batch 1:** Reserved for fracture toughness testing at the room condions, which is discussed in detail in Section 5.2.
- **Batch 2:** Exposed to a Hot-Dry environment at a temperature of $50\,^{\circ}\mathrm{C}$ and $30\,\%$ relative humidity (RH). These samples were maintained in the climatic chamber for approximately *25 days* until equilibrium moisture content was achieved.
- **Batch 3:** Subjected to Hot-Wet conditions of $50\,^{\circ}\mathrm{C}$ and $90\,\%\mathrm{RH}$, following a similar procedure as Batch 2. Once the equilibrium state was reached, this batch was further divided into two subgroups. The first subgroup was transferred to a Severe Cold environment at $-20\,^{\circ}\mathrm{C}$ to establish moisture equilibrium under freezing conditions, while the second subgroup remained under the

Hot-Wet equilibrium state.

After equilibrium was reached under each environmental condition, the specimens were subjected to fracture toughness testing, as described in Section 5.2. Figure 5.1 provides an overview of the experimental procedure and the sequence of hygrothermal conditioning stages used in this study.

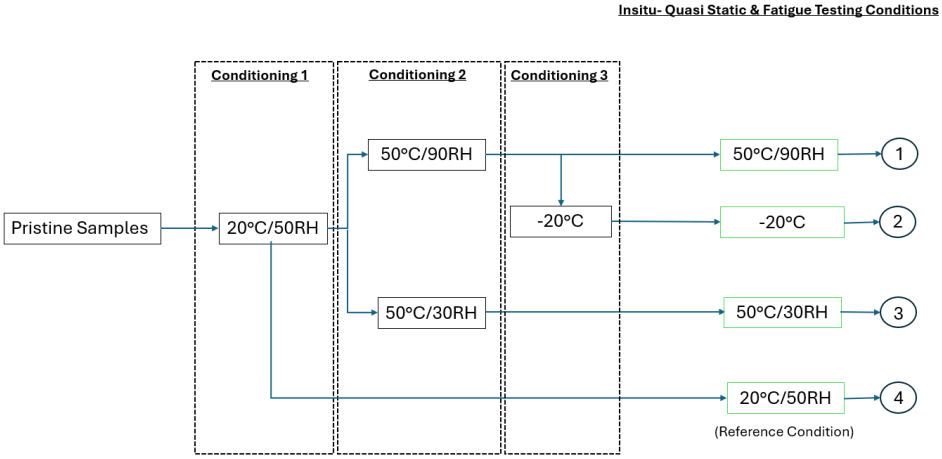

Figure 5.1: Figure illustrates step-by-step hygrothermal conditioning protocol used to establish four equilibrium conditions

To monitor moisture absorption and desorption behaviour during the conditioning process, gravimetric analysis was performed. The mass of each specimen was recorded at intervals of one to two days. When environmental conditions were adjusted and larger variations in mass were expected, the frequency of measurement was increased.. As the specimens approached equilibrium, the measurement intervals were gradually extended. The *moisture evolution* (M) was calculated using the following relation:

$$M = \frac{W_i - W_0}{W_0} \times 100 \tag{5.1}$$

where W_i is the mass of the specimen at a given time interval, and W_0 represents the initial mass before conditioning.

Equilibrium was determined by analyzing the moisture uptake curves, in which the moisture evolution (M) was plotted as a function of time. When consecutive mass measurements showed negligible variation, the specimen was considered to have reached equilibrium. The results of all codntioning exprients are presented and discussed in results an discussion section.

5.2. Fracture toughness Tests

Currently, there are no specific testing standards established for determining the Mode I interlaminar fracture toughness of flax fibre reinforced polymer composites. Therefore, the present work follows the ASTM D5528 standard, which provides the procedure for evaluating Mode I interlaminar fracture toughness of unidirectional glass or carbon fibre composites containing either brittle or tough single-phase polymer matrices [20]. The Double Cantilever Beam (DCB) specimens with attached aluminium loading blocks were prepared in accordance with this standard, as described in Section 4.1.

All fracture toughness experiments were conducted under in-service environmental conditions using a climatic chamber that precisely controlled both temperature and humidity. The interlaminar fracture toughness was investigated under two types of loading conditions: quasi-static loading and fatigue loading. The methodology adopted for experiment is given below

5.2.1. Quasi-static

The quasi-static Mode I interlaminar fracture toughness tests were performed using an Instron 100 kN universal testing machine, which was modified by externally attaching a Weiss environmental chamber to simulate in-service conditions. To ensure accurate measurement, especially at lower load levels, a 200 N load cell was incorporated into the setup.

Crack propagation was monitored using an optical crack measurement system. A digital camera was connected to the computer interface of the Instron machine to automatically capture images at regular intervals of approximately 3 to 10 seconds during testing. The images were synchronised with the load and displacement data recorded by the testing software. This enabled precise tracking of crack growth in relation to the load–displacement response, ensuring accurate fracture toughness evaluation. The complete experimental setup is presented in Figure 5.2. All tests were conducted at the Faculty of Civil Engineering, TU Delft.

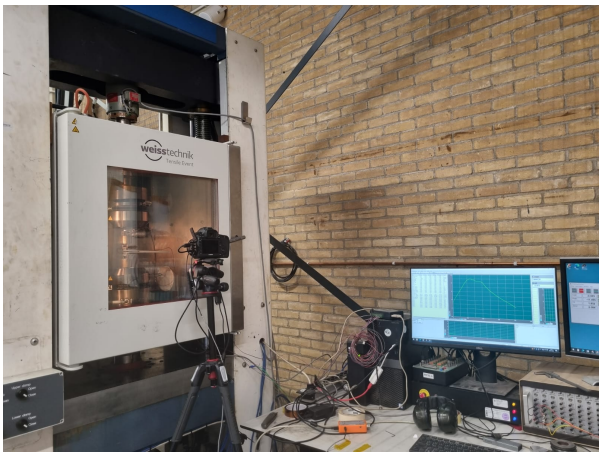

Figure 5.2: Experimental Setup

Before the main tests, a sharp starter crack was introduced to promote stable crack propagation during loading. According to ASTM D5528, this pre-crack can be produced using either the pre-crack cycling method or the wedge insertion method. In the pre-crack cycling approach, specimens without an initial crack are subjected to displacement-controlled loading at a constant crosshead speed of approximately $2\,\mathrm{mm\,min^{-1}}$. Loading is manually stopped once a crack length of 3–5 mm is achieved, after which the specimen is unloaded. However, this method may induce small amounts of permanent deformation in the DCB specimen, which can affect test accuracy.

To avoid this limitation, the wedge insertion method was adopted in this study. In this method, a thin, sharp-edged metal blade (the wedge) is carefully inserted into the delamination plane until a controlled pre-crack of 3–5 mm forms, as specified by the ASTM D5528 standard. This approach ensures that the initial crack is sharp and DCB specimen have minimal permanent deformation.

Following pre-cracking, the specimens were mounted on the tensile test bench for single-cycle loading. The tests were carried out under displacement control at a crosshead speed of $2\,\mathrm{mm\,min^{-1}}$. The loading was continued until the machine reached its maximum displacement limit of 35 mm, at which point unloading was initiated. The resulting crack length corresponding to each force-displacement level was used to construct the R-curve, which represents the variation of fracture toughness with crack propagation under different hygrothermal conditioning environments.

5.2.2. Fatigue

The fatigue fracture toughness tests were performed using the same experimental setup used for the quasi-static experiments. The Instron 100 kN tensile testing machine, equipped with the Weiss climatic chamber, was capable of operating under both quasi-static and cyclic loading regimes. The primary difference between the two testing procedures lies in the control scripts used in the testing software. For fatigue testing, a dedicated script was implemented to apply cyclic loading while simultaneously

capturing images of the crack front at regular cycle intervals.

Before initiating the fatigue tests, it was necessary to determine the baseline fracture toughness value in order to define the loading parameters. Therefore, a pre-cracking cycle was carried out as described in Section 5.2.1, and the Mode I fracture toughness (G_{Ic}) was calculated. Following this, the fatigue experiments were conducted using a load ratio (R) of 0.2, where $R = P_{\text{min}}/P_{\text{max}}$. The cyclic frequency was maintained at $3\,\text{Hz}$, and each test continued until the crack growth reached approximately 200,000 cycles.

Initial trials were conducted at a lower load ratio of $R = 0.1$, during which a small amount of permanent deformation was observed in the specimens. Although this deformation remained below the minimum displacement value of the load cycle and did not result in negative loading, it was anticipated that greater plastic deformation could occur under elevated temperature and humidity conditions. Therefore, all subsequent fatigue experiments were carried out using a load ratio of $R = 0.2$.

Under most hygrothermal conditions, including the hot-dry, room, and cold environments, the specimens exhibited minimal plastic deformation and stable crack propagation at $R = 0.2$. However, under hot-wet conditions, a noticeable increase in plastic deformation was observed. To mitigate this effect and maintain consistent loading behaviour, an additional $1\,\text{mm}$ thick aluminium plate was bonded to both sides of the DCB specimens. This reinforcement enhanced the stiffness of the beam, allowing the load ratio of $R = 0.2$ to be maintained throughout the test without the introduction of compressive loads.

Crack propagation during cyclic loading was continuously monitored using the optical camera system. Images were captured every 200 cycles until the end of the test at 200,000 cycles. In parallel, load data of the cycles, were recorded by the system at the same 200 cycle intervals. These datasets were later synchronised to generate the Paris curves, which describe the relationship between the crack growth rate and strain energy release rate.

Throughout both the quasi-static and fatigue experiments, a thermocouple was attached to the surface of the specimen to monitor temperature variations during testing. This enabled detection of any potential temperature increase resulting from cyclic loading at $3\,\text{Hz}$. No significant temperature rise was observed during the experiments, indicating that isothermal conditions were effectively maintained throughout the entire testing campaign. Furthermore, the thermocouple readings were used to confirm that each specimen had reached thermal equilibrium before the fatigue tests commenced, ensuring consistency across all hygrothermal conditions.

5.3. Analysis

This section outlines the methodology employed for analysing the experimental data obtained from the fracture toughness tests. The analysis begins with the determination of crack length, which is essential for calculating the strain energy release rate and evaluating the progression of delamination. Subsequently, the data reduction methods used to derive the fracture toughness values of the tested specimens are presented in accordance with the ASTM D5528 standard. In addition to these core analyses, the section also describes the procedures and analysis conducted before and after mechanical testing, including microscopic examinations, fractographic observations using high-resolution Scanning Electron Microscopy (SEM), and surface roughness measurements. These complementary analyses provide a comprehensive understanding of the material's damage mechanisms, fracture behaviour, and the influence of hygrothermal conditions

5.3.1. Crack Length Determination

The post-processing of the fracture toughness data begins with the accurate determination of the crack length. Precise measurement of crack length is essential for applying the equations used to calculate fracture toughness in both quasi-static and fatigue tests. The fundamental principles used for crack length measurement remain consistent across both testing regimes.

Each specimen was fabricated with an initial delamination length of $57\,\text{mm}$, which was marked along the specimen edge to serve as the reference point for crack initiation. The location of this initial delamination was identified by directing a bright light across the specimen's thickness. The delamination

interface, corresponding to the release film inserted during manufacturing, appeared as a distinct dark line along the specimen's edge. The exact position of the initial delamination front was then marked and measured with a scale for the accuracy. From this reference point, additional markings were made at $1\,\mathrm{mm}$ intervals along the specimen edge. These markings provided a reliable scale for measuring crack length progression using the captured images during testing.

In the quasi-static experiments, images were captured at regular time intervals, resulting in several hundred frames per test. Similarly, the fatigue experiments generated approximately 800 images for each specimen. Given this large dataset, it was not feasible to manually analyse every image during post-processing. Therefore, the measured crack lengths were correlated with the corresponding compliance values, and the results were plotted on a logarithmic scale. A linear regression was then performed to establish a relationship between compliance and crack length. The regression models describing the relationship between compliance and crack length are presented in Section 5.3.3. This linear regression model enabled the continuous estimation of crack propagation throughout the entire test while minimising the need for detailed image-by-image analysis.

The post-processing of images not only provided accurate crack length data but also allowed observation of the direction of crack propagation and the evolution of the crack tip. Across all tests, the crack was observed to propagate stably along the intended delamination plane. No evidence of transverse crack deviation or crack jumping ahead of the tip was detected, confirming the reliability of the specimen preparation and testing procedure. Figure 5.3 presents representative images showing crack tip propagation observed during the experiments.

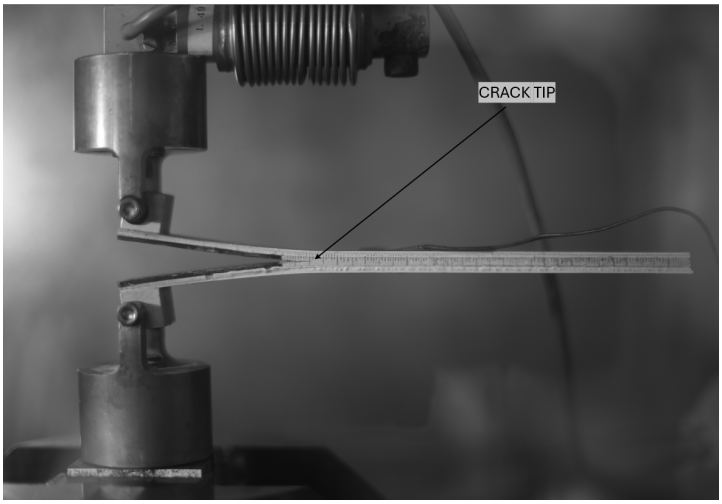

Figure 5.3: Image used for the crack growth analysis

5.3.2. Interlaminar Fracture Toughness

Linear Elastic Fracture Mechanics (LEFM) provides the theoretical foundation for analysing crack initiation and propagation in materials that behave elastically up to the point of fracture. This approach assumes that the region of nonlinear deformation or damage at the delamination front is small compared to the smallest specimen dimension, which is typically the laminate thickness in the case of the Double Cantilever Beam (DCB) test. Under these conditions, the stress and strain distribution around the crack tip can be accurately described using linear elastic theory.

In LEFM, the fracture toughness of a material is expressed in terms of the strain energy release rate, denoted by G. The strain energy release rate represents the amount of elastic strain energy released from the specimen per unit increase in crack area during delamination growth. It is defined as the differential loss of strain energy (dU) per unit specimen width (b) for an infinitesimal increase in delamination length (da), assuming self-similar crack growth under constant displacement conditions as given in equation 5.2. In essence, G quantifies the energy available to drive a crack through the material and serves as a critical parameter in understanding fracture behaviour.

$$G = \frac{1}{b}\frac{dU}{da} \tag{5.2}$$

According to LEFM, crack propagation occurs when the applied strain energy release rate G reaches a critical value, known as the fracture toughness G_c. To facilitate controlled Mode I or opening-mode crack propagation, specimens are specifically designed and manufactured in the Double Cantilever Beam configuration. The DCB geometry is preferred because it provides a simple, stable, and controlled crack propagation mechanism that isolates the Mode I component of fracture without introducing shear or mixed-mode effects.

During a DCB test, as the delamination propagates from the initial insert, a resistance-type fracture behaviour is typically observed. The calculated critical energy release rate G_{Ic} generally increases monotonically and stabilizes as delamination continues. This behaviour can be represented by a resistance curve, often referred to as the R-curve, which plots G_{Ic} as a function of delamination length. The R-curve characterizes both the initiation and propagation phases of delamination in a unidirectional composite specimen. The observed increase in resistance is primarily attributed to the development of fibre bridging, where intact fibres span the crack wake and provide additional resistance to crack growth.

Fibre bridging commonly occurs when delamination propagates between two 0° unidirectional plies. However, in multidirectional laminates, where delamination typically occurs between plies of dissimilar orientation, fibre bridging is less likely to develop. As a result, it is generally considered an artefact of the DCB test in unidirectional materials, although it provides useful insight into toughening mechanisms that may enhance interlaminar resistance.

5.3.3. Data Reduction Methods

The ASTM D5528 standard specifies three data reduction methods for determining the strain energy release rate (G) from experimental load and displacement data. These include the Modified Beam Theory (MBT), the Compliance Calibration Method (CCM), and the Modified Compliance Calibration Method (MCC). Each method is based on the principles of LEFM but incorporates different approaches to account for experimental and geometric deviations from ideal beam theory assumptions.

Modified Beam Theory (MBT)

In its simplest form, the beam theory expression for the strain energy release rate of a double cantilever beam may lead to an overestimation of G_{Ic} To correct for the overestimation, the Modified Beam Theory introduces an effective crack length correction term (Δ)and the corrected expression is:

$$G_I = \frac{3P\delta}{2b(a + |\Delta|)} \tag{5.3}$$

where P is the applied load (N), δ is the load point displacement (m), b is the specimen width (m), a is the measured delamination length (m), and Δ is the effective crack length correction factor (m).

The Δ parameter is determined experimentally by plotting the cube root of compliance ($C^{1/3}$) against the delamination length (a), where compliance is defined as $C = \delta/P$. The resulting relationship is linear and can be expressed as

$$C^{1/3} = m(a + |\Delta|) \tag{5.4}$$

where m is the slope of the fitted line. The value of Δ is obtained from the negative x-intercept of plot as shown in the figure 5.4, which represents the additional effective crack length required to correct for real deformation behaviour. This correction ensures that the computed G_I accurately reflects the true strain energy release rate associated with delamination growth. The least-squares fit of $C^{1/3}$ versus a graphically demonstrates this linear correlation and is widely used in data reduction.

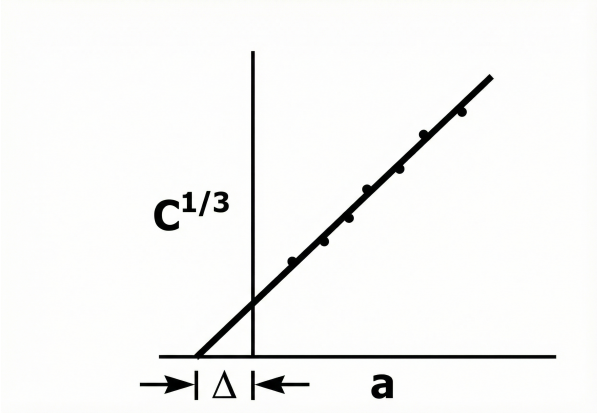

Figure 5.4: Relation between compliance and crack length for mode I fracture toughness analysis using MBT method [20]

Compliance Calibration Method (CCM)

The Compliance Calibration Method determines the Mode I interlaminar fracture toughness (G_I) from the empirical relationship between specimen compliance (C) and crack length (a). Compliance, defined as $C = \delta/P$, is experimentally measured at several delamination lengths during the DCB test. When plotted on a log-log scale, the relationship between C and a typically follows a power law form:

$$C = ka^m \tag{5.5}$$

Taking the logarithm of both sides gives a linear relationship:

$$\log C = \log k + m \log a \tag{5.6}$$

where k is a proportionality constant and m is the slope of the fitted line, which describes how compliance varies with crack length. The Mode I strain energy release rate is then calculated using

$$G_I = \frac{mP\delta}{2ba} \tag{5.7}$$

where P is the applied load (N), b is the specimen width (m), C is the compliance, a is the crack length (m), and m is the slope obtained from the log-log plot.

This method inherently accounts for deviations from ideal beam behaviour but it requires multiple measurements over a range of crack lengths.

Modified Compliance Calibration Method (MCC)

The Modified Compliance Calibration (MCC) Method is an advancement of the Compliance Calibration approach that incorporates additional correction factors to account for compliance variations arising from experimental and geometric influences. This refinement enables a more accurate determination of the Mode I strain energy release rate (G_I) under conditions where large displacements, load block stiffening, or other nonideal effects may influence the test results.

In this method, the parameter A_1 is obtained by plotting $(C_i/N)^{1/3}$ against a_i/h, where C_i is the measured compliance, N is the load block correction factor, a_i is the delamination length, and h is the specimen thickness. A linear regression is then applied to the plotted data to determine the slope, as illustrated in Figure 5.5.

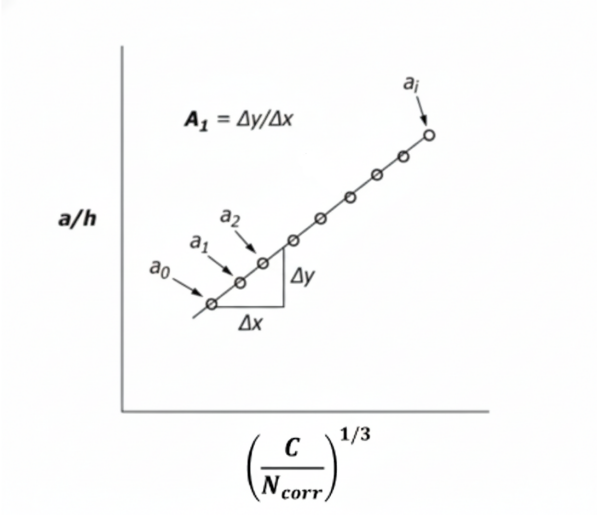

Figure 5.5: Relation between compliance and crack length for mode I fracture toughness analysis using MCC method

To further enhance accuracy, a *large-displacement correction factor*, denoted as F, is introduced to compensate for geometric nonlinearity occurring at higher opening displacements. The value of F is calculated as follows:

$$F = 1 - \frac{3}{10}\left(\frac{\delta}{a}\right)^2 - \frac{3}{2}\left(\frac{\delta d}{a^2}\right) \tag{5.8}$$

Here, 'd' represents the distance from the mid-plane of the specimen to the centre of the loading pinhole.

In addition, a loading-block correction factor, denoted as N_{corr}, is applied to account for the stiffness contribution of the loading blocks. It is determined using the following expression:

$$N_{\text{corr}} = 1 - \left(\frac{l}{a}\right)^3 - \frac{9}{8}\left[1 - \left(\frac{l}{a}\right)^2\right]\left(\frac{\delta t}{a^2}\right) - \frac{9}{35}\left(\frac{\delta}{a}\right)^2 \tag{5.9}$$

where 'l' is the horizontal distance from the centre of the loading block pinhole to the edge of the loading block.

5.3.4. Comparison and Method Selection

A Round Robin interlaboratory study reported that the Mode I fracture toughness values obtained using the three data reduction methods (Modified Beam Theory, Compliance Calibration Method, and Modified Compliance Calibration Method) differed by no more than 3.1 percent [20]. None of the three methods demonstrated clear superiority in terms of accuracy. Therefore, the Compliance Calibration Method was adopted in this study for data reduction and analysis, as it provides a suitable balance between accuracy, simplicity, and experimental practicality.

5.4. Surface Roughness Test

The analysis of the fracture surface offers valuable insights into the mechanisms governing crack initiation and propagation, as well as the underlying phenomena influencing the material's fracture behaviour. Consequently, the fracture toughness tests were followed by detailed surface roughness examinations to further understand the post-fracture characteristics. The surface roughness measurements were carried out using the Keyence VK-X1000 Confocal Laser Scanning Microscope (CLSM).

Laser scanning confocal microscopy provides high vertical resolution and three-dimensional topographical data through a non-contact optical technique. This makes it particularly suitable for measuring the surface roughness of complex or delicate fracture surfaces without introducing mechanical damage.

The primary objective was to examine the extent to which hygrothermal exposure affects crack propagation, with the resultant changes reflected in the fracture surface morphology. Variations in surface roughness can indicate changes in the intrinsic or extrinsic fracture mechanisms. A rougher fracture surface generally suggests increased energy dissipation during crack propagation, which can be attributed to enhanced resistance offered by mechanisms such as fibre pull-out, crack deflection, or crack bridging, thereby contributing to higher fracture toughness.

The quantitative characterization of fracture surface topography was carried out using areal roughness parameters, which describe the statistical variation of the surface height within a defined area. These parameters provide insight into the influence of hygrothermal conditioning on surface morphology and, consequently, on the fracture behaviour of the material. The three key parameters considered are the arithmetical mean height (S_a), the root mean square height (S_q), and the maximum height (S_z).

Arithmetical Mean Height (S_a): The arithmetical mean height, S_a, represents the mean of the absolute height deviations of the surface from the mean plane across the evaluation area. It is analogous to the two-dimensional roughness parameter R_a and serves as a general indicator of the average surface roughness. However, it does not emphasize isolated peaks or valleys, thereby providing a balanced estimation of the overall surface texture.

$$S_a = \frac{1}{A} \iint_A |z(x,y)| \, dx \, dy \tag{5.10}$$

Root Mean Square Height (S_q): The root mean square height, S_q, is defined as the square root of the mean of the squares of surface height deviations from the mean plane. In contrast to S_a, the S_q parameter is more sensitive to larger deviations due to the squaring operation, which amplifies the contribution of extreme peaks and valleys. Consequently, S_q provides a more representative measure of the statistical dispersion of the surface topography.

$$S_q = \sqrt{\frac{1}{A} \iint_A z^2(x,y) \, dx \, dy} \tag{5.11}$$

Maximum Height (S_z): The maximum height, S_z, is defined as the vertical distance between the highest peak and the lowest valley within the measured area. It quantifies the total vertical range of the surface profile and is particularly useful for identifying surface asperities or irregularities that that arise during crack initiation and propagation.

$$S_z = z_{\text{max}} - z_{\text{min}} \tag{5.12}$$

In general, higher values of these parameters correspond to a rougher fracture surface, which often indicates greater energy dissipation during crack propagation. Among these, S_a is considered the primary parameter for assessing the influence of hygrothermal conditions on fracture surface roughness, as it provides a reliable measure of the average height deviation while being less sensitive to noise or isolated surface anomalies.

5.5. Microscopy Analysis

Microscopy examinations were carried out on hygrothermally aged specimens as well as on the corresponding fracture surfaces, using the Keyence VHX-7000 digital microscope, which allows high-resolution imaging across a variable magnification range suitable for microstructural analysis.. The primary objective of these analysis was to identify any microstructural damage or morphological changes induced by hygrothermal conditioning. Such analyses provide essential insight into how environmental exposure influences the internal integrity of flax fibre-reinforced composites prior to mechanical testing.

Yarn Analysis: The microscopic examination of the yarns was performed to detect the presence of cracks that may have developed during the conditioning process. These defects can occur due to the differential swelling or shrinkage of the fibres as they absorb or desorb moisture under varying

temperature and humidity conditions. Monitoring these effects is critical, as damage at the yarn level can significantly influence the overall mechanical response and durability of the composite.

Fibre–Matrix Interface: The fibre–matrix interface was closely examined to identify any signs of interfacial debonding or degradation caused by hygrothermal exposure. The strength of this interface plays a vital role in determining the load transfer efficiency and in governing damage mechanisms such as fibre pull-out, matrix cracking, and fibre bridging during fracture. A well-bonded interface contributes to improved stress distribution, while degradation at the interface can accelerate delamination growth and reduce fracture toughness.

Matrix Analysis: The epoxy matrix was also analysed to evaluate potential microcrack formation resulting from internal stresses generated by fibre swelling or shrinkage during conditioning. Hygrothermal exposure can lead to matrix softening, local plasticization, or the initiation of microcracks that may compromise the material's environmental resistance. Understanding these effects is essential for correlating the microstructural integrity of the matrix with the mechanical performance degradation observed during subsequent fracture toughness tests.

Overall, microstructural characterization plays a crucial role in establishing the relationship between environmental exposure and the resulting mechanical behaviour of the composites. Microscopy tests performed before mechanical testing provide evidence of any pre-existing damage induced by hygrothermal conditioning, while post-fracture microscopy offers insight into the damage evolution and crack propagation mechanisms. A more detailed assessment of the fracture surface morphology and failure modes was further carried out through Scanning Electron Microscopy (SEM), as discussed in the following section.

5.6. Scanning Electron Microscopy (SEM) Analysis

The Scanning Electron Microscopy (SEM) analysis was carried out to closely examine the fracture surfaces of the tested specimens and to understand how cracks developed and evolved under different loading and environmental conditions. By observing the morphology and microstructural features of the fractured surfaces, the aim was to gain a deeper understanding of the damage mechanisms that occurred in the flax fibre-reinforced epoxy composites subjected to quasi-static and fatigue tests.

SEM is a surface characterization technique widely used in for studying fracture morphology, interfacial behaviour, and microstructures. It operates by scanning a focused beam of electrons over the specimen surface, where interactions between the electrons and the material generate signals such as secondary electrons, backscattered electrons, and characteristic X-rays. These signals are detected and converted into high-resolution images that reveal the fine details of the surface topography. Due to its high magnification capability and excellent depth of field, SEM is particularly suitable for analysing features such as fibre–matrix interfaces, fibre pull-out, matrix cracking, and void formation.

Since flax fibres and the epoxy matrix are hydrophilic and non-conductive by nature, careful sample preparation was essential before imaging. Conventional SEM requires a high-vacuum environment typically between 10^{-4} and 10^{-7} Pa to ensure that the electron beam remains stable and focused. This vacuum also prevents contamination of the electron source and detectors by air molecules, maintaining the accuracy and quality of the images. However, operating under vacuum can cause moisture loss and potential structural changes in hydrophilic materials, such as flax-based composites.

Initially, Environmental Scanning Electron Microscopy (E-SEM) was considered to minimize moisture loss during imaging. E-SEM allows imaging under controlled humidity and temperature, which helps preserve delicate fracture surfaces by reducing desorption effects. However, due to practical constraints, conventional SEM was ultimately chosen for detailed analysis.

For the SEM tests„ the samples were coated with a thin conductive layer of carbon using the *carbon evaporation method*. In this process, a high-purity carbon rod was resistively heated in a vacuum chamber, causing the carbon to vaporize and deposit as a thin, uniform film over the sample surface. A coating thickness of approximately 20 ± 3 nm was determined through preliminary trials to provide good surface conductivity without obscuring the fine microstructural features.

Delamination in fibre-reinforced composites typically occurs through the fibre–matrix interface or within

the matrix itself, and often through a combination of both. The SEM observations therefore focused on identifying key features that could explain how hygrothermal exposure influenced the crack propagation mechanisms:

- **Fibre–Matrix Adhesion:** High-magnification images were used to assess the quality of bonding between fibres and the polymer matrix. Intact interfaces generally indicated minimal influence of hygrothermal degradation, while visible fibre pull-out or debonding pointed to weakened interfacial strength due to exposure to heat and moisture.
- **Yarn Damage:** The flax reinforcement is composed of twisted yarns made up of smaller technical fibres. SEM analysis of these yarns helped identify whether moisture or temperature exposure along the loads caused yarn breakage or technical fibre breakage indicating failure mechanisms such as fiber bridging.
- **Matrix Residue on Yarns:** The amount of residual matrix adhering to the yarn surfaces after fracture served as an indicator of the dominant failure mode. A high level of matrix residue suggested cohesive failure within the matrix, while reduced residue indicated interfacial debonding, which could be intensified under extreme hydrothermal conditions.
- **Matrix Damage:** The matrix regions were inspected for microscopic features such as cusps, scarps, branched cracks, chevron markings, hackles, and river lines. These features provide insight into how the matrix fractured, the direction of crack propagation, and the extent of environmental degradation.

In summary, the SEM analysis provided valuable insight into the microstructural processes governing fracture in flax fibre composites. Comparing the fracture surfaces across different hygrothermal conditions revealed how environmental exposure influenced fibre–matrix bonding, matrix toughness, and overall damage development. Together, these observations contribute to a clearer understanding of how hygrothermal aging affects the long-term mechanical performance of natural fibre-reinforced composites.

6

Results & Discussion

This chapter presents the results obtained from the hyrgrothermal conditoning and *in-situ* quasi-static as well as fatigue fracture toughness tests conducted under the designed hygrothermal conditions. The main objective is to evaluate how fracture resistance changes under different environmental exposures and to understand the underlying mechanisms by comparing the findings with the corresponding fractographic observations. The chapter begins with an results from hygrothermal experiments, overview of the overall results and is then divided into two subsections that individually discuss the effects of relative humidity and temperature.

6.1. Hygrothermal Conditioning

The experiments began with the conditioning of the samples in a controlled environmental chamber. The results presented in Figure 6.1 and 6.2 show that the moisture content of the specimens reached a stable plateau after a certain period of conditioning. This plateau indicates that the specimens had attained their equilibrium moisture content under the respective hygrothermal environments. From the figure 6.1, it can be observed that the maximum moisture uptake for the flax fibre composite specimens was approximately 3.4%, reflecting the near limit of diffusion-driven absorption from the surrounding air. On day 24, a 1% decrease in recorded mass is evident, traced to an inadvertent chamber opening that went unnoticed. Therefore, the conditioning was extended by one additional week, during which the moisture content recovered and was realigned with the expected equilibrium trajectory.

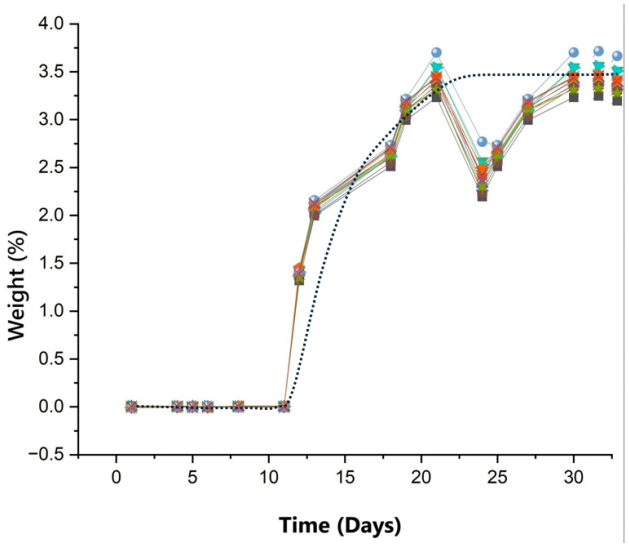

Figure 6.1: Moisture absorption behaviour of flax fibre composites at 50 °C/90% RH condition.

For specimens conditioned at room temperature and under severe cold environments, no significant variation in moisture content was recorded throughout the conditioning period. In these cases, the rate of moisture diffusion within the composite material is considerably reduced, particularly under subzero conditions where the absorbed water remains immobilised within the matrix. Consequently, the moisture uptake curves for the room and cold conditions are not presented, as the specimens exhibited negligible changes in mass and remained effectively at equilibrium throughout the testing.

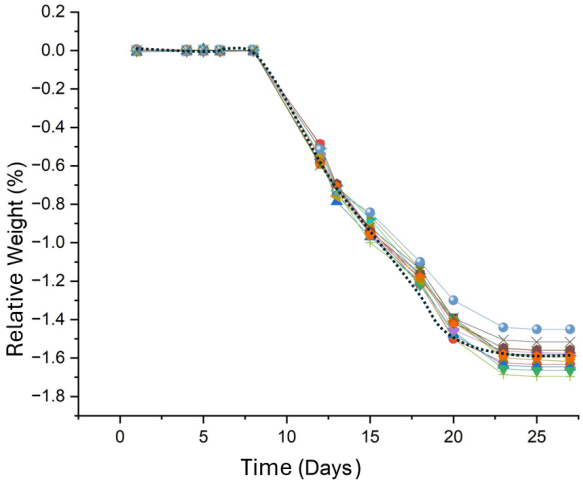

Figure 6.2: Moisture absorption behaviour of flax fibre composites at 50 °C/30% RH condition.

The results of the specimens conditioned under low-humidity conditions are shown in Figure 6.2. It was observed that the specimens experienced a moisture desorption of approximately 1.6% by weight. This indicates that the rate of diffusion during desorption is lower compared to the rate of absorption observed under high-humidity conditions. Such behaviour is typical for natural fibre composites, as moisture molecules are more strongly bound within the fibre with hydrophilic bonds, leading to slower moisture release during drying.

The microscopy results of the samples immediately after hygrothermal conditioning are shown in Figure 6.3. A comparison of all images reveals no visible changes in the microstructure of the specimens, such as inter- or intra-yarn cracking, indicating that the conditioning process did not induce any observable structural damage. However, since the specimens absorbed moisture at 90% RH and desorbed moisture at 30% RH, residual stresses are expected to have developed at the fibre–matrix interfaces. These residual stresses are likely compressive under high-humidity conditions and tensile under low-humidity conditions, which could influence the subsequent fatigue or quasi-static fracture behaviour of the composites.

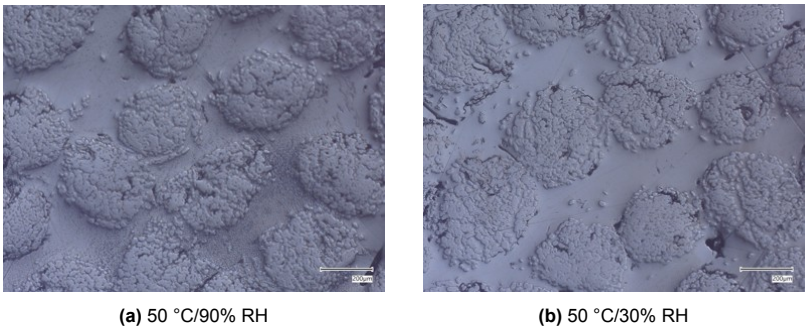

(a) 50 °C/90% RH **(b)** 50 °C/30% RH

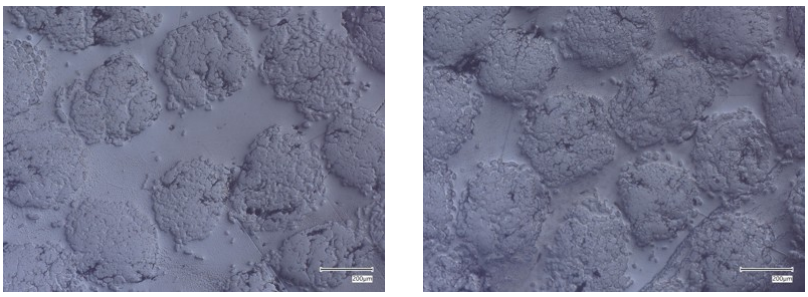

(c) 20 °C/50% RH **(d)** –20 °C

Figure 6.3: Microscopy images of cross-sections of samples after hygrothermal conditioning.

6.2. Overview of Hygrothermal Effects on Quasi static and Fatigue behaviour

Figure 6.4 shows the force–displacement curves for all the quasi statically tested specimens. At the beginning of loading, the specimens are expected to behave elastically, which results in a linear increase in force with displacement. During this stage, the crack tip remains stationary, and both arms of the DCB specimen bend elastically. A slight nonlinearity is observed in this region, which is typical for flax fibre composites. This nonlinear behavior primarily depends on the orientation and distribution of the fibres within the laminate, which influences the local stiffness and load transfer capability.

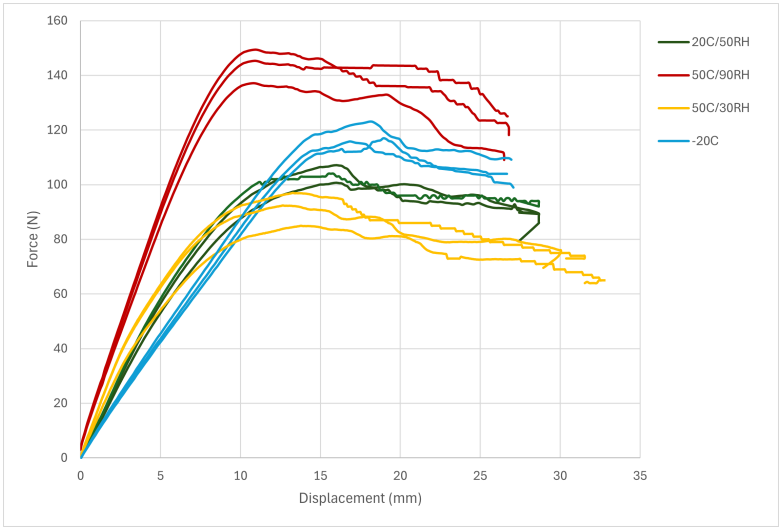

Figure 6.4: Force–displacement curves of FFRP under quasi-static loading across tested hygrothermal conditions

As the applied load approaches the critical energy release rate corresponding to crack initiation, delamination begins to propagate. The peak of the curve generally exhibits a near-plateau behavior, after

which the force decreases gradually until the maximum displacement is reached, depending on the calibrated stroke of the testing machine.

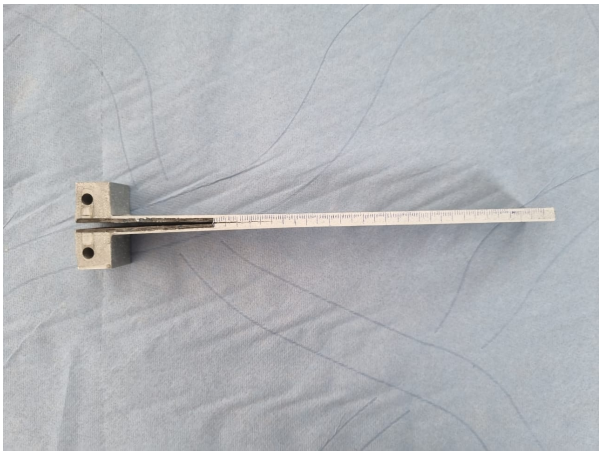

Figure 6.5: DCB specimen after testing.

During unloading, a small residual force is observed when the specimen returns to its initial position. This indicates the presence of minor plastic deformation within the material. According to ASTM D5528, the arms of the specimen are considered permanently deformed if restoring them to their original shape requires more than manual pressure applied using an index finger. Specimens that show such permanent deformation are considered invalid for fracture toughness evaluation because the assumptions of linear elastic fracture mechanics (LEFM) no longer apply. In this study, all specimens were able to return to their original position with slight manual pressure, which indicates that the deformation was not permanent. A deformed specimen after the experiment is shown in Figure 6.5 to illustrate the small curvature that developed after loading. It is important to note that the ASTM D5528 criteria were developed primarily for glass and carbon fibre composites, which behave differently compared to the FFRP composite tested in this study and typically require greater force to remove small curvature after loading.

From the recorded force–displacement data and the corresponding crack length measurements obtained from the images, the Mode I interlaminar fracture toughness (G_{IC}) was calculated for all specimens tested under different hygrothermal conditions. In total, four distinct environmental conditions were examined as shown in figure 6.6. The results show that fracture toughness increases with increasing crack length in all tested specimens. This indicates that FFRP composites exhibit a progressive toughening mechanism that contributes to an increase in resistance as the crack propagates.

The results further show that specimens conditioned and tested under cold conditions ($-20\,^{\circ}\mathrm{C}$) exhibited the highest G_{IC} values, while those tested under hot dry conditions had the lowest values, with no overlap observed between their R-curves. Distinct differences in fracture toughness were observed among all four hygrothermal conditions. However, a slight overlap was found during the initiation phase between the specimens tested at room, hot wet & dry conditions, which can be attributed to statistical variation. As will be shown in Section 6.3.1, ANOVA indicates that this difference is statistically insignificant. Overall, a clear trend was identified across all conditions. The highest fracture toughness was obtained for specimens tested under cold conditions, followed by those tested under hot–wet, room, and hot–dry environments.

In the case of fatigue loading, the Paris curve was constructed from the measured and derived crack length data together with the calculated strain energy release rate values to characterize the fatigue crack growth rate of the tested specimens. The plots in Figure 6.7 represent the crack growth rate (da/dN) as a function of the maximum strain energy release rate of each cycle ($G_{\max}$). These results provide insight into the relationship between cyclic loading conditions and crack propagation behavior under different hygrothermal environments.

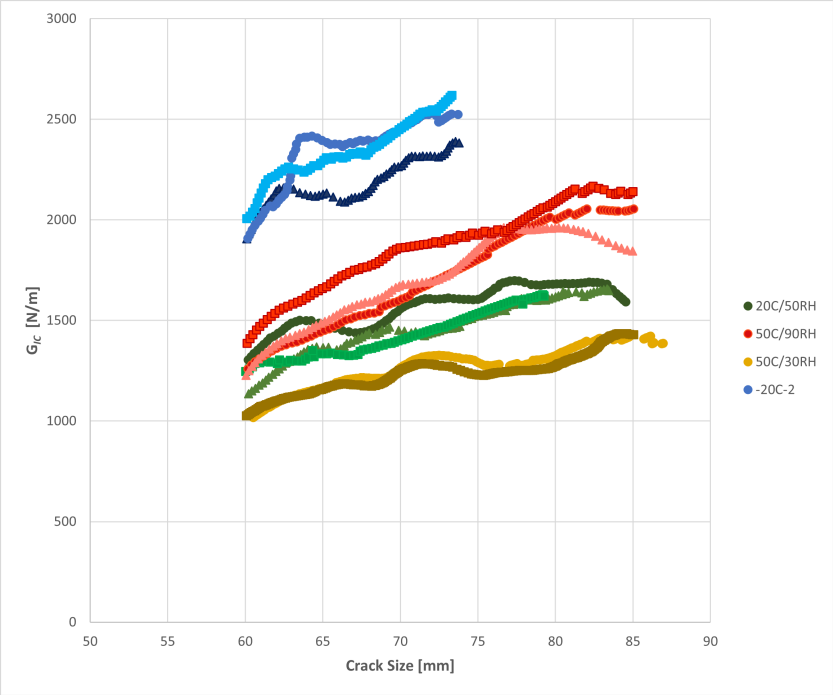

Figure 6.6: R-curve comparing fracture toughness evolution across tested hygrothermal conditions.

From the plotted data, a noticeable shift in the Paris curves can be observed for all tested conditions, accompanied by small variations in slope. This suggests that there may be a common mechanism influencing the crack propagation behavior of flax fibre composites under varying environmental exposures. The results also show that the crack growth rate is highest for specimens tested under hot–dry conditions, followed by those tested at room temperature. This indicates that the combination of elevated temperature and low humidity promotes interfacial degradation and accelerates crack growth.

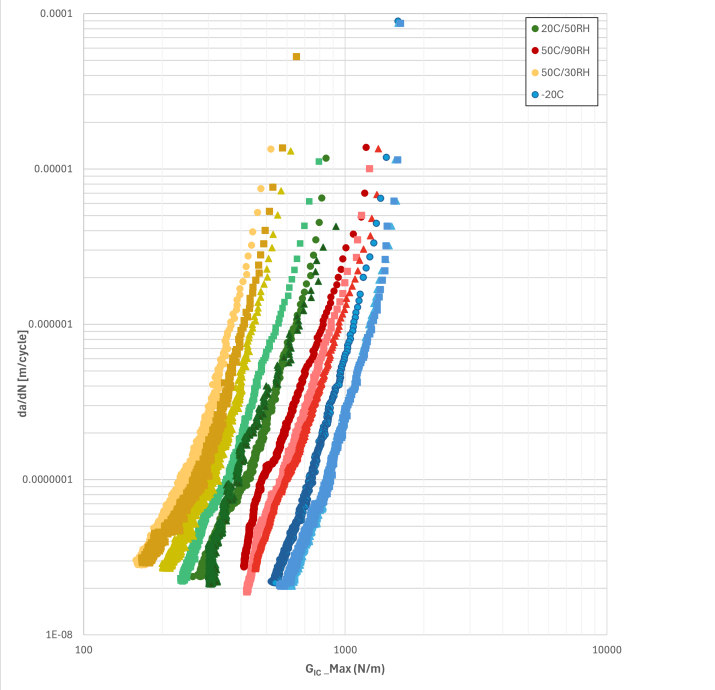

Figure 6.7: Paris curves for FFRP under the tested hygrothermal conditions.

To gain a deeper understanding of these phenomena, the effects of humidity and temperature are analyzed separately in the following sections. The fracture results are then compared with the corresponding fractographic observations to explain the mechanisms responsible for the observed differences in fracture behavior.

6.3. Effect of Relative Humidity

This section discusses the effect of relative humidity by comparing the results of the hot–wet, hot–dry, and room conditions, marked in graphs as 50 °C/90% RH, 50 °C/30% RH, and 20 °C/50% RH, respectively. The influence of humidity is isolated by keeping the temperature constant while varying the relative humidity. The hot–wet condition represents a high-humidity environment, whereas the hot–dry condition represents a low-humidity environment. The results from these two conditions are compared with the room condition to provide an overall understanding of the influence of moisture. Additionally, fractographic results obtained from SEM and optical microscopy analyses are evaluated to further interpret the crack growth phenomena associated with varying humidity levels.

6.3.1. Quasi Static behaviour

Figure 6.8 shows the R-curve plotted for the hot-wet, room, and hot-dry hygrothermal conditions. Distinct R-curves are observed for all three conditions, demonstrating clear differences in fracture behavior. The initiation fracture toughness of the low-humidity condition (50 °C/30% RH) is measured as 1073 ± 90 N/m, and the fracture toughness near the maximum crack length reaches 1399 ± 45 N/m. Similarly, the initiation fracture toughness of the high-humidity condition (50 °C/90% RH) is 1291 ± 84 N/m, while the fracture toughness near the maximum crack length reaches 2033 ± 114 N/m. This significant increase in fracture toughness for the high-humidity condition indicates that moisture enhances the crack propagation resistance as the crack advances. In contrast, the low-humidity condition shows a relatively slower increase in fracture toughness. This difference is reflected in the slopes of the R-curves, where the hot–wet condition exhibits a steeper slope compared to the hot–dry condition, indicating a stronger toughening effect due to moisture.

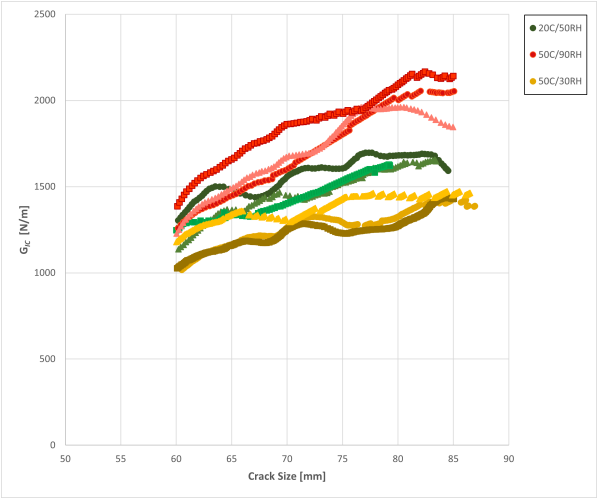

Figure 6.8: R-curves showing the effect of relative humidity on fracture toughness.

At room conditions (20 °C/50% RH), the initiation fracture toughness is 1229 ± 85 N/m, and the fracture toughness near the maximum crack length is 1644 ± 34 N/m. From Figure 6.8, it can be observed that the slope of the R-curve for the room condition lies between that of the hot–dry and hot–wet conditions, showing a moderate moisture influence on fracture toughness.

It is also observed that for the room and hot–dry conditions, the fracture toughness exhibits a slight fluctuation along the crack propagation path. The values initially increase, then decrease, and increase again as the crack progresses. Despite these fluctuations, the overall trend of fracture toughness remains increasing with crack length, indicating a gradual stabilization of resistance as the delamination

advances. Such fluctuations are not observed under the high-humidity condition, where the fracture toughness increases more uniformly with crack growth, suggesting a steadier and more consistent propagation behavior.

For further analysis, the initiation and propagation fracture toughness values are extracted from the R-curves. It is noted that for all specimens, the R-curve does not reach a complete plateau at the maximum crack length. However, as the crack propagates, the slope of the curve decreases significantly, indicating that the rate of increase in fracture toughness slows down and the curve is approaching a stable region where the fracture toughness begins to level off. This region is therefore considered representative of the propagation phase. The limitation arises from the displacement capacity of the fatigue test bench, which restricts the maximum measurable crack length and prevents the curve from fully reaching the plateau experimentally. For comparative analysis, the fracture toughness at a crack length of approximately 80–85 mm is taken as the propagation value for the hot and humid conditions. For the room-temperature specimens, the fracture toughness at a crack length of approximately 78–83 mm is used. These regions correspond to the part of the curve where the slope becomes minimal, signifying that the fracture toughness is nearing stabilization as the crack length further increases.

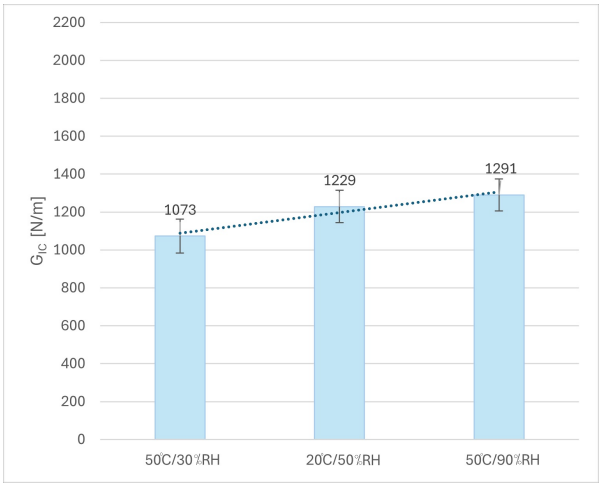

Figure 6.9: Intiation fracture toughness under hot-dry, room, and hot-wet conditions

Figure 6.9 plots the initiation fracture toughness values for the hot–wet, room, and hot–dry conditions arranged in order of increasing moisture content. It can be observed that the hot dry and hot wet conditions exhibit distinctly different initiation toughness values. The fracture toughness values obtained at room condition lie between those of the hot–wet and hot–dry conditions, with the corresponding error bars showing a slight overlap. This indicates that although the average value at room condition is intermediate, there is minor statistical overlap between the results due to experimental variability. This trend shows that as relative humidity increases, the initiation fracture toughness also increases. Statistical analysis through ANOVA method comparing the room, hot wet and hot dry groups yielded $p=0.421$ ($p < 0.05$ to be statistically significant) indicating these values are statistically insignificant. Overall, it can be concluded that, at constant temperature, increasing relative humidity does not have much influence on the initiation fracture toughness.

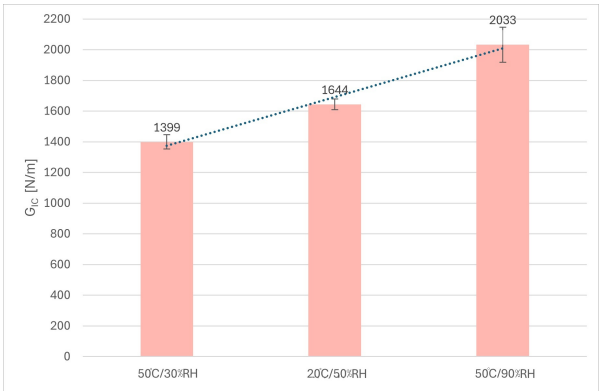

Figure 6.10: Propagation fracture toughness under hot-dry, room, and hot-wet conditions.

Similarly, Figure 6.10 shows the propagation fracture toughness values for the same three conditions arranged in order of increasing moisture content. All three conditions exhibit distinct propagation values. The propagation fracture toughness increases with increasing relative humidity, as the material offers greater resistance to crack growth under moist conditions and the crack advances more gradually with rising humidity.

6.3.2. Fatigue behavior

Figure 6.11 presents the Paris curves from fatigue crack-growth tests conducted under low humidity ($50\,^{\circ}\mathrm{C}$/30% RH), room conditions ($20\,^{\circ}\mathrm{C}$/50% RH), and high humidity ($50\,^{\circ}\mathrm{C}$/90% RH). The curves show the relationship between the fatigue crack-growth rate $(\mathrm{d}a/\mathrm{d}N)$ and the maximum strain-energy release rate $(G_{\max})$. Distinct, non-intersecting curves are observed for the three environments, indicating that humidity consistently influences the fatigue crack-propagation behavior of the FFRP composites.

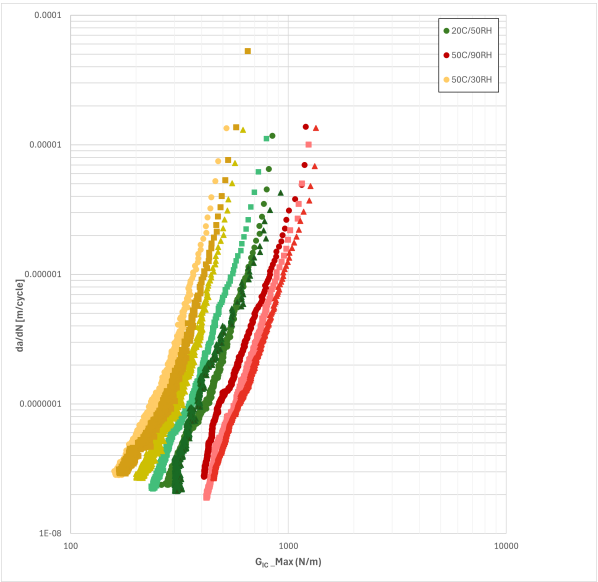

Figure 6.11: Paris curves showing the effect of relative humidity on fatigue crack growth resistance

A clear rightward shift of the Paris curves is observed with increasing relative humidity. The curve corresponding to the low humidity condition lies on the left, followed by the room condition, while the high humidity condition appears furthest to the right. This rightward shift signifies that a higher $G_{\max}$ is required to achieve the same crack growth rate under high humid conditions. In other words, the fatigue crack growth resistance increases as the relative humidity rises.

The gradient of the Paris curve also varies across the three conditions. As shown in the table 6.1,the

Table 6.1: Influence of relative humidity on the slope (m) of Paris curves.

	50°C/30% RH	20°C/50% RH	50°C/90% RH
Slope (m)	0.01503 $\pm$ 0.0015	0.0111 $\pm$ 0.0008	0.0079 $\pm$ 0.0009

low humidity specimens show the steepest gradient, indicating that their crack growth rate varies more sharply with changes in the strain energy release rate during cyclic loading. In contrast, the high humidity specimens exhibit a gentler gradient, meaning that their crack growth rate changes more gradually as the crack propagates. The room condition displays an intermediate behavior between the two cases. This reduction in gradient with increasing humidity suggests that the material responds more steadily to variations in strain energy release rate, resulting in more stable and controlled crack propagation under cyclic loading.

These results clearly demonstrate that humidity plays a significant role in influencing fatigue behavior. Under low humidity conditions, cracks propagate more rapidly, reflecting a relatively brittle response of the material. As humidity increases, the crack growth rate decreases, and the propagation becomes more gradual and stable. The consistent rightward shift of the Paris curves, together with the reduction in gradient, confirms that higher humidity enhances the material's resistance to fatigue crack growth and promotes steadier crack propagation under cyclic loading.

Overall, the results highlight a clear environmental dependence. The fatigue crack growth resistance improves progressively with increasing relative humidity. The distinct and non-intersecting nature of the Paris curves further confirms that this trend is consistent across the full range of G_{max} values tested, indicating a reproducible and predictable influence of humidity on fatigue crack growth behavior.

6.3.3. Fractography

This section presents the fractography results obtained from both quasi-static and fatigue tests. Figure 6.12 shows the microscopy images of the fracture surfaces for the hot–dry, room, and hot–wet conditions, arranged from left to right. It can be observed that the specimens tested at 50 °C/90 % RH exhibit a noticeably lighter surface colour compared with the others, which could be attributed to the higher moisture content absorbed under high humidity conditions. From the microscopic observations, the fracture surfaces appear relatively rough, characterized by broken fibres, fibre bundle imprints, and visible twists within the fibre bundles. Overall, the fracture surfaces across the different hygrothermal conditions do not display any pronounced differences observable to the naked eye or under low-magnification microscopy.

(a) $50\,^{\circ}$C/30% RH **(b)** $20\,^{\circ}$C/50% RH **(c)** $50\,^{\circ}$C/90% RH

Figure 6.12: Microscopy images comparing effects of humidity on fracture surfaces.

Further examination of the specimens using SEM provided a detailed view of the fracture morphology across the surfaces. Figure 6.14-6.16,shows the SEM images of the fracture surfaces obtained from specimens tested under hot–wet, cold, and room conditions during fatigue loading. The microstructural features observed were largely consistent across all environmental conditions. Common features included fibre breakage, fibre imprints, fibre patches, yarn loosening, scarp formation, and fibre elongation.

Figure 6.14-6.16, highlight the loosening of yarns on the fracture surface. This phenomenon occurs

due to the opening of the fracture plane, which induces a pulling effect on the fibres within the yarn. As a result, local debonding and fibre breakage are observed. it can be also noted that the interface between the yarn and the surrounding matrix appears relatively strong, which allows the yarn structure to remain intact during loading. However, since the load is transferred through the fibres within the yarn, individual fibres experience higher stresses and eventually fracture. This failure behavior is influenced by inherent defects in the technical fibres, such as kink bands along the fibre axis, which act as weak points. Consequently, the opening of the crack leads to fibre breakage at these defect sites rather than failure of the entire yarn structure.

In several regions on fracture surface, fibre patches can also be observed on the fracture surface. These patches are idendified by sudden change in the twist direction along axis of the yarn. Their presence indicates that stress concentrations may develop in certain regions during crack propagation, leading to localized fibre bundle breakage and the detachment of small fibre clusters.

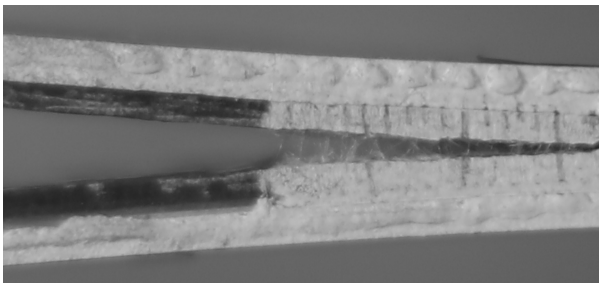

Figure 6.13: Technical Fibre briding

Overall, the observed yarn loosening, fibre breakage, and fibre patches suggest the presence of fibre bridging of technical fibres across the crack plane. This observation is further supported by the magnified image of the crack-propagation zone in Figure 6.13. The figure corresponds to the specimen tested under hot–wet conditions, where fibre bridging is clearly visible. Notably, this is the same condition that exhibited the highest fracture toughness values, indicating a strong correlation between the extent of fibre bridging and the material's resistance to crack propagation.

In theory, delamination may initiate through matrix cracking and/or fibre–matrix debonding, with both mechanisms often acting concurrently rather than in isolation. Here, technical fibre bridging and fibre pull-out indicate the fibre–matrix debonding mechanism and matrix cracking is observed on the surface as the formation of scarps.

It is observed that a scarp forms perpendicular to the twist direction of the yarn rather than aligned with the yarn. This could be because the technical fibres in the yarn carry the load, and the interface between the technical fibres and the matrix is more important than the yarn–matrix interface. The formation of a scarp perpendicular to the technical fibre instead of the yarn direction could be considered as a unique feature of FFRP.

The formation of scarps represents a very fascinating and important feature observed on the failure surfaces of FFRP. These structures typically appear as relatively bright, linear markings in microscopic images, oriented along the fibre direction. Scarps are formed as a result of the convergence of two adjacent crack planes during fracture.

The development of scarp lines begins with localized failure at high-stress regions, such as the interface between the matrix and the technical fibres. This localized damage initiates the formation of microcracks within the matrix and around the fibres. Initially, these microcracks propagate approximately perpendicular (90°) to the fibre direction. However, as the primary crack progresses along the fibres, the microcracks gradually reorient toward the global crack growth direction. With continued loading, the matrix microcracks extend as microflows along several planes and, upon intersection, coalesce to form distinct linear features referred to as scarps.

Scarps are characteristic features of toughened matrix systems. The epoxy matrix used in this study has an impact strength of approximately 70 kJ/m², indicating a relatively tough and ductile behavior.

Hence, the presence of comparable scarp features across all fracture surfaces suggests that the matrix shows ductile characteristics under the room, hot–wet, and hot–dry conditions.

The SEM images also reveal noticeable changes in the failure mechanism of the fibres. As shown in Figure 6.14c-6.16c, the technical fibres exhibit ductile failure features, and this ductility increases with rising humidity due to the higher moisture content in the fibres. This transition is evident in the form of greater fibre elongation at the point of fracture, as observed in the hot–wet condition (Figure 6.16c) compared with the hot–dry condition (Figure 6.15c).

Overall, the matrix patches on the fracture surface is observed to be low, even though the fibre volume fraction of the specimens is around 45% this could be attributed to the relatively weak fibre-matrix interface in FFRP.

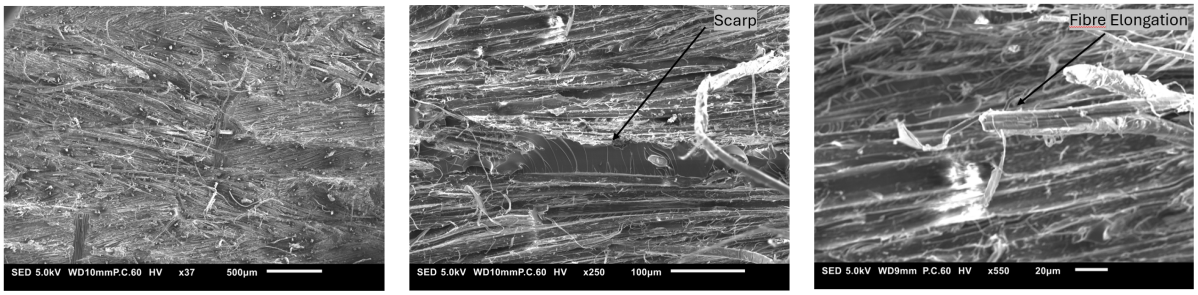

(a) 37x **(b)** 250x **(c)** 550x

Figure 6.14: SEM images of the fracture surfaces of specimens tested at $20\,^{\circ}\mathrm{C}$ and 50% RH under quasi-static loading, at different magnifications.

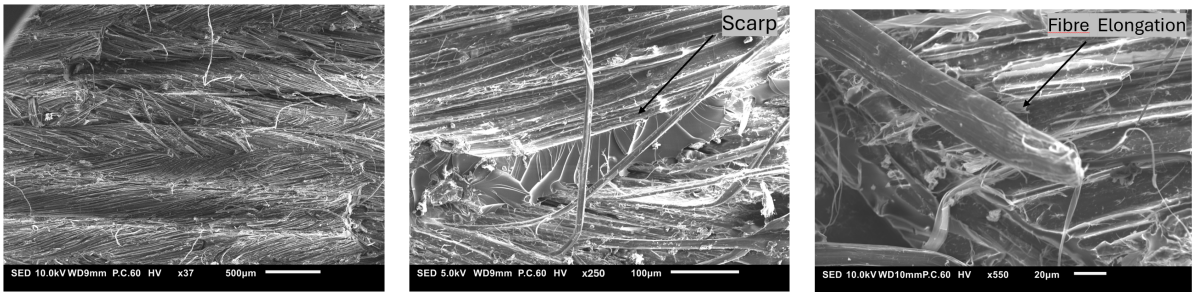

(a) 37x **(b)** 250x **(c)** 550x

Figure 6.15: SEM images of fracture surfaces at $50\,^{\circ}\mathrm{C}$/30% RH under quasi-static loading, at different magnifications.

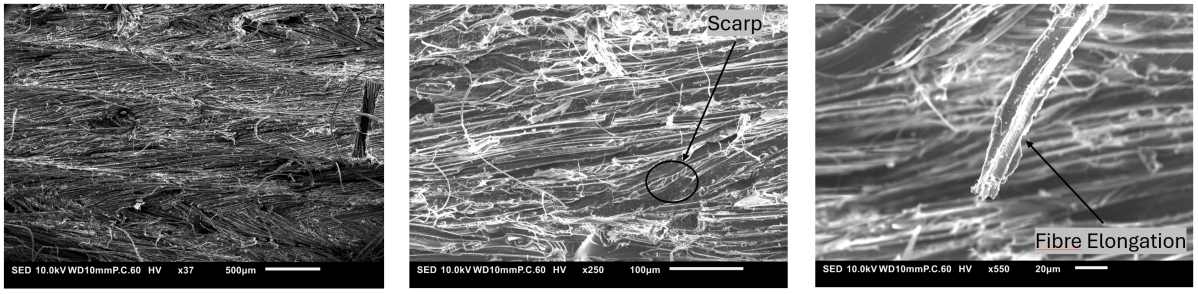

(a) 37x **(b)** 250x **(c)** 550x

Figure 6.16: SEM images of fracture surfaces at $50\,^{\circ}\mathrm{C}$/90% RH under quasi-static loading,at different magnifications.

6.3.4. Surface Roughness

The surface roughness of all specimens was analyzed using a Keyence VK-X1000 Confocal Laser Scanning Microscope. To assess both the initiation and propagation regions, measurements were

taken on the bottom arm of each specimen. The top arm was not analyzed because the specimen is symmetric about its mid-plane, implies the fracture characteristics of the top and bottom surfaces are equivalent. For the fatigue specimens, the crack propagation length was relatively short. Therefore, the surface roughness was measured near the central region of the crack growth zone, which best represents the typical fatigue fracture surface. The results of these measurements are summarized in Table 6.2. The measured roughness values (S_a) are discussed in relation to the observed fracture mechanisms below.

Table 6.2: Average surface roughness values (S_a) measured on fracture surfaces for quasi-static (QS) and fatigue tests under hot-dry, room conditon, hot-wet conditions

	50 °C / 30 % RH	20 °C / 50 % RH	50 °C / 90 % RH
QS–Initiation	90 $\pm$ 5 (μm)	92 $\pm$ 7(μm)	94 $\pm$ 5 (μm)
QS–Propagation	93 $\pm$ 7 (μm)	94 $\pm$ 9 (μm)	98 $\pm$ 11 (μm)
Fatigue	88 $\pm$ 3 (μm)	89 $\pm$ 5 (μm)	95 $\pm$ 9 (μm)

In the quasi-static tests, a considerable degree of statistical variation was observed in the surface roughness values measured under the hot dry, room & hot wet hygrothermal conditions. This variation primarily arises from high varations in the non uniform surface roughness across fracture surface of each specimen. During crack propagation, fibre bridging occurs as several flax fibres remain partially intact and resist separation across the crack plane. The number and thickness of these bridging fibres vary between specimens, leading to localized differences in fracture morphology. In addition, yarn loosening and the presence of fibre patches on the fracture surface contribute to the irregular topographical features. These fibre-rich regions create uneven fracture zones and localized surface roughness variations. Furthermore, the relatively large thickness of individual flax fibres amplifies these irregularities, producing pronounced peaks and valleys along the fracture surface. As a result, significant scatter in the measured surface roughness values was observed under all environmental conditions.

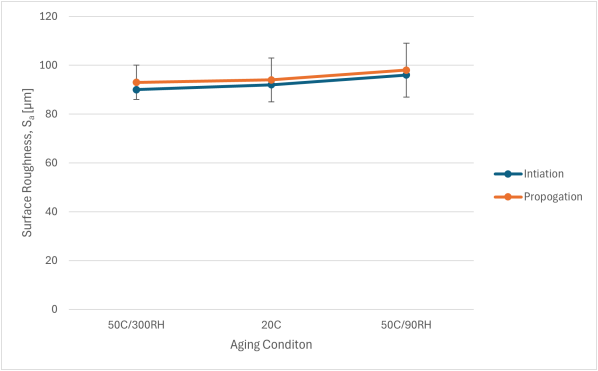

Figure 6.17: Surface roughness (S_a) of quasi-static specimens under dry, room, and wet conditions

Despite this variation, the mean values displayed a clear trend, with surface roughness increasing progressively with relative humidity as shown in figure 6.17. The specimens tested under hot dry conditions (50 °C/30 % RH) exhibited the lowest average roughness, while those tested under hot wet (50 °C/90 % RH) showed the highest values, and the room condition (20 °C/50 % RH) lay in between. This indicates that humidity influences the fracture morphology by promoting greater fibre pull-out and matrix deformation, resulting in rougher fracture surfaces. It was also evident that, for each environmental condition, the propagation roughness values were consistently higher than the initiation values. This suggests that as the crack advanced, the fracture process became increasingly complex due to progressive fibre breaking, pull-out, and the accumulation of micro-damage, leading to more irregular fracture surfaces and enhanced energy dissipation. Although the large scatter prevented a definitive quantitative conclusion, the trend in average values supports the interpretation that increasing humidity and crack progression both contribute to more complex and energy-dissipative fracture behavior under quasi-static loading.

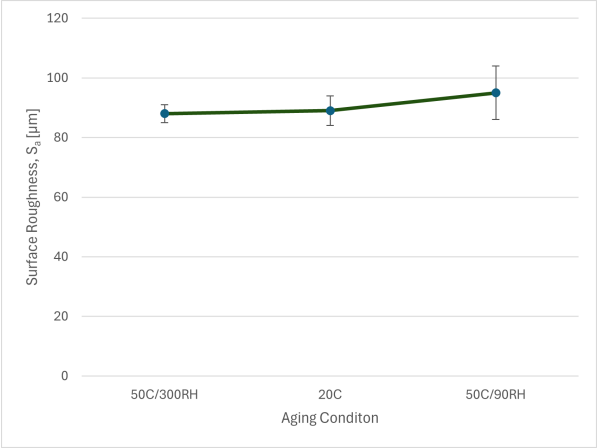

Figure 6.18: Surface roughness (S_a) of fatigue specimens under dry, room, and wet conditions

A similar degree of statistical scatter was also observed in the fatigue surface roughness results as shown in figure 6.18 . The SEM fractography observations revealed comparable fracture surface features between the fatigue and quasi static specimens, indicating that similar microstructural mechanisms such as fibre bridging, fibre pull out, and fibre patch govern the fracture process in both cases. Therefore, the scatter observed in the fatigue results could be arising from the same inherent material characteristics that cause variability in the quasi static tests. Despite this, the mean fatigue roughness values followed the same general trend as the quasi static results, showing an increase in surface roughness with increasing relative humidity.

When comparing the quasi-static and fatigue results, the fatigue specimens generally exhibited slightly lower average surface roughness values than their quasi-static counterparts under similar environmental conditions. This difference can be attributed to the progressive and cyclic nature of fatigue crack propagation, where repeated loading promotes gradual interfacial degradation and encourages the crack to follow through the weak fibre–matrix interfaces. As a result, the fatigue fracture surfaces appeared smoother and more uniform. In contrast, quasi-static failure occurred through a single, abrupt event, producing greater local deformation, fibre pull-out, and rougher topographical features.

However, when tested statistically, the apparent differences in mean roughness did not hold. The ANOVA analysis yielded $p = 0.474$ for the initiation region and $p = 0.786$ for the propagation region in quasi-static tests, and $p = 0.386$ for fatigue fracture surfaces, indicating no significant differences between conditions. Therefore the mean-based comparison in fracture-surface roughness should therefore be viewed as anticipated trend rather than statistically inferential results. The large variability is attributed to the fracture morphology of FFRP composites. The relatively large fibre diameter, together with fibre-bridging and fibre pull-out, produces highly localized surface features that amplify roughness variability within and between specimens, yielding overall in-significant differences across conditions.

6.3.5. Summary of findings

The results demonstrate that relative humidity has a pronounced effect on the fracture and fatigue behavior of flax fibre-reinforced polymer composites. Under quasi-static loading, the propagation fracture toughness values increased systematically with rising relative humidity. The hot–wet condition (50 °C/90 %RH) exhibited the highest fracture resistance, while the hot–dry condition (50 °C/30 % RH) showed the lowest. The R-curves confirmed that moisture enhances resistance to crack growth by promoting more gradual and stable crack propagation.

Fatigue results displayed a similar trend, with the paris curves shifting rightward as humidity increased, indicating that higher strain energy release rates were required to achieve comparable crack growth rates under humid conditions. The slope of the Paris curves decreased with increasing humidity, reflecting a more controlled and stable crack growth response. Overall, consistency between quasi-static and fatigue trends suggests that environmental humidity significantly improves crack propagation resistance across different loading modes.

Fractographic analysis supported these mechanical observations. Common microstructural features, such as fibre bridging, fibre pull-out, yarn loosening, and scarp formation, were observed across all humidity levels. Technical fibre bridging was most pronounced under the hot–wet condition, correlating with the highest fracture toughness. The appearance of scarps across all conditions indicated that the epoxy matrix maintained ductile characteristics across all the humidity levels. Increased fibre elongation and ductile failure of the technical fibres were evident under higher humidity, demonstrating moisture-induced softening and enhanced deformability of the fibres.

Surface roughness measurements did not statistically corroborate the qualitative observations, although the mean trends were similar. High scatter was present because of the heterogeneous FFRP fracture surface, and the mean roughness tended to increase with relative humidity for both quasi-static and fatigue tests. However, ANOVA analysis showed no significant differences between conditions. The substantial variability is consistent with the fracture surface morphology of FFRP composites, where large technical fibres, fibre bridging, and fibre pull-out create highly localised surface features that increase specimen-to-specimen scatter. Fatigue specimens exhibited slightly smoother surfaces than quasi-static ones, which aligns with the more gradual crack propagation under cyclic loading and the associated reduction in fibre pull-out and matrix deformation.

Overall, the results confirm that increased humidity enhances fracture toughness, fatigue resistance in flax fibre composites. Moisture plays a key role in modifying both the fibre and matrix behavior, leading to more ductile failure characteristics and greater energy absorption during crack growth.

6.4. Effect of Temperature

This section discusses the effect of temperature by comparing the results obtained under the room, hot–wet, and cold conditions, represented in the graph as 20 °C/50 % RH, 50 °C/90 % RH, and –20 °C, respectively. The influence of temperature is isolated by maintaining a nearly constant moisture content while varying the test temperature. This approach was adopted because controlling relative humidity accurately at sub-zero temperatures is experimentally challenging. The hot–wet condition corresponds to an elevated temperature environment, whereas the cold condition represents a low-temperature environment. The results from these two cases are compared with the room condition to develop an overall understanding of the influence of temperature on the fracture behaviour of the flax fibre composite. Furthermore, fractographic observations obtained from SEM and optical microscopy analyses are examined to interpret the crack growth mechanisms associated with different temperature conditions.

6.4.1. Quasi Static

Figure 6.19 shows the R-curve for the cold, room, and hot–wet temperature conditions. Distinct R-curves are observed for all three conditions, demonstrating clear differences in fracture behaviour. Among these, the cold condition ($-20\ ^\circ\mathrm{C}$) exhibits the steepest R-curve, indicating a pronounced increase in fracture toughness as the crack propagates. The initiation fracture toughness for the cold condition is $1939 \pm 57\ \mathrm{N\,m^{-1}}$, and the value near the maximum crack length reaches $2459 \pm 107\ \mathrm{N\,m^{-1}}$. In contrast, room condition ($20\ ^\circ\mathrm{C}/50\%$ RH) previously discussed in the humidity section shows considerably lower R-curve values, while the the hot–wet condition ($50\ ^\circ\mathrm{C}/90\%$ RH) lies in between. This trend highlights that the fracture resistance of FFRP composites increases significantly as the temperature decreases.

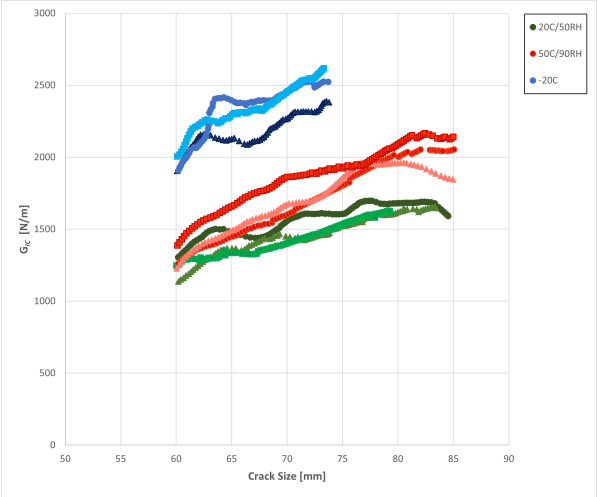

Figure 6.19: R-curves showing the effect of relative humidity on fracture toughness of FFRP.

It is also noted that the maximum crack length reached in the cold condition is smaller than in the other two cases, which is due to the limitation in stroke displacement of the testing machine. Despite this, the cold condition displays a rapid rise in fracture toughness with crack length, emphasizing increased crack resitance of the the FFRP at lower temperatures.

It is further observed that the R-curves for the cold and room conditions exhibit slight fluctuations along the crack propagation path. The values initially increase, then decrease, and rise again as the crack progresses. These fluctuations likely result from local variations in fibre bridging and crack path resistance. Nevertheless, the overall trend remains increasing, suggesting a progressive stabilization of fracture resistance with crack extension. Such fluctuations are less evident under the hot–wet condition, where the fracture toughness increases more uniformly with crack growth, indicating steadier and more consistent crack propagation behavior at elevated temperature.

Similar to the analysis conducted for the effect of humidity, the initiation and propagation fracture toughness values were extracted from the corresponding R-curves. It is observed that, for all specimens, the R-curve does not reach a complete plateau at the maximum crack length. In the case of the high-humidity and room-temperature conditions, the slope of the R-curve gradually decreases as the crack length increases, indicating that the fracture toughness begins to stabilize. However, under the low-temperature condition, the slope continues to increase even near the maximum crack length, suggesting that the material has not yet reached the plateau region within the limits of the test. Since this study focuses on a comparative evaluation, the maximum crack length recorded in each test is considered representative of the propagation region. For the cold condition, the fracture toughness is averaged around a crack length of approximately 70–73 mm and taken as the propagation value. For the room and hot–wet conditions, the same approach used in the relative humidity analysis is applied, where the propagation fracture toughness is averaged over a crack length range of approximately 78–85 mm.

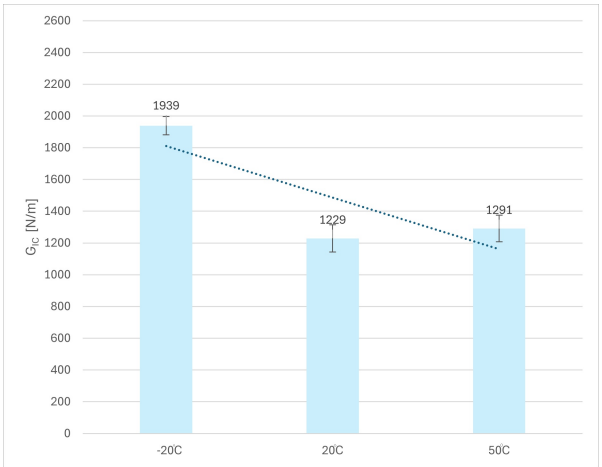

Figure 6.20: Initiation fracture toughness under cold, room, and hot conditions

Figure 6.20 shows the initiation fracture toughness values for the cold, room, and hot–wet conditions, arranged in order of increasing temperature. It can be observed that the cold and hot–wet conditions exhibit distinct initiation fracture toughness values with no overlap in their statistical variation. The fracture toughness values obtained at room temperature lie close to hot–wet conditions, with the corresponding error bars showing a slight overlap with the hot–wet condition. Overall, it can be concluded that the initial fracture resistance of flax fibre composites is enhanced at lower temperatures, while higher temperatures reduce the material's overall resistance to crack initiation.

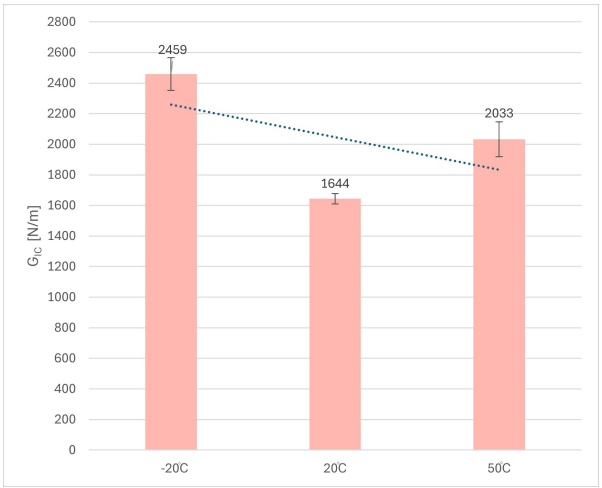

Figure 6.21: Propagation fracture toughness under cold, room, and hot conditions

Similarly, Figure 6.21 presents the propagation fracture toughness values for the cold, room, and hot–wet conditions, arranged in order of increasing temperature. Distinct propagation values are observed for all three cases, following a trend consistent with that of the initiation toughness. The cold condition exhibits the highest propagation fracture toughness, while the room condition shows the lowest, with the hot wet condition lying between them. This indicates that the material's resistance to crack growth decreases progressively as the temperature increases. It is also noted that, the specimen at 20 °C/50 % RH likely contains less moisture than the one at 50 °C/90 % RH; if both specimens had comparable moisture contents, the propagation fracture toughness at room temperature could potentially exceed that of the hot–wet condition. Overall, these results suggest that both the initiation and propagation fracture toughness values are enhanced at lower temperatures, demonstrating that flax fibre composites exhibit greater resistance to crack growth under cold conditions.

6.4.2. Fatigue

Figure 6.22 presents the Paris curves from fatigue crack-growth tests conducted under cold conditons ($-20\,^{\circ}\mathrm{C}$), room ($20\,^{\circ}\mathrm{C}/50\%\ \mathrm{RH}$), and high-humidity ($50\,^{\circ}\mathrm{C}/90\%\ \mathrm{RH}$) conditions. These curves illustrate the relationship between the fatigue crack-growth rate $(\mathrm{d}a/\mathrm{d}N)$ and the maximum strain-energy release rate $(G_{\max})$. Distinct, non-intersecting trends are observed for the three environments, indicating consistent differences in fatigue crack-growth behaviour. At higher $G_{\max}$ values (above $\sim 1000\ \mathrm{N/m}$), a slight overlap appears among some specimens, which can be attributed to experimental variability. Applying ANOVA to hot wet and cold conditions for values $G_{\max} > 1000\ \mathrm{N\,m^{-1}}$ yielded $p = 0.002$, showing that values are statitically significant. Overall, the results demonstrate that temperature consistently influences the fatigue crack-propagation behaviour of FFRP composites.

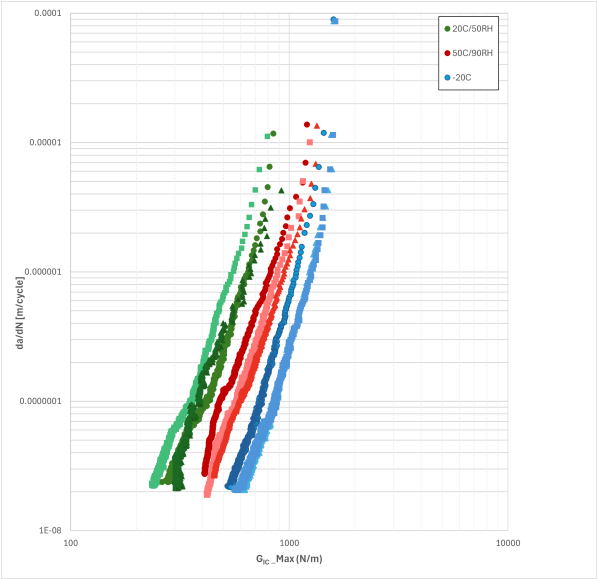

Figure 6.22: Paris curve showing the effect of temperature on Fatigue crack growth resistance.

The gradient of the Paris curves also varies across the three conditions as shown in table 6.3. The room condition specimens exhibit the steepest gradient, suggesting that their crack growth rate changes more sharply with variations in the strain energy release rate during cyclic loading. The cold specimens show a moderate gradient, while the hot wet specimens display the lowest gradient, indicating hot wet conditions shows better stable crack growth rate than cold conditions during cyclic loading. The overall rightward shift of the curves with decreasing temperature shows that FFRP composites exhibit improved fatigue crack growth resistance under cold conditions. When compared with the trends observed for the effect of humidity, this suggests that the lower moisture content at reduced temperatures could also contribute to the higher gradients of the Paris curves. Nevertheless, an overall improvement in crack growth resistance is also governed by the influence of temperature.

Table 6.3: Influence of temperature on the slope (m) of Paris curves.

	20°C/50% RH	50°C/90% RH	-20°C
Slope (m)	0.0111 $\pm$ 0.0008	0.0065 $\pm$ 0.0006	0.0079 $\pm$ 0.0008

The enhanced resistance to crack growth at low temperature under both quasi-static and fatigue loading can be attributed to the behaviour of the bridging fibres. At lower temperatures, FFRP exhibit higher tensile strength, allowing the bridging fibres to sustain greater loads across the crack surfaces (refer fig:2.5). This increased load-bearing capacity leads to higher energy absorption during crack propagation, thereby improving the overall fracture and fatigue resistance of the material in cold environments.

6.4.3. Fractography

This section shows the fractography analysis of specimens tested under different temperature conditions for both quasi-static and fatigue loading. Figure 6.23 present the microscopy images of the fracture surfaces corresponding to the cold, room, and hot conditions, arranged from left to right. The specimens tested at –20 °C and 50 °C/90% RH display noticeably lighter surface coloration compared with those tested at room temperature, which may be attributed to the same moisture content retained under both hot and cold environments. Microscopic observations reveal that the fracture surfaces are relatively rough and feature broken fibres, fibre-bundle imprints, and loosening of bundle within the yarn structure. These characteristics are similar to those observed under study effect of humidty conditions. Another interesting observation is that specimens conditioned in hot–wet and cold environments display similar overall coloration on fracture surface, indicating that temperature variations do not drastically alter the colour of the specimens. Overall, no significant differences in surface morphology are apparent when viewed with the under optical mircrocpy.

(a) -20C°C **(b)** $20\,^{\circ}$C/50% RH **(c)** $50\,^{\circ}$C/90% RH

Figure 6.23: Microscopy images comparing the effects of temperature on fracture surface.

A closer examination of the fracture surfaces of the fatigue and quasi static specimens using SEM is presented in Fig. 6.24, Fig. 6.25, and Fig. 6.26. The SEM images of the quasi-static specimens have already been presented in the section on the effect of humidity, where the room and hot–dry conditions are shown in Fig. 6.14 and Fig. 6.16. As discussed there, the room and hot–dry conditions exhibit fibre breakage, fibre imprints, fibre patches, ductile fibre behaviour, and scarps. When compared with these room and hot–dry conditions, the cold condition still shows several similar features, such as fibre imprints and fibre patches. However, both the fibre and the matrix appear markedly more brittle. Figure 6.26c shows brittle failure of the fibres, while Fig. 6.26b depicts matrix failure characterised by scarps, river lines, and distinct facets.

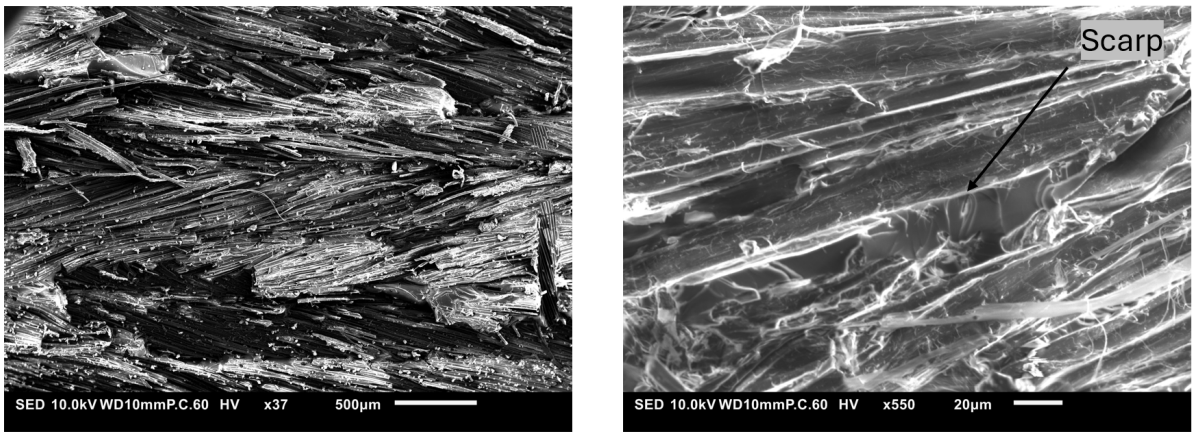

(a) 37x **(b)** 550x

Figure 6.24: SEM images of fatigue fracture surfaces at $20\,^{\circ}$C/50% RH.

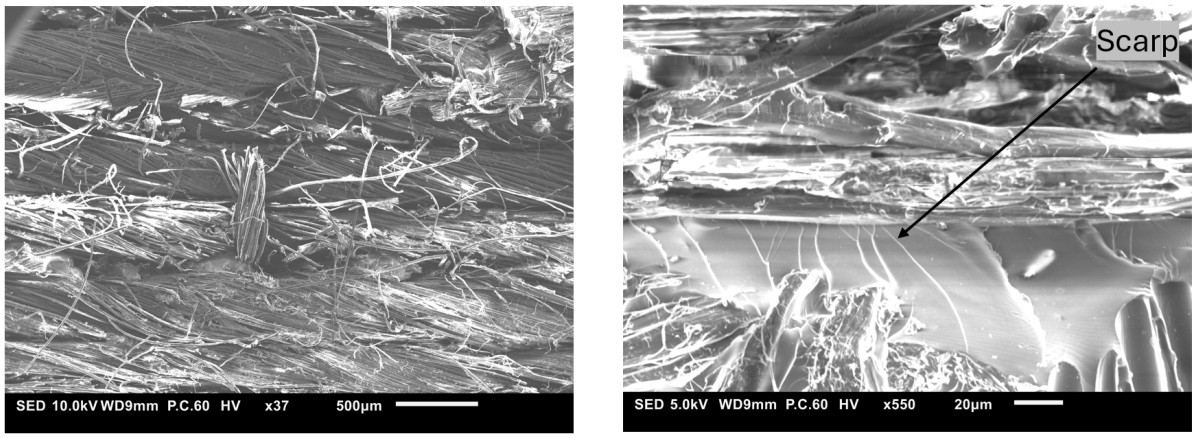

(a) 37x **(b)** 550x

Figure 6.25: SEM images of fatigue fracture surfaces at $50\,^{\circ}\mathrm{C}$/90% RH.

At high humidity and room temperature, the presence of scarps can be observed, although their appearance under cold conditions is noticeably different. The SEM images reveal the formation of textured microflows that gradually develop into distinct riverline patterns on the fracture surface. Scarps accompanied by riverlines are typical features of a brittle matrix. These riverlines can be interpreted as the result of several crack planes that originate separately and then merge together, forming tributary-like paths that eventually join into a single dominant crack. The direction of crack growth follows the direction in which the riverlines come together. In Figure 6.26b, the convergence of riverlines in resin-rich regions shows how matrix microcracks growing on different planes have met and formed large scarps, which appear as prominent facets on the fracture surface.

These observations indicate a clear shift in fracture behaviour with temperature. At lower temperatures, both the fibres and the matrix exhibit a more brittle response. At higher temperatures, the matrix soften and behaves more ductile, and the fibres likewise show more ductile failure characteristics.

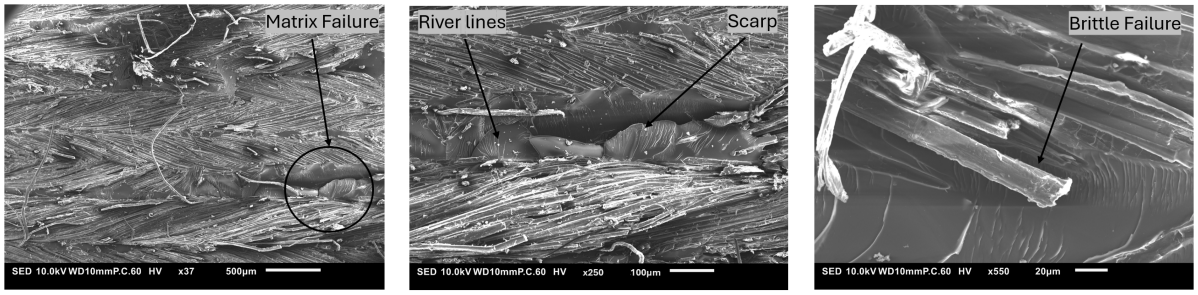

(a) 37x **(b)** 250x **(c)** 550x

Figure 6.26: SEM images of quasi static fracture surfaces at -20C.

6.4.4. Surface Roughness

The same approach used in the study of effects of the humidty is used for the surface roughness measurements. To assess both the initiation and propagation regions, measurements were taken on the bottom arm of each specimen for the quasi static samples. For the fatigue specimens the surface roughness was measured near the central region of the crack growth zone. The results of these measurements are summarized in Table 6.4. The measured roughness values (S_a) are discussed in relation to the observed fracture mechanisms in this section.

Table 6.4: Average surface roughness values (S_a) measured on fracture surfaces for quasi-static (QS) and fatigue tests under cold, room, and hot–wet temperature conditions.

	–20 °C	20 °C / 50 % RH	50 °C / 90 % RH
QS–Initiation	93 $\pm$ 6 (μm)	92 $\pm$ 7 (μm)	94 $\pm$ 5 (μm)
QS–Propagation	99 $\pm$ 10 (μm)	94 $\pm$ 9 (μm)	98 $\pm$ 11 (μm)
Fatigue	91 $\pm$ 8 (μm)	89 $\pm$ 5 (μm)	95 $\pm$ 9 (μm)

Similar to the results observed in the quasi-static tests under varying humidity, a considerable degree of statistical variation was also found in the surface roughness values measured under the cold, room, and hot conditions. This variation primarily arises from the highly non-uniform surface topography across the fracture surface of each specimen. Fractographic observations revealed that fibre bridging, yarn loosening, and the presence of fibre patches contribute significantly to these irregularities. As observed in the effect of humidity, the relatively large thickness of individual flax fibres may further amplifies this variation, while at lower temperatures, matrix cracking accentuates the formation of pronounced peaks and valleys along the fracture surface. Consequently, substantial scatter in the measured surface roughness values was observed across all environmental conditions.

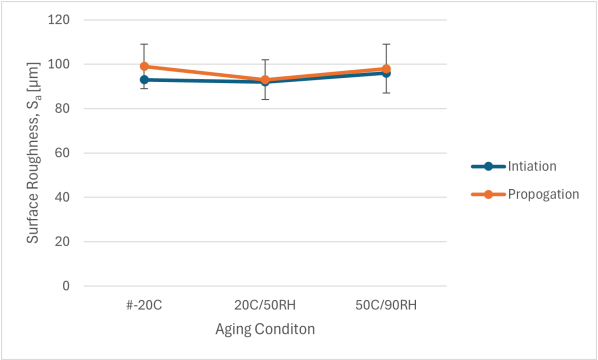

Figure 6.27: Surface roughness (S_a) of quasi-static specimens under cold, room, and hot conditions

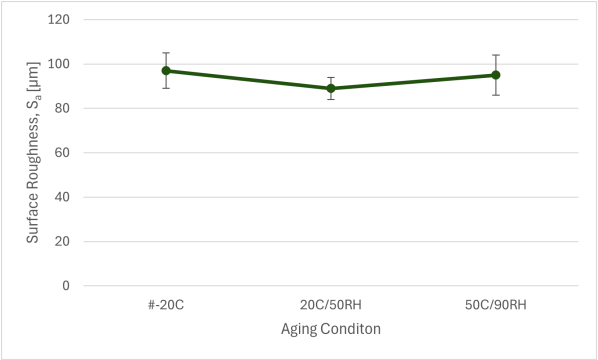

Figure 6.28: Surface roughness (S_a) of fatigue specimens under cold, room, and hot conditions

A similar degree of statistical scatter was observed in the fatigue surface roughness results, as shown in Figure 6.28. Similar to the observations from the humidity study, SEM fractography revealed comparable surface features between fatigue and quasi-static specimens, suggesting that the same microstructural mechanisms such as fibre bridging, fibre pull-out, matrix cracking, and the presence of fibre patches govern the fracture process in both cases. Therefore, the scatter observed in the fatigue results likely originates from the same inherent material heterogeneity responsible for variations in the quasi-static tests.

However, at low temperatures, higher surface roughness was expected on the fracture surfaces of the fatigue specimens. The increased brittleness of the matrix at –20 °C causes cracks to propagate

primarily through the matrix rather than along the fibre–matrix interfaces. This results in more irregular and fragmented fracture surfaces compared with the smoother, interface-driven morphology observed under room and hot–wet conditions. At higher temperatures, cyclic loading promotes gradual interfacial degradation and fibre–matrix separation, leading to smoother fracture surfaces.

When comparing quasi-static and fatigue conditions, the fatigue specimens generally exhibited slightly lower average surface roughness than their quasi-static counterparts under similar environments, consistent with the observations from the humidity study. This difference arises because quasi-static failure occurs through a single, abrupt event that induces greater fibre pull-out and matrix crackig, producing rougher and more irregular fracture surfaces.

The significant experimental scatter observed across the temperature conditions makes it challenging to establish a definitive quantitative relationship. The ANOVA showed $p = 0.715$ for the initiation region, $p = 0.746$ for the propagation region in quasi static, and $p = 0.449$ for fatigue, indicating no statistically significant differences in surface roughness across temperatures.This finding contrasts with the mechanical behavior reported earlier, where specimens tested at lower temperatures exhibited higher fracture toughness and were expected to show more energy-dissipative crack propagation that would normally yield higher surface roughness. Taken all results together, the absence of a significant temperature effect on roughness suggests that small changes in surface roughness are masked by the intrinsic variability created by fibre-dominated mechanisms. In other words, the observed features that govern fracture fibre bridging, pull-out, and associated matrix cracking introduce enough local variation that mask the variations caused by temperature dependent differences.

6.4.5. Summary of findings

The results of the quasi-static and fatigue tests, supported by fractographic analyses, demonstrate that temperature has a significant influence on the fracture and fatigue behaviour of flax fibre-reinforced polymer composites. A consistent trend was observed across all mechanical tests, where the fracture resistance increased markedly as the temperature decreased. The R-curve results showed that the specimens tested at low temperature exhibited the highest initiation and propagation fracture toughness, while those tested under room temperature displayed the lowest values, with hot–wet conditions specimens lying in between.This indicates that crack growth resistance are enhanced under cold conditions.

In the case of fatigue loads, the Paris curves exhibited a distinct rightward shift with decreasing temperature, signifying that a higher strain energy release rate is required to achieve the same crack growth rate in cold environments. The cold-temperature specimens demonstrated improved fatigue crack growth resistance, while those tested at elevated temperatures showed lower crack growth resistance. This trend confirms that lower temperatures promote higher resistance to cyclic damage, likely due to the increased tensile strength of the flax fibres and the higher load-bearing capacity of the bridging fibres across the crack plane.

Fractographic observations provided additional insight into the underlying failure mechanisms. Under cold conditions, the fracture surfaces exhibited features such as scarps, river lines, and distinct matrix facets, all of which are characteristic of brittle matrix failure. In contrast, specimens tested at room and hot–wet conditions displayed more ductile features, including fibre deformation and matrix cracking of similar nature across both environments. These observations indicate that the fracture mechanism shifts from a predominantly brittle, matrix-controlled mode at low temperatures to a more ductile fibre–matrix debonding mode at higher temperatures.

From a practical application perspective, these findings highlight that FFRP components are most reliable in cooler and room-temperature environments, whereas performance becomes more critical to manage at elevated temperatures and high humidity. At higher temperatures, the material becomes more sensitive to moisture uptake and release as ambient humidity fluctuates, which can lead to changes in fracture toughness and fatigue resistance in service. For design and certification, this implies that FFRP structures intended for hot–wet service conditions should be used with more conservative design allowables, tighter inspection intervals, and carefully defined environmental operating windows. Conversely, applications in colder climates or controlled indoor environments are likely to benefit more fully from the material's favourable fracture toughness and fatigue resistance, making

FFRP particularly attractive for lightweight, sustainability-driven structures in such conditions.

7

Conclusion

This study investigated the hygrothermal effects on the fracture toughness of FFRP composites, focusing on both quasi-static (QS) and fatigue responses under Mode I loading. The experiments were conducted under four representative hygrothermal conditions hot-wet, hot-dry, room, and cold environments, to simulate the range of natural weathering conditions. To evaluate these effects, Double Cantilever Beam (DCB) specimens were designed and manufactured. Prior to testing, all specimens were conditioned to their respective environments until equilibrium was reached. This resulted in moisture absorption in hot-wet conditions, moisture desorption in hot-dry conditions, and no change in the equilibrium state for room conditions.

Testing was performed under in-situ quasi-static and fatigue loading conditions in environmental chamber. The limited stroke length of the testing machine restricted measurable displacement, affecting the complete capture of crack propagation data during some tests. Despite these constraints, reliable and consistent results were achieved across all environmental conditions.

Overall conclusions of the experimental campaign are presented by addressing each of the research questions.

How does the hygrothermal environment influence the Mode I fracture toughness of flax–epoxy composites under quasi-static and fatigue loading conditions?

The hygrothermal environment strongly influences crack initiation and growth resistance, but in different ways for humidity and temperature. In terms of relative humidity, the initiation toughness does not change significantly with relative humidity, whereas the propagation toughness increases and the fatigue Paris curves shift to the right with gentler slopes at higher humidity, indicating more stable crack growth. Temperature, by contrast, has a clearer effect on crack initiation: specimens tested at –20 °C show higher initiation and propagation toughness and improved fatigue resistance, while hot–wet conditions lead to reduced values. The underlying mechanisms differ, with increased humidity promoting fibre bridging and other energy-dissipative processes, whereas low temperature strengthens the fibres and enhances load transfer during fibre bridging.

Sub-Reseach Questions

1. How does temperature variation affect the fracture toughness of flax epoxy composites under Mode I quasi-static and fatigue loading conditions?

Cold temperature (–20 °C) yields the highest initiation and propagation toughness and the steepest R-curves; fatigue data show improved resistance via a rightward Paris-curve shift. Hot–wet (50 °C/90% RH) and especially hot–dry (50 °C/30% RH) conditions reduce toughness and accelerate fatigue crack growth. Thus, decreasing temperature enhances Mode I fracture and fatigue resistance, while elevated temperature diminishes it.

2. How do dry and wet environmental conditions influence the fracture toughness of flax–epoxy composites under Mode I quasi-static and fatigue loading conditions?

Under increasing humidity, the initiation toughness did not show a statistically significant change, whereas the propagation toughness increases. Under fatigue loading, the Paris curves shift to the right and exhibit lower slopes at higher humidity, indicating more stable crack growth. Overall, the hot–wet condition provides the highest toughness and crack growth resistance, hot–dry the lowest, with room conditions in between. This improvement in resistance under wet conditions is attributed to moisture promoting technical fibre bridging, which increases energy dissipation during crack propagation.

3. What is the effect of hygrothermal exposure on the surface morphology and damage mechanisms in flax–epoxy composites subjected to Mode I quasi-static and fatigue loading conditions?

Across all environments, the fracture surfaces exhibit fibre bridging, fibre imprints/patches, yarn loosening, and scarps. Increased humidity enhances technical fibre pull-out and fibre bridging, which improves fracture resistance and stabilises the crack-growth curves, but does not noticeably change the nature of matrix cracking. At low temperature, the fracture morphology is markedly different, with more pronounced scarps, river lines, and faceted regions, indicating that matrix and fiber fail in a brittle manner. Fatigue fracture surfaces are generally smoother than their quasi-static counterparts, reflecting more interface-guided crack paths under cyclic loading.

In conclusion, the results demonstrate that the fracture toughness of FFRP composites is highly sensitive to both temperature and relative humidity, under both quasi-static and fatigue loading. The environmental exposure significantly affects the crack propagation behaviour and energy absorption mechanisms, underscoring the need to account for hygrothermal effects in the design and durability assessment of FFRP composite structures. These findings provide valuable insights for improving the long-term reliability of sustainable natural fibre composites in outdoor structural applications exposed to variable climatic conditions.

8

Recommendations

This thesis has investigated the effect of hygrothermal conditions on the fracture toughness under quasi-static loading and on the crack growth resistance under fatigue loading in Mode I conditions. The findings presented here represent only the tip of the iceberg in understanding the fracture mechanics of FFRP composites. The behaviour of these natural fibre composites is highly complex, and much remains to be explored to fully capture the influence of environmental factors on their mechanical performance. Based on the outcomes of this study, several recommendations for future research are proposed:

1. **Extend fracture toughness testing to Mode II and mixed-mode loading.**
   The current work focuses solely on Mode I delamination. However, in real structural components, delamination frequently occurs through shear-dominated or mixed-mode mechanisms. Investigating the influence of hygrothermal conditions on Mode II and mixed-mode fracture behaviour is therefore essential to develop a comprehensive understanding of the overall fracture response of FFRPs.
2. **Study the effect of hygrothermal conditions on thermoplastic composites.**
   The present research was conducted on epoxy-based thermoset composites. Future studies should examine thermoplastic flax fibre composites, which are more recyclable and better suited for sustainable engineering applications. Understanding how hygrothermal conditions affect their fracture and fatigue behaviour will provide valuable insights for designing environmentally durable composites.
3. **Investigate combined environmental degradation effects.**
   This study considered temperature and humidity as independent parameters. However, real-life service environments often involve more complex exposure conditions, including fluctuations in moisture and temperature, ultraviolet (UV) radiation, and salt-laden atmospheres. Exploring these combined effects would provide a more realistic understanding of the long-term durability of FFRPs in practical applications.
4. **Develop numerical and analytical models.**
   There is currently no established numerical framework to predict the fracture toughness of flax fibre composites under hygrothermal environments. Future research should aim to develop computational or analytical models that incorporate the effects of moisture absorption, fibre swelling, and matrix plasticisation. Such models would enable accurate prediction of fracture behaviour across a wide range of environmental conditions and reduce reliance on experimental testing.
5. **Explore the influence of fibre architecture.**
   This thesis focused exclusively on unidirectional flax fibre composites. Extending the investigation to other fibre architectures, such as woven or hybrid flax fabrics, would help in understanding how fibre orientation and interlacing influence crack propagation and energy dissipation mechanisms. Exploring different fibre layups could further improve the fracture toughness and structural performance of FFRPs.

6. **Examine the effect of fibre treatments and surface modifications.**
   Surface modification of flax fibres (for example, silane, alkali, or enzymatic treatments) could be explored to enhance interfacial bonding and reduce moisture uptake. Comparing treated and untreated composites under identical hygrothermal conditions would clarify how chemical treatments influence long-term durability and fracture mechanisms.
7. **Explore hybridisation with synthetic fibres or metal laminates.**
   Hybrid composites combining flax with glass, carbon, or metal reinforcements could be studied to determine whether hybridisation improves mechanical and environmental performance. For instance, fibre–metal laminates such as GLARE have demonstrated enhanced impact and fatigue resistance. Replacing glass fibres with flax fibres to form a sustainable variant (FLARE) could be an interesting direction for future investigation to balance strength, weight, and sustainability.

References

[1] Jack R. Vinson and Robert L. Sierakowski. *The Behavior of Structures Composed of Composite Materials*. Springer, 2008.

[2] Yusif Alovsat Tanriverdiyev. “Classification and properties of composites based on matrix material”. In: *World Journal of Advanced Research and Reviews* 24.2 (2024), pp. 314–320. DOI: 10.30574/wjarr.2024.24.2.3608. URL: https://doi.org/10.30574/wjarr.2024.24.2.3608.

[3] Saptarshi Maiti et al. “Sustainable Fiber-Reinforced Composites: A Review”. In: *Advanced Sustainable Systems* 6.11 (2022), p. 2200258. DOI: 10.1002/adsu.202200258.

[4] Libo Yan, Nawawi Chouw, and Krishnan Jayaraman. “Flax fibre and its composites – A review”. In: *Composites Part B: Engineering* 56 (2014), pp. 296–317. ISSN: 1359-8368. DOI: https://doi.org/10.1016/j.compositesb.2013.08.014. URL: https://www.sciencedirect.com/science/article/pii/S1359836813004228.

[5] Yan Li and Bing Xue. “Hydrothermal ageing mechanisms of unidirectional flax fabric reinforced epoxy composites”. In: *Polymer Degradation and Stability* 126 (2016), pp. 144–158. ISSN: 0141-3910. DOI: https://doi.org/10.1016/j.polymdegradstab.2016.02.004. URL: https://www.sciencedirect.com/science/article/pii/S0141391016300271.

[6] L. Calabrese et al. “Toughness Evolution of Flax-Fiber-Reinforced Composites under Repeated Salt Fog–Dry Aging Cycles”. In: *Polymers* 16.13 (2024), p. 1926. DOI: 10.3390/polym16131926. URL: https://doi.org/10.3390/polym16131926.

[7] Elisa Pietropaoli and Aniello Riccio. “On the robustness of finite element procedures based on Virtual Crack Closure Technique and fail release approach for delamination growth phenomena: Definition and assessment of a novel methodology”. In: *Composites Science and Technology* 70.8 (2010), pp. 1288–1300. DOI: 10.1016/j.compscitech.2010.04.006.

[8] L. Tong, A. P. Mouritz, and M. K. Bannister. *3D Fibre Reinforced Polymer Composites*. Elsevier, 2002.

[9] H. S. Sharath Shekar and M. Ramachandra. “Green Composites: A Review”. In: *Materials Today: Proceedings* 5.1, Part 3 (2018). International Conference on Advanced Materials and Applications (ICAMA 2016), June 15–17, Bengaluru, Karnataka, India, pp. 2518–2526. DOI: https://doi.org/10.1016/j.matpr.2017.11.034. URL: https://www.sciencedirect.com/science/article/pii/S2214785317322666.

[10] W. Woigk et al. “Interface properties and their effect on the mechanical performance of flax fibre thermoplastic composites”. In: *Composites Part A: Applied Science and Manufacturing* 122 (2019), pp. 8–17. ISSN: 1359-835X. DOI: https://doi.org/10.1016/j.compositesa.2019.04.015. URL: https://www.sciencedirect.com/science/article/pii/S1359835X19301435.

[11] A. Moudood et al. “Flax fiber and its composites: An overview of water and moisture absorption impact on their performance”. In: *Journal of Reinforced Plastics and Composites* 38.7 (2018), pp. 323–339. DOI: 10.1177/0731684418818893.

[12] Sikiru Oluwarotimi Ismail, Emmanuel Akpan, and Hom N. Dhakal. “Review on natural plant fibres and their hybrid composites for structural applications: Recent trends and future perspectives”. In: *Composites Part C: Open Access* 9 (2022), p. 100322. ISSN: 2666-6820. DOI: https://doi.org/10.1016/j.jcomc.2022.100322. URL: https://www.sciencedirect.com/science/article/pii/S2666682022000858.

[13] M. Angulu and H.-J. Gusovius. “Retting of Bast Fiber Crops Like Hemp and Flax—A Review for Classification of Procedures”. In: *Fibers* 12.3 (2024), p. 28. DOI: 10.3390/fib12030028. URL: https://doi.org/10.3390/fib12030028.

[14] W. Mahjoub and O. Harzallah. “Physical and Mechanical Characterization of Flax Fibers: From Elementary Fiber to Yarn”. In: *Fibers* 13.7 (2025), p. 87. DOI: 10.3390/fib13070087. URL: https://doi.org/10.3390/fib13070087.

[15] Syed Hussnain et al. “Degradation and mechanical performance of fibre-reinforced polymer composites under marine environments: – A review of recent advancements.” In: *Polymer Degradation and Stability* 215 (June 2023). DOI: 10.1016/j.polymdegradstab.2023.110452.

[16] A. Athijayamani et al. “Effect of moisture absorption on the mechanical properties of randomly oriented natural fibers/polyester hybrid composite”. In: *Materials Science and Engineering: A* 517.1 (2009), pp. 344–353. ISSN: 0921-5093. DOI: https://doi.org/10.1016/j.msea.2009.04.027. URL: https://www.sciencedirect.com/science/article/pii/S0921509309005152.

[17] Thomas Cadu et al. “Cyclic hygrothermal ageing of flax fibers’ bundles and unidirectional flax/epoxy composite. Are bio-based reinforced composites so sensitive?” In: *Industrial Crops and Products* 141 (2019), p. 111730. ISSN: 0926-6690. DOI: https://doi.org/10.1016/j.indcrop.2019.111730. URL: https://www.sciencedirect.com/science/article/pii/S092666901930740X.

[18] Valentin Perruchoud, René Alderliesten, and Yasmine Mosleh. “The Effects Of In-Situ Temperature And Relative Humidity On The Tensile Response Of Flax Vs. Glass Frp Composites”. In: July 2024.

[19] Eva Preiß. “Fracture Toughness of Freestanding Metallic Thin Films Studied by Bulge Testing”. In: *Doctoral thesis* (2018). PhD dissertation.

[20] *Standard Test Method for Mode I Interlaminar Fracture Toughness of Unidirectional Fiber-Reinforced Polymer Matrix Composites*. ASTM International, 2021. URL: https://www.astm.org/d5528_d5528m-21.html.

[21] *Fibre-reinforced plastic composites — Determination of mode I interlaminar fracture toughness (G_IC) for unidirectional fibre-reinforced materials*. International Organization for Standardization, 2023. URL: https://www.iso.org/standard/84263.html.

[22] *ASTM D7905/D7905M-19E01: Standard Test Method for Determination of the Mode II Interlaminar Fracture Toughness of Unidirectional Fiber-Reinforced Polymer Matrix Composites*. ASTM International, 2019. URL: https://compass.astm.org/document/?contentCode=ASTM%7CD7905_D7905M-19E01%7Cen-US&proxycl=https%3A%2F%2Fsecure.astm.org&fromLogin=true.

[23] *ISO 15114:2014 – Fibre-reinforced plastic composites — Determination of the mode II fracture resistance for unidirectionally reinforced materials using the calibrated end-loaded split (C-ELS) test and an effective crack length approach*. International Organization for Standardization (ISO), 2014. URL: https://www.iso.org/standard/55357.html.

[24] Yangyang Ge et al. “Test methods for measuring pure Mode III delamination toughness of composite laminates”. In: *Polymer Testing* 55 (2016), pp. 261–268. ISSN: 0142-9418. DOI: 10.1016/j.polymertesting.2016.08.025. URL: https://u-bourgogne.hal.science/hal-01445372.

[25] Qihui Chen et al. “Improved interlaminar fracture toughness of carbon fiber/epoxy composites by a combination of extrinsic and intrinsic multiscale toughening mechanisms”. In: *Composites Part B: Engineering* 252 (2023), p. 110503. ISSN: 1359-8368. DOI: https://doi.org/10.1016/j.compositesb.2023.110503. URL: https://www.sciencedirect.com/science/article/pii/S1359836823000069.

[26] Enes Akca and Ali Gursel. “A Review on the Matrix Toughness of Thermoplastic Materials”. In: *Periodicals of Engineering and Natural Sciences* 3 (Aug. 2015), pp. 1–8. DOI: 10.21533/pen.v3i2.52.

[27] Carolina Furtado et al. “J-Integral Experimental Reduction Reveals Fracture Toughness Improvements in Thin-Ply Carbon Fiber Laminates with Aligned Carbon Nanotube Interlaminar Reinforcement”. In: *ACS Applied Materials & Interfaces* 16.16 (2024). PMID: 38624137, pp. 20980–20989. DOI: 10.1021/acsami.3c17333. eprint: https://doi.org/10.1021/acsami.3c17333. URL: https://doi.org/10.1021/acsami.3c17333.

[28] M. F. Hibbs, M. K. Tse, and W. L. Bradley. “Interlaminar Fracture Toughness and Real-Time Fracture Mechanism of Some Toughened Graphite/Epoxy Composites”. In: *Toughened Composites, ASTM STP 937*. Ed. by N. J. Johnston. ASTM International, 1987, pp. 115–130. DOI: 10.1520/STP24374S.

[29] A. Korjakin et al. “Comparative study of interlaminar fracture toughness of GFRP with different fiber surface treatments”. In: *Polymer Composites* 25.2 (2004), pp. 125–133. DOI: 10.1002/pc.10154.

[30] Yao Chen et al. “Enhancing interfacial performance and fracture toughness of carbon fibre reinforced thermoplastic composites”. In: *Composites Part A: Applied Science and Manufacturing* 187 (2024), p. 108434. ISSN: 1359-835X. DOI: 10.1016/j.compositesa.2024.108434. URL: https://www.sciencedirect.com/science/article/pii/S1359835X24004317.

[31] Vishnu Prasad et al. “Enhancing Mode I and Mode II interlaminar fracture toughness of flax fibre reinforced epoxy composites with nano TiO_2”. In: *Composites Part A: Applied Science and Manufacturing* 124 (2019), p. 105505. ISSN: 1359-835X. DOI: 10.1016/j.compositesa.2019.105505. URL: https://www.sciencedirect.com/science/article/pii/S1359835X19302544.

[32] Mike van der Panne and John-Alan Pascoe. “Fatigue delamination growth – Is UD testing enough?” In: *Procedia Structural Integrity* 42 (2022), pp. 449–456. DOI: 10.1016/j.prostr.2022.12.057.

[33] W. S. Johnson and P. D. Mangalgiri. “Investigation of Fiber Bridging in Double Cantilever Beam Specimens”. In: *Journal of Composites Technology & Research* 9.1 (1987), pp. 10–17. DOI: 10.1520/CTR10421J. URL: https://ntrs.nasa.gov/api/citations/19860014187/downloads/19860014187.pdf.

[34] Rafiullah Khan. “Fiber bridging in composite laminates: A literature review”. In: *Composite Structures* 229 (2019), p. 111418. ISSN: 0263-8223. DOI: https://doi.org/10.1016/j.compstruct.2019.111418. URL: https://www.sciencedirect.com/science/article/pii/S0263822318346051.

[35] P. Kumar, Ravinder Reddy Pinninti, and A. Gupta. “Thickness Effect of DCB Specimen on Interlaminar Fracture Toughness in Carbon/Epoxy Composites”. In: *International Journal of Mechanical and Production Engineering Research and Development* 8 (June 2018), pp. 541–548. DOI: 10.24247/ijmperdjun201858.

[36] Liaojun Yao et al. “Bridging effect on mode I fatigue delamination behavior in composite laminates”. In: *Composites Part A: Applied Science and Manufacturing* 63 (2014), pp. 103–109. ISSN: 1359-835X. DOI: https://doi.org/10.1016/j.compositesa.2014.04.007. URL: https://www.sciencedirect.com/science/article/pii/S1359835X14001092.

[37] George C. Jacob et al. “The Effect of Loading Rate on the Fracture Toughness of Fiber Reinforced Polymer Composites”. In: *Journal of Applied Polymer Science* 96.3 (2005), pp. 899–904. DOI: 10.1002/app.21535. URL: https://onlinelibrary.wiley.com/doi/10.1002/app.21535.

[38] Younes Saadati et al. “A Study of the Interlaminar Fracture Toughness of Unidirectional Flax/Epoxy Composites”. In: *Journal of Composites Science* 4.2 (2020), p. 66. DOI: 10.3390/jcs4020066. URL: https://doi.org/10.3390/jcs4020066.

[39] M. Ravandi et al. “The effects of through-the-thickness stitching on the Mode I interlaminar fracture toughness of flax/epoxy composite laminates”. In: *Materials & Design* 109 (2016), pp. 659–669. ISSN: 0264-1275. DOI: 10.1016/j.matdes.2016.07.093. URL: https://www.sciencedirect.com/science/article/pii/S0264127516309911.

[40] Y. Li, D. Wang, and H. Ma. “Improving interlaminar fracture toughness of flax fiber/epoxy composites with chopped flax yarn interleaving”. In: *Science China Technological Sciences* 58 (2015), pp. 1745–1752. DOI: 10.1007/s11431-015-5911-3. URL: https://doi.org/10.1007/s11431-015-5911-3.

[41] B. Yu, Y. Li, H. Tu, et al. “Experimental and numerical investigation into interlaminar toughening effect of chopped fiber-interleaved flax fiber reinforced composites”. In: *Acta Mechanica Sinica* 40 (2024), p. 423287. DOI: 10.1007/s10409-023-23287-x. URL: https://doi.org/10.1007/s10409-023-23287-x.

[42] Zia Mahboob and Habiba Bougherara. “Fatigue of flax-epoxy and other plant fibre composites: Critical review and analysis”. In: *Composites Part A: Applied Science and Manufacturing* 109 (2018), pp. 440–462. ISSN: 1359-835X. DOI: 10.1016/j.compositesa.2018.03.034. URL: https://www.sciencedirect.com/science/article/pii/S1359835X18301362.

[43] Antigoni Barouni et al. “Investigation into the fatigue properties of flax fibre epoxy composites and hybrid composites based on flax and glass fibres”. In: *Composite Structures* 281 (2022), p. 115046. ISSN: 0263-8223. DOI: https://doi.org/10.1016/j.compstruct.2021.115046. URL: https://www.sciencedirect.com/science/article/pii/S0263822321014665.

[44] N.H. Nash, T.M. Young, and W.F. Stanley. “The reversibility of Mode-I and -II interlaminar fracture toughness after hydrothermal aging of Carbon/Benzoxazine composites with a thermoplastic toughening interlayer”. In: *Composite Structures* 152 (2016), pp. 558–567. ISSN: 0263-8223. DOI: https://doi.org/10.1016/j.compstruct.2016.05.086. URL: https://www.sciencedirect.com/science/article/pii/S0263822316304998.

[45] L. A. Khan et al. “Effect of hygrothermal conditioning on the fracture toughness of carbon/epoxy composites cured in autoclave/Quickstep”. In: *Journal of Reinforced Plastics and Composites* 32.16 (2013), pp. 1165–1176. DOI: 10.1177/0731684413486367.

[46] Amar Garg and Ori Ishai. *Hygrothermal Influence on Delamination Behavior of Graphite/Epoxy Laminates*. Tech. rep. NASA TM-85935. NASA Ames Research Center, 1984. URL: https://ntrs.nasa.gov/citations/19840013836.

[47] Liaojun Yao et al. “Does hygrothermal degradation of Mode I fatigue delamination resistance in carbon fibre reinforced polymer laminates depend on the ageing conditions?” In: *Composite Structures* 342 (2024), p. 118240. ISSN: 0263-8223. DOI: https://doi.org/10.1016/j.compstruct.2024.118240. URL: https://www.sciencedirect.com/science/article/pii/S0263822324003684.

[48] Luca A. Baak. “Hygrothermal Effects on Fracture Toughness of Flax Fiber Reinforced Epoxy”. In: *TU Delft, Faculty of Aerospace Engineering* (2024). MSc thesis.